Ministry of Higher Education and Scientific Research
University of Baghdad
Institute of Laser for Postgraduate Studies

Studying Enhancement of Humidity Sensor Based on Photonic Crystal Fiber Interferometer

A Thesis Submitted to the Institute of Laser for Postgraduate Studies/ University of Baghdad in Partial Fulfillment of Requirements for the Degree of Master of Science in Laser/ Physics

By
Hassan Faleh Hassan
B.Sc. Physics –2000

Supervisor
Asst. Prof. Dr. Hanan J. Taher

2017 AD **1439 AH**

Certification

I certify that this thesis was prepared under my supervision at the Institute of Laser for Postgraduate Studies, University of Baghdad, as a partial fulfillment of requirements for the degree of "Master of Science in Laser/ Physics.

Signature:

Name: **Dr. Hanan J. Taher**

Title: **Asst. Professor**

Address: Institute of Laser for Postgraduate Studies,

University of Baghdad.

Date: / / 2017

(Supervisor)

In view of the available recommendation, I forward this thesis for debate by Examining Committee.

Signature:

Name: **Asst. Prof. Dr. Shelan Khasro Tawfeeq**

Title: Head of the Scientific Committee.

Address: Institute of Laser for Postgraduate Studies,

University of Baghdad.

Date: / / 2017

بِسْمِ اللَّهِ الرَّحْمَنِ الرَّحِيمِ

قَالُوا سُبْحَانَكَ لَا عِلْمَ لَنَا إِلَّا مَا عَلَّمْتَنَا إِنَّكَ أَنْتَ الْعَلِيمُ الْحَكِيمُ

صدق الله العلي العظيم

الآية (32) سوره البقرة

DEDICATION

This thesis is dedicated to:

The sake of Allah, my Creator and my Master,

My great teacher and messenger, Mohammed (May Allah bless and grant him),and holy Imams of his household who taught us the purpose of life,

My homeland Iraq, the warmest womb,

The great martyrs and Iraq army, the symbol of sacrifice,

The University of Baghdad / Institute of Laser for Postgraduate studies, my second magnificent home,

My great parents, who never stop giving of themselves in countless ways, My dearest wife, who leads me through the valley of darkness with light of hope and support,

My beloved brothers and sisters, the symbol of love and giving,

My beloved kids: Mohammed muntadher, Fatima . tuqa . and zahraa, whom I can't force myself to stop loving ,

My friends who encourage and support me, particularly my dearest friend the lawyer Ahmed Al-Jobory who stands by me when things look bleak.

All the people in my life who touch my heart, I dedicate this research.

Hassan *2017*

Acknowledgements

First and foremost, I am grateful to the creator "ALLAH" for giving me the strength, enablement, knowledge and understanding required to complete this work.

I am heartily thankful to my supervisor,Dr. Hanan J. Taher, whose encouragement, guidance and support from the initial to the final level enabled me to develop and understand the project. I would like to thank Prof. Dr. Abdul Hadi M. Al- Janabi, the Dean of Institute of Laser for Postgraduate Studies and for welcoming me into their groups, and for his continuous help and encouragement through this work.

Also I would like to introduce a great thank to Dr. Mohamed K. Dhahir who helped me so many times for resolving different experimental and theoretical problems and for Fraternal support and continuous help through this work. I would like to thank Dr. Zainab Fadhil Mahdi for allowing use some devices and thank to Nor Abid Almalek for helping me in chemical processes in nanotechnology lab. A great thank to Dr. Fadhil Abbas Umran , Dr. Tahreer Safaa Mansour, Hiba Kadhim and Dr. Alawan Mohamed in the university of Technology / Applied Sciences department for their help and support.

Special thanks to Eng. Saif Akeel, for his help and his assistance during the project in the lab. of the photonic fiber.

I would like to thank to all the staff of the Institute for their effort during this research work especially to Eng. Atheer who help me to make coated setup in CNC machine CO_2 laser lab. My sincere thanks go to all my friends, for their help and support.

Finally, thanks to almighty **ALLAH** for giving me the strength to complete my master degree.

Abstract

Photonic Crystal Fiber Interferometers (PCFIs) are generally utilized for sensing applications. This work presents the fabrication and studies the characterization of a relative humidity sensors. A stub of (LMA-10) PCF infiltrated with a polymer (agarose) in order to improve the sensitivity of the humidity sensor that operates in a Mach- Zehnder Interferometer (MZI) reflection mode . The other sensor was coated with same material that operates in a (MZI) transmission type. The fabrication of the sensors only involves splicing and cleaving PCF with Single Mode Fiber SMF (Corning-28). For agarose infiltrated PCFI that based in MZI reflection type, the sensor operation involved on the adsorption and desorption of water vapor at the silica-air interface within the PCF. The sensor shows a high sensitivity to RH variations from (27% RH - 95% RH), with a change in its reflected power, the position of the interference peaks is found to be shifted to long wavelength (red shift) with high humidity sensitivity of (8.49 pm / %RH) is achieved with compact (4mm) PCF length and the response time of the sensor is found to be 1.4 s for a change in RH of 50%RH. The sensor has the focal points for reasonable for checking the humidity in microenvironments such as a human breath rate monitor in a clinical situation. The other RH sensor based on coated agarose PCFI that operates in (MZI) transmission type, the experimental results show that a high humidity sensitivity of -29.37 pm/%RH is achieved within measurement range of 27–95% RH at thickness of agarose solution 5.996μm, the sensitivity of the RH sensor had a considerable reliance on the thickness of coating and the highest sensitivity of the sensor showed a linear response for RH change that shifted interference peaks to short wavelength (blue shift) with a fast response time of 0.8 s for an RH changed from 50% - 90%.

The two sensors also show good repeatability, small size, long-term stability, measurement accuracy and wide humidity range.

Some simulation results have been achieved by using the COMSOL 5.1 multiphase's program. It used to design the photonic crystal fiber large-mode area of the empty and with infiltrated or coated agarose PCFI and find a guiding diode laser 1550 nm inside the optical crystal fiber.

Table of Contents

Subject	*Page*
Abstract	i
Table of Contents	iii
List of Tables	v
List of Figures	vi
List of Abbreviations	ix
List of Symbols	x
CHAPTER ONE :Introduction and Basic Concept	
1.1. Introduction	1
1.2 Optical Fiber	2
1.2.1Classification of Optical Fibers	3
1.2.2 Propagation of Light within an Optical Fiber	4
1.٣Photonic Crystal (PC)	6
1.٣.1Configuration of Photonic Crystals	7
1.4 Photonic Crystal Fibers (PCFs)	10
1.4.1 Classification and Guidance Mechanisms of PCF	12
1.4.1.1 Solid Core (Index-Guiding) PCFs	14
1.٤.١.١.1 Large mode area	17
1.٤.١.٢ Hollow- core PCF	1٨
1.٥ Optical Properties of PCFs	19
1.5.1 Dispersion	19
1.5.2 The nonlinearity	21
1.5.3 The losses	21
a- Confinement losses	21
b- Bending losses	22
1.6 Photonic Crystal Fiber Interferometer (PCFI)	23
1.7Humidity sensing	27
1.7.1Fiber optic humidity sensor	28
1.7.1.1 Operating principle of the RH sensor based on PCFI	28
1.7.1.2 Evanescent wave (EW)sensing method based humidity sensors	33
1.8Literature survey	35
1.5The motivation , aims and objectives of the research	45
Chapter Two: Experimental Set Up and Procedures	
2.1 Introduction	٤6
2.2 PCFs cleaving	47

2.3 PCF-SMF fusion splicing:	49
2.4 Fabrication of a PCFI:	50
2.5 PCF Humidity Sensors Based on Modal Interferometer Setup	52
2.6 Controlling the humidity environment	55
2.7 Chemical processes:	56
2.8 RH sensor based on Agarose infiltrated photonic crystal fiber interferometer (AI-PCFI)	57
2.8.1 System Layout:-	57
2.8.2 Experimental Procedures	57
2.9 RH sensor based on Agarose coated photonic crystal fiber interferometer (AC-PCFI)	58
2.9.1 System Layout:-	58
2.9.2 Experimental Procedures	59
2.10 Simulation Design:	61
Chapter Three Results and Discussion	
3.1 Introduction:-	62
3.2The Interferometer Fabrication	٦2
3.3Physical properties of agarose gel	65
3.4 Experimental investigationand discussion of RH sensor based on an agarose infiltration reflection-type photonic crystal fiber interferometer (AI-PCF)	67
3.4.1 The Effect of the PCF Length on The infiltration region	٦8
3.4. 2 Performance Analysis of the RH Sensor Based on AI-PCFI	٧0
3.4. 3 The Effect of the PCF Length on The Sensor Sensitivity	74
3.4.4 The Rise Time of RH Sensor Based on AI-PCFI	77
3.4. 5The Repeatability of the RH Sensor Base on AI-PCFI	78
3.5 Experimental investigationand discussion of RH sensor based on an agarose coated transmission type photonic crystal fiber interferometer	79
3.5.1Effect of coating thickness on the sensor sensitivity	٨1
3.5. 2The rise time of RH sensor based on AI-PCFI	86
3.5. 3Long term stability of the RH sensor based on AC-PCFI	87
3.6 Performance comparison of the RH sensors	88
3.7 Simulation Result for COMSOL Multiphsics Program for Soild Core PCF(LMA-10)	90

3.7.1 Infiltrated Solid Core PCF(LMA-10) with agarose solution	٩1
3.7.٢coated Soild Core PCF(LMA-10) with agarose solution at thickness 5.996 µm	92
3.7.3coated Soild Core PCF(LMA-10) with agarose solution at thickness 3530 nm	93
3.7.4coated Soild Core PCF(LMA-10) with agarose solution at thickness 630 nm	٩4
3.7.4coated Soild Core PCF(LMA-10) with agarose solution at thickness 300 nm	95
Conclusions and Future Work	
3.8Conclusion	96
3.8.1 RH sensor based on AI-PCFI	96
3.8.2RH sensor based on AC-PCFI	97
3.9 Future Work	97
References	
References	98

LIST OF TABALS

Table	Title	Page
1.1	Summary of the published works in RH sensor	3٥
3.1	The optimized parameters of arc fusion splicer (FSM-60S) for splicing SMF-28 with PCF (LMA-10)	٦٢
3.2	parameters of (A,B,C,D)proportions	66
3.3	Different Parameters of the AC-PCFI Devices	82
3.4	RH Sensitivity of AC-PCFI Devices.	86
3.5	Comparison of RH sensors	89

List of Figures

Figure No.	Page
Fig. (1-1): Traditional structure of optical fiber	٢
Fig. (1-2): Different types of optical fibers	٣
Fig (1-3): The block diagram of classification of optical fiber	4
Fig. (1-4) Propagation of light through an optical fiber	5
Fig. (1.5) Examples of (a) one-dimensional, (b)two-dimensional, and (c) three-dimensional photonic crystals	8
Fig. (1.6) One-dimensional photonic crystal structure	٨
Fig. (1.7) photonic crystal structure of Two-dimensional	9
Fig. (1.8) Three-dimensional photonic crystal structure	10
Fig. (1.9) Geometrical parameters describing PCFs	١١
Fig.(1.10) PCF SEM images: (a) hybrid PCF; (b) sub-wavelength air core PCF; (c) PCF for quantum dot applications; (d) hollow-core; (e) all-solid PBGF; (f) index -guiding PCF	١١
Fig. (1.11) Cross-section drawing of (a) Single-Mode Fiber (SMF), (b) solid core PCF, and (c) hollow-core PCF	١٢
Fig.(1.12) Classification of PCFs	١٣
Fig. (1.13) Schematic illustration of (a) the cross-section and (b) the refractive index profile for an index-guiding photonic crystal fiber	١٥
Fig. (1.14) Solid core (Index guidance)PCF ; n1=1.45(silica) , n2=1(air)	١٦
Fig. (1.15) HC- PCF ; n1=1.45(silica) , n2=1(air)	١٨
Fig (1.16): Schematic of the bending of the PCF	٢٢
Figure (1.17): the schematic of an MZI. Two couplers are used to split and recombine the signals	٢٣
Fig (1.17): Reflection type PCF interferometer	٢٤
Fig (1.18): Transmission type interferometer PCFI	٢٥
Fig. 1.19 Examples of applications of humidity sensors in different areas	٢٧
Fig.(1.20): Water vapor adsorption mechanisms on an SiO2 surface	29
Fig.(1.21)a) drawing of the reflection type PCF interferometer and b)a diagram of the cross section of the PCF employed.	31
Fig.(1.22)a) drawing of the transmission type PCF interferometer and b)a diagram of the cross section of the PCF employed	32
Fig.(1.23)Schematic diagram of a fiber optic breath sensor system, (upper) microscope image of an AI-PCFI and (lower) a photograph of the mask placed on the volunteer's face showing the position of the sensor inside the mask (dotted line). FOC- Fiber optic circulator, SMF-Single mode fiber, AI-PCFI-Agarose infiltrated-photonic crystal fiber interferometer, PC/BAAP-Personal computer/Breath analysis application program	33
Fig. (1-24) Evanescent wave in the optical fiber cladding[	34
Fig. (2-1): Schematic diagram for the structural work of the study	٤7
Fig. (2. 2) Fiber cleaver (CT-30)	48
Fig (2. 3): Microscope images of PCFs (LMA-10) end after cleaving	48
Fig (2. 4): Arc fusion splicer (FSM-60S)	50

Fig (2.5): Scanning electron microscope image of the cross section of the PCF used for the experiment	51
Fig (2.6): Microscope image of the PCF collapsing interferometer	51
Fig. 2.7 Block diagram of the generic experimental set-up to study the RH response of the transmission type sensor	52
Fig. 2.8 Block diagram of the generic experimental set-up to study the RH response of reflection type	52
Fig.(2.9)Fiber Optic Circulator (FOC)	53
Fig. (2.10) Light source (S1FC1550)	53
Fig (2.11): photograph of optical spectrum analyzer (OSA)	54
Fig. (2.12) Power meter	54
Fig.(2.13) The Transmission Microscope	55
Fig.(2.14) Humidity chamber a) front view, b) top view, and c) side view	56
Fig. (2.15) Temperature and Humidity Controller	56
Fig.(2. 16)The Spectrophotometer sp-3000 from optima Company	56
Fig. (2.18) The photographic picture for the PCFI humidity sensor set up (reflection type)	٥7
Fig.(2.20)The photographic picture for the PCFI humidity sensor set up (transmission type)	٥9
Fig. (2.21) Schematic diagram of the experimental setup for Agarose coating	60
Fig. (2.22) The photographic picture for setup of Agarose coating	60
Fig.(2.23) procedures of design the PCFI in the COMSOL multphysics.	61
Fig.(3.1): The splicing process and the loss obtained in (dB)	63
Fig.(3.2): Microscope images of the splice regions, between PCF (LMA-10) and the SMF-28, a)the collapsed length is ~235.2 µm, and b)the collapsed length is ~287.8µm, when the magnification power of the transmission microscope is (10X)	٦4
Fig.(3.3): Output Spectrum of laser diode 1550 nm	65
Fig.(3.4) spectrophotometer UV/visible absorption spectrum of (A,B,C,D) proportions.	66
Fig.(3.5)a Change in the reflection spectrum of a PCFI with length 4.5 cm with respect to different ambient relative humidity values. b) Change in the reflection power of a PCFI with length 4.5 cm with respect to different ambient relative humidity values.	67
Fig.(3.7) Microscope image show a)length of infiltration region in PCF b) cross section of agarose infiltration in PCF (AI-PCF)	69
Fig. (3.8) The infiltration lengths of the five different AI-PCFI devices at R.T.	69
Fig.(3.٨)a) Interference peaks shift of wavelength shift with RH for length(4.5) cm of PCF b) Interference peaks shift of reflection power with RH for length(4.5) cm of PCF	70
Fig.(3.9a) Interference peaks shift of wavelength shift with RH for length(3.5)cm of PCF. b) Interference peaks shift of reflection power with RH for length (3.5) cm of PCF	٧1
Fig.(3.10)a) Interference peaks shift of wavelength shift with RH for length(2.5)cm of PCF b) Interference peaks shift of reflection power with RH for length(2.5)cm of PCF	٧1
Fig.(3.11)a) Interference peaks shift of wavelength shift with RH for length(1.5)cm of PCF b) Interference peaks shift of reflection power with RH for length(1.5)cm of PCF	72

Fig.(3.12)a) Interference peaks shift of wavelength shift with RH for length(0.4)cm of PCF b) Interference peaks shift of reflection power with RH for length(0.4)cm of PCF	72
Fig. (3.13 a) : behavior of all lengths for wavelength shift with RH . b)behavior of all lengths for reflection power with RH	73
Fig (3.14) The sensitivity values obtained from different PCF lengths	74
Fig.(3.15) COMSOL image snapshot of infiltrated PCF	75
Fig. (3.16) OSA Graphics peaks shift of AI- PCFI with respect humidity of the length 4 mm.	76
Fig. (3.17):The relationship between PCF lengths and sensitivity of the sensor	76
Fig. (3.18):The rise time of the RH sensor with length (4mm)	78
Fig. (3.19): The repeatability of the RH sensor with PCF length (4mm)	79
Fig.(3.2٠) The shift in Wavelength peak of PCFI without coating in humidity chamber	٨0
Fig.(3.21)a) Change in the transmission spectrum of a PCFI without coating of length 10mm with respect to different ambient RH values. b) Change in the transmission power of a PCFI without coating of length 10mm with respect to different ambient RH values.	٨0
Fig.(3.21)a) Wavelength peak of PCFI before coating. b) The shift in Wavelength peak of PCFI after coating is about 1.014 nm	81
Fig. (3.22) The average spectral peak shift of AC-PCFI A and B with respect to relative humidity.	٨3
Fig. (3.2٣) OSA Graphics peaks shift of AC- PCFI(A) with respect humidity. b) OSA Graphics peaks shift of AC- PCFI(B) with respect humidity.	٨4
Fig. (3.2٤) The spectral peak shift of AC-PCFI C and D with respect to relative humidity.	85
Fig. (3.25)a) OSA Graphics peaks shift of AC- PCFI(C) with respect RH .	85
Fig. (3.٢5)b) OSA Graphics peaks shift of AC- PCFI(D) with respect humidity.	86
Fig.(3.٢٦). Response time of the sensor.	87
Fig. (3.٢٧): The repeatability of the AC-PCFI sensor (D)	88
Fig. (3.28) (A) geometry of cladding PCF with refractive index of air =1(B) Mesh of PCF (C) Laser beam profile that exist from PCF(LMA-10) without infiltration (empty).	90
Fig. (3.29) (A) geometry of cladding PCF infiltrated agarose with refractive index =1.12 (B) Mesh of PCF (C) Laser beam profile that exist from PCF(LMA-10) with infiltration.	91
Fig. (3.30) (A) geometry of cladding PCF with coating of agarose thickness=5966nm (B) Mesh of PCF (C) Laser beam profile that exist from PCF(LMA-10) with PCF agaros coated.	92
Fig. (3.31) (A) geometry of cladding PCF with coating of agarose thickness=3530 nm (B) Mesh of PCF (C) Laser beam profile that exist from PCF(LMA-10) with PCF agaros coated.	93
Fig. (3.32) (A) geometry of cladding PCF with coating of agarose thickness=630 nm (B) Mesh of PCF (C) Laser beam profile that exist from PCF(LMA-10) with PCF agaros coated.	94
Fig. (3.33) (A) geometry of cladding PCF with coating of agarose thickness=300nm (B) Mesh of PCF (C) Laser beam profile that exist from PCF(LMA-10) with PCF agaros coated.	95

LIST OF ABBREVIATONS

NA	Numerical Aperture
PCF	Photonic Crystal Fiber
MOF	Microstructured Optical Fiber
MTIR	Modified Total Internal Reflection
PBG	Photonic Band Gap
RH	Relative Humidity
PC	Photonic Crystal
TIR	Total Internal Reflection
1D, 2D, 3D	One, Two, and three dimensional
OFC	Optical Fiber Conference
SEM	Scanning Electron Microscope
LMA	Large Mode Area
HC	Hollow-Core
SMF	Single Mode Fiber
PCFI	Photonic Crystal Fiber Interferometer
ATR	Attenuated Total Reflection
MZI	Mach- Zehnder Interferometer
MFD	Mode-Field Diameter
FOC	Fiber Optic Circulator
DWDM	Dense Wavelength Division Multiplexing
FBG	Fiber Bragg Grating
PVC	Polyvinyl Chloride
OSA	Optical Spectrum Analyzer
RI	Refractive index
EW	Evanescent wave
AI-PCFI	agarose infiltration photonic crystal fiber interferometer
AC-PCFI	agarose coated photonic crystal fiber interferometer
PC/BAAP	Personal computer/Breath analysis application program

List of Symbols

θ_{in}	the incident angle
θ_1	Refraction angle
n_c	Refractive index of core
n_{cl}	Refractive index of cladding
n1,n2	Refractive index of silica , refractive index of air
θ_c	critical angle
θ	internal reflection angle
d	hole diameter (μm)
Λ	hole pitch (μm)
ρ	core diameter (μm)
β	propagation constants (m^{-1})
n_{eff}	effective index
k_0	vacuum wave number (cm^{-1})
λ	wavelength of light (nm)
k	wave vector (cm^{-1})
R_0	radius of curvature (cm)
ω	frequency (Hz)
n	refractive index
V_{eff}	effective frequency parameter
$\Delta\varphi$	phase difference
Δn	effective refractive index deference
P_w	partial pressure of the water vapor (pascal)
P_{ws}	saturation water vapor pressure (pascal)
L	PCF length (cm)
d_p	penetration depth

Chapter One

Introduction and Basic Concepts

1.1 Introduction

This chapter introduces the basic concepts of optical fiber ,research background, literature survey, motivation and objectives of the research. Over the past decades, optical fibers have revolutionized the fields of the sensing and telecommunications. Numerous kinds of optical fiber sensors have been well-designed and developed to measure various parameters, more than 70 different parameters could be measured or monitored, such as, temperature[1], rotation [2], strain [3], vibration[4], magnetic fields[5], pressure[6], acoustics[7], humidity[8], refractive index [9], acceleration [10], etc. Optical fiber sensors have become more and more important; they gradually become indispensable, such as in civil [11, 12] medical [13, 14] and military applications [15].

Although optical fibers offer an excellent performance in fiber communication, the silica's intrinsic properties have imposed limitation in the development of this technology. The first limitation is selection of material for the core and cladding, so as to have matching optical, chemical, and thermal properties. Different limitations are identified with the fiber geometry and its refractive file profile, which does not permit designing optical fiber attributes for uninhibitedly, for example, nonlinearity, scattering, and birefringence keeping in mind the end goal to advance in applications, for example, fiber sensors or high power lasers, among others[16].To avoid these problems, new sensors are designed and constructed in depending on optical fibers, photonic crystal fibers (PCFs).

PCF is a particularity optical fiber made out of a single material (silica) based on the properties of photonic crystals with unique manufacture [17]. The PCF has cross-section of an array of air holes running along its entire length, It is microstructure provides distinctive characteristics different from the conventional optical fiber [18], the air holes presence provides a possibility of light propagation in air, or instead of that gives the ability to

inject gases/liquids into holes. This leads a good controlled interaction between light and matter leading to novel sensing applications that cannot get it with conventional optical fibers [19, 20, 21].

Photonic Crystal Fiber Interferometers (PCFI) are attractive because of their compactness and fundamental intrinsic temperature compensation [22].

Humidity is a serious factor in various fields, such as, food process and storage, chemical, biomedical, agriculture,weather conditions monitoring and others[23].

1.2 Optical Fiber

The optical fiber is dielectric waveguide, that is utilized to keep and direct the light [24]. An Optical fiber is made of three parts; the core, the cladding, and the coating. The basic composition of a traditional optical fiber is shown in Fig. (1.1). The core is a thin center of the fiber where the light guides,it is generally made of glass with refractive index (n_c) [24, 25]. Typically, the core section has a diameter of between (5μm) and (100μm) [26].

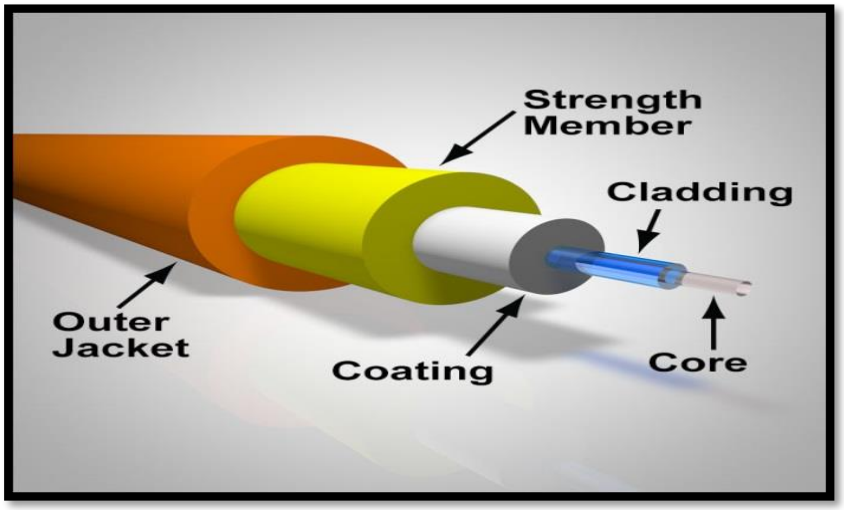

Fig. (1-1): Traditional structure of optical fiber [25].

The outer optical substance around the core is cladding layer that reflects the light back into the core and made of a dielectric material with an index of refraction (n_{cl}). The index of refractive of the cladding material is less than that of the core material[25]. Generally, the clad is made of glass or plastic. The cladding executes such functions as reducing loss of light from core into the surrounding air, decreasing loss of scattering at the surface of the core, maintaining the fiber from absorbing the surface contaminants and including mechanical strength [24]. Most cladding diameter of fibers are about (125 to 200) μm [24]. The coating is a coat of material utilized to keep an optical fiber from physical hazards. The substance utilized for a coating is plastic which is prevents abrasions and it is elastic in nature [25].

1.2.1 Classification of Optical Fibers

An optical fibers can be classified into two kinds, single mode or multimode as shown in Fig. (1.2). The classification of optical fiber has been presented in block diagram seen in fig. (1.3).

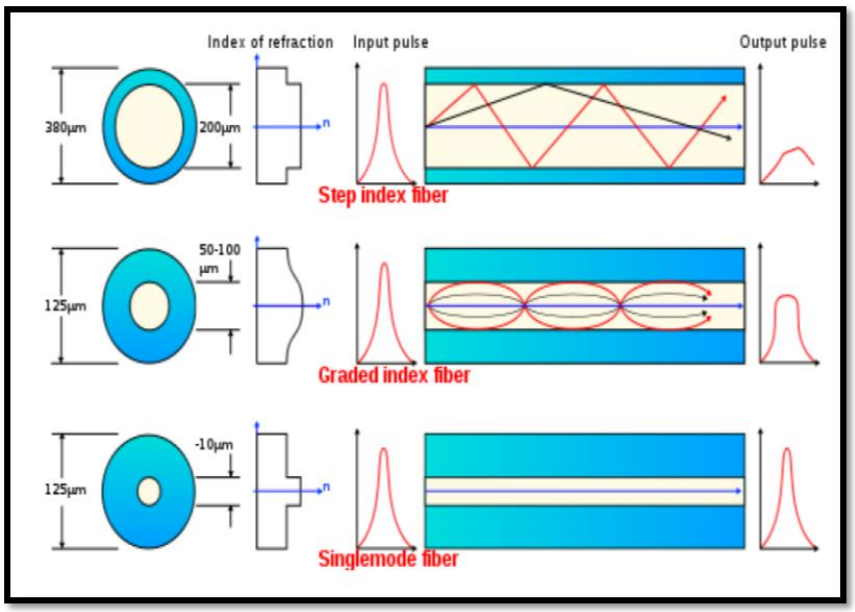

Fig. (1-2): Different types of optical fibers [25].

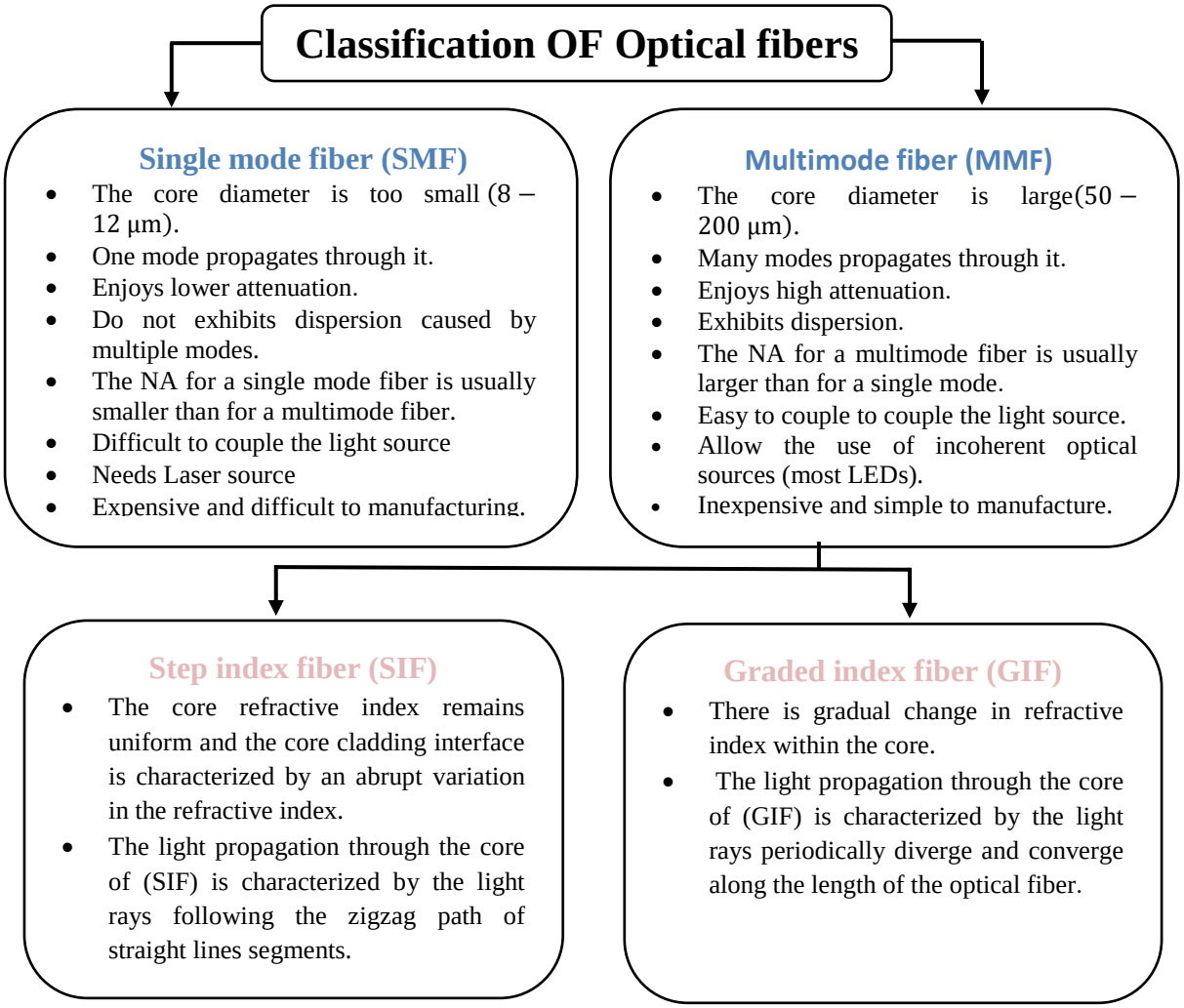

Fig. (1-3): The block diagram of classification of optical fiber [26].

1.2. 2Propagation of Light within an Optical Fiber

When the light gets in one end of a fiber at a certain angle to its axis, it travels a zigzag path through a number of total internal reflections (TIR) at the interface of core- clad and propagates to the other end of the fiber. TIR phenomenon occurs when light travels in a medium of "refractive index" n_c, strikes the boundary of a second, relatively lower "refractive index", medium, n_{cl}, at an angle, measured with respect to normal, greater than the critical angle" [26], defined as:

$$\theta_c = \sin^{-1}\frac{n_{cl}}{n_c} \dots\dots\dots (1-1)$$

The refraction phenomena in fibers follow the well-known Snell's law:

$$\mathbf{n_2 \sin \theta_{in} = n_c \sin \theta_1} \ldots\ldots\ldots (\mathbf{1-2})$$

Where θ_{in},θ_1 are the incident and refraction angle and n_2,n_c are the index of refraction of launch region and core respectively. It is seen from the Fig. (1.4) that the internal incidence angle and refraction angle are related by the expression $\theta_1 = (90 - \theta_c)$, so that, Snell's law becomes $n_2 \sin \theta_{in} = n_c \cos \theta_c$.

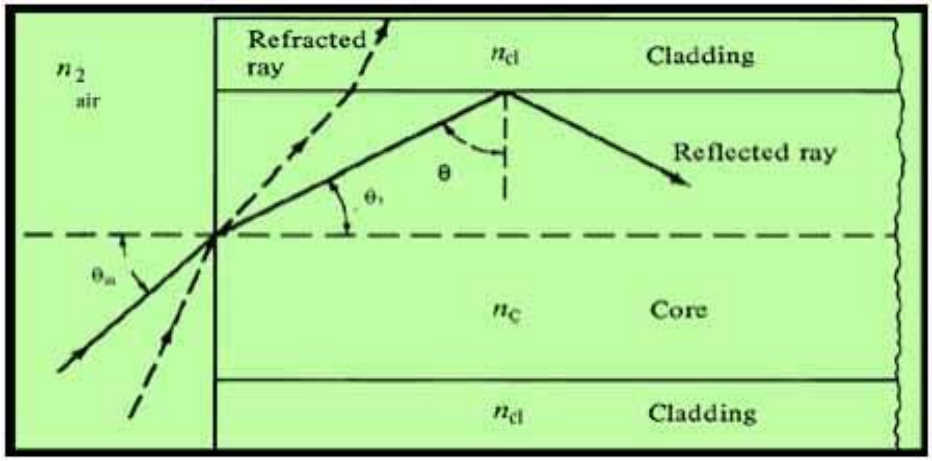

Fig. (1-4) Propagation of light through an optical fiber [12].

As long as the light gets in the fiber at an incident angle so that the internal reflection angle θ isn't less than the critical angle θ_c , the light will be included within fiber and will travel to the far end by a series of reflections. Thus by using the expression for critical angle , the maximum value of incidence angle for which light will travel through the fiber is given by:

$$\mathbf{\theta_{in}(max) = \sin^{-1}\left[\left(n_c^2 - n_{cl}^2\right)^{1/2}/n_2\right]} \ldots\ldots\ldots (\mathbf{1-3})$$

This maximum angle is called the acceptance angle. The maximum sine of acceptance angle is used as the merit figure of the fiber and is called numerical aperture (NA) [27]:

$$\mathbf{NA = \sin\theta_{in}(max) = \left[\left(n_c^2 - n_{cl}^2\right)^{1/2}/n_2\right] \ldots\ldots\ldots (1-4)}$$

If the light is launched from air, $n_2 = 1$ the numerical aperture NA becomes [28]:

$$\mathbf{NA = \left(n_c^2 - n_{cl}^2\right)^{1/2} \ldots\ldots\ldots (1-5)}$$

1.٣ Photonic Crystal (PC):-

The term crystal is meaning an organized arrangement of atoms (or molecules). The crystal lattice will be formed if the atoms (or molecules) are repeated spatially in a small basic structure. In semiconductor materials there is a bandgap between the valence and conduction bands, and the electrons are occupy a specific energy level if have a certain bandgap. Thus, if the material have dielectric steady changes periodically in space, the material is called as a Photonic Crystal (PC) [29].

The common method for guiding light along a defining path in space is to use Total Internal Reflection (TIR), at which light transferring in a higher index core will be reflected efficiently100% at the border with a lower index cladding. This main principle underlies the working of planar waveguide devices and almost all fiber optic in use today[30] .

Recently, there is a promising and alternative model for controlling the flow of light. Photons can be used as very good information transporter. The features of photons lie in high information transport speed and the great information capacity. To obtain very high speed information treatment and optical computing based on photonic appliances is one of the goals of integrated photonic technology. Suitable photonic materials are the fundamental basis for the achievement of photonic devices. PCs are types

of materials that can control the propagation cases of photons. The propagation cases of photons can be designed by use of PC in much the same method as controlling of electrons by semiconductor materials. PCs are materials made of two (or even more) types of dielectric materials placed periodically in space[30, 31].

The Photonic Crystal (PC) dielectric distribution differs periodically in space, which gives a “periodic potential” for light waves entering in the PC. In the interfaces of different dielectric components, the light waves encounter great coherent scattering. Due to the strong modulation of the light wave by the spatially frequent distribution of dielectric constant, the PBGs arise in the dispersion relationship curves of PC. The incident waves whose frequencies fall in the PBG can't transfer in the PC. The propagation states of light waves can be designed at will by use of PCs due to their special PBG effect[31].

When a constructing defect is inserted in a perfect PC, defect cases will appear in the PBG .Light waves with a specific resonant frequency will be confined strongly around the defect structure location. The defect cases can possess high transmittance with perfect designed defect constructing. An incident wave could transfer through the PC based on the photon tunneling influence, when it's frequency resonant with that of the defect mode. The job of PCs in the photonic technology is similar semiconductor (SC) materials in the microelectronic technology. Several novel integrated photonic appliances can be achieved based on PCs [31].

1.3. 1Configuration of Photonic Crystals:-

The dielectric function distribution has a spatial periodicity. PC can be organized (asto various spatial periodicities of dielectric materials) into

one-dimensional (1D) PC, two-dimensional(2D) PC, and three-dimensional (3D) PC, examples are shown in Fig. (1.5) [29, 31,32] .

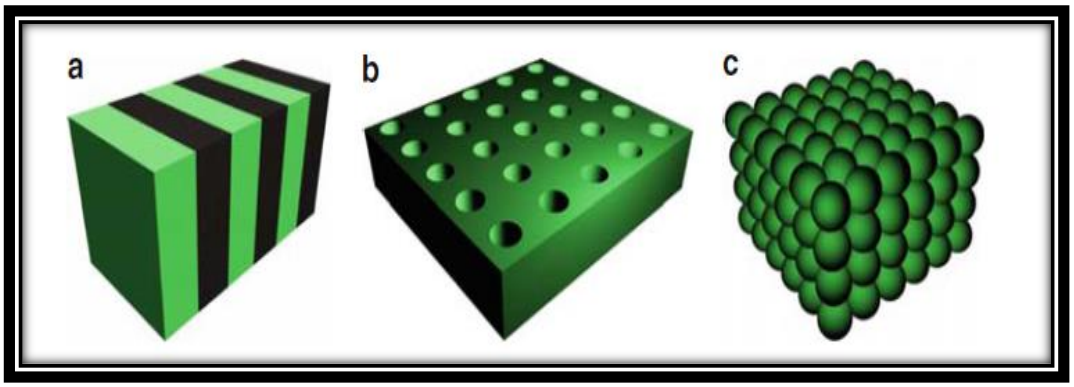

Fig. (1.5) Examples of (a) one-dimensional, (b)two-dimensional, and (c) three-dimensional photonic crystals [32]

In One-Dimensional Photonic crystal (1D-PC), the refractive index change only along one direction.1D-PCs can be constructed by placing a dielectric layer alternatively with a high refractive index and another dielectric layer with a low refractive index. PC can be given the Bragg grating with periodicity in z direction, and it is shown in Fig. (1.6) , the material is periodic in z-direction[29, 31,32].

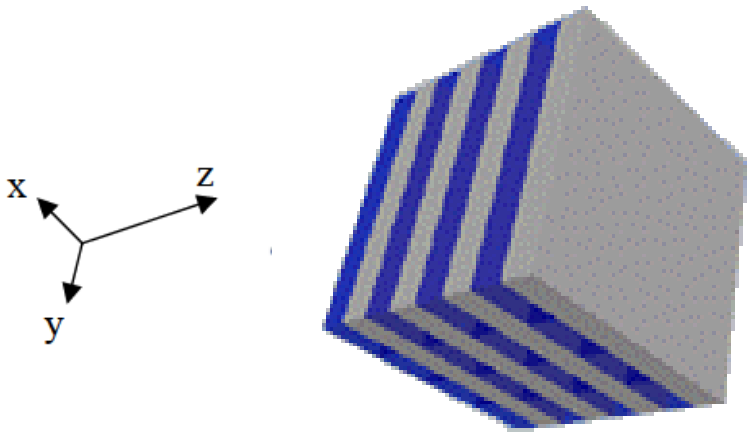

Fig. (1.6) One-dimensional photonic crystal structure[29]

Two-Dimensional Photonic crystal (2D-PC) structure (which is the topic of interest for PCFs) have the dielectric periodicity in two directions, such as in *X* and *Y* axle directions. 2D-PCs have two kinds of arrangement:

the air-hole-type and the dielectric-rod-type PC[29, 31,32]. The schematic structure of a 2D-PC is shown in Fig. (1.7) [33].

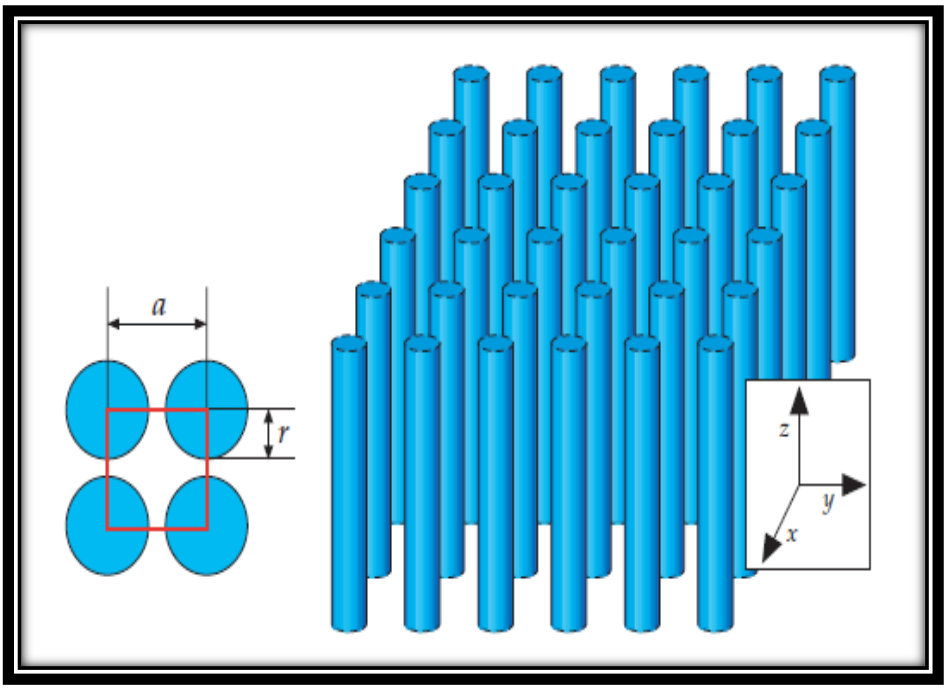

Fig. (1.7) photonic crystal structure of Two-dimensional [33]

Photonic Crystals of three-Dimensional (3D-PCs) have dielectric periodicity in the three directions, i.e., the *X*, *Y*, and *Z* axle directions. So, the PC has a number of possible configurations much larger than in case of 1D or2D PC. Figure (1.8) shows an example of a 3D-PC.

The most 3D-PC known naturally formed is worthy stone opal. This stone plays different colors when turned around. These features caused by the opal microstructure. The optical properties of PCs can be determined by the presence of the periodic modulation of the permittivity or the refractive index of the medium[29, 31,32].

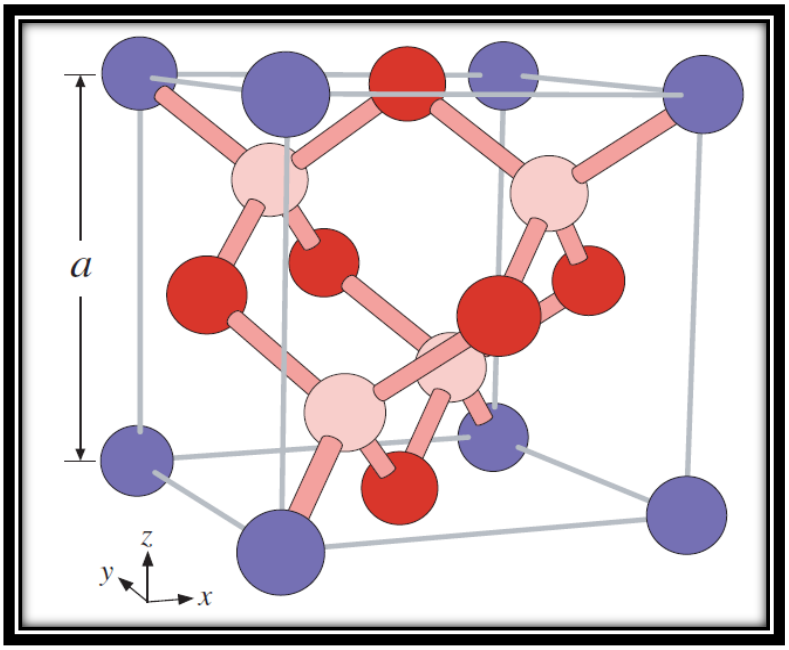

Fig. (1.8) Three-dimensional photonic crystal structure[21]

1.4 Photonic Crystal Fibers (PCFs)

Photonic Crystal Fibers (PCFs) are fibers made of capillaries with an internal periodic structure, filled with air, designed in a hexagonal form lattice. Light can transfer through the PCF in defects of its crystal structure.

A defect can be achieved by removing at least one capillaries. In order to develop new optical medium, since the1980s has been attracted by the capacity to made materials on the scale of the wavelength (a fraction of micrometers or less), known as Photonic Crystals PCs. PCFs are a new kind of optical fibers, joining properties of optical fibers and PCs, they have a remarkable highlights features impossible to obtain in conventional fibers [34, 35, 36] **.**

The Photonic Crystals (PCs) have high reflection coefficient, even with a small number of periods. The PC width around the defect can be decreased to a few layers, this means the optical fibers consisting of a core (in scale of micrometer) surrounded by a PC cladding (that only a few times wider than the core). The resulting fiber is called (PCF)[37].

PCF configuration is very flexible, and there are numerous parameters to control: shape of air hole and diameter, type of lattice, and refractive index of the glass[35].

The major geometrical parameters concerned: hole diameter *d*, the hole pitch *Λ*(distance between the center of two consecutive air holes), and the core diameter *ρ* (which is defined for solid core PCF as the diameter of the ring formed by the innermost air holes), used in the realization are shown in Fig. (1.9) [34].

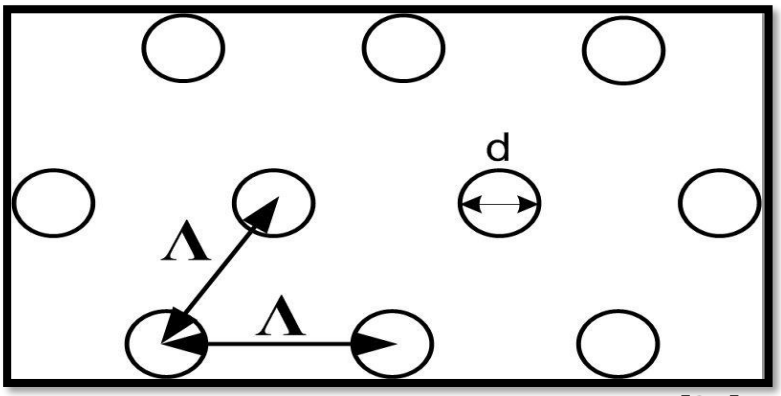

Fig. (1.9) Geometrical parameters describing PCFs[35]

Fig.(1.10) shows some Scanning Electron Microscope (SEM) images of different type PCFs and shows the enormous variety of this technology[38] .

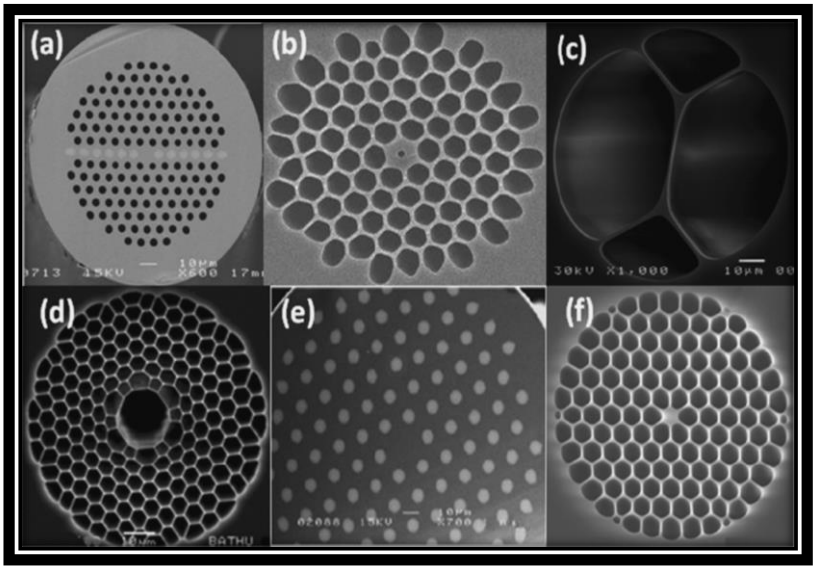

Fig.(1.10) PCF SEM images: (a) hybrid PCF; (b) sub-wavelength air core PCF; (c) PCF for quantum dot applications; (d) hollow-core; (e) all-solid PBGF;

1.4.1Classification and Guidance Mechanisms of PCF:-

Light guidance in the traditional fiber is based on the small refractive index difference between the core and cladding [39, 21], as shown in figure (1.11(a)) . PCFs can be classified in two types in view of their geometry: solid core and hollow-core PCFs, as appeared in Fig.(1.11 (b), (c)) [39] .

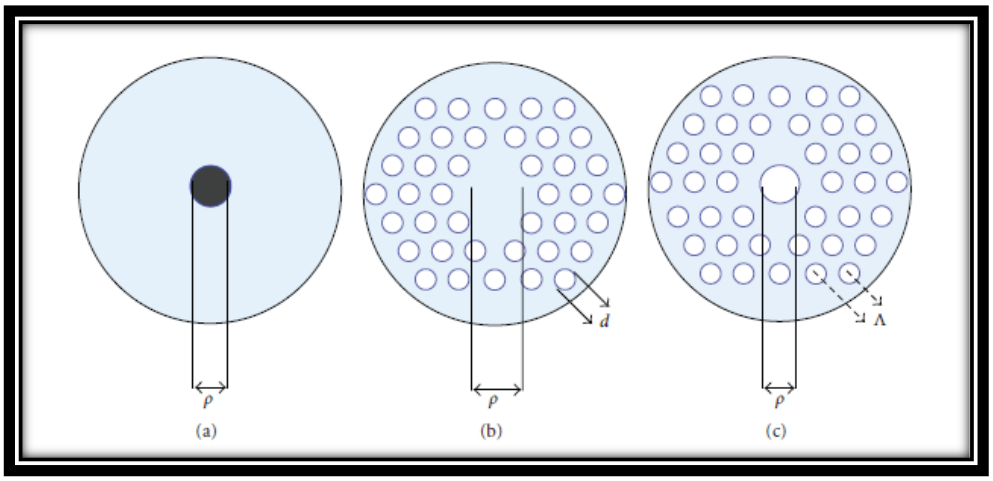

Fig. (1.11) Cross-section drawing of (a) Single-Mode Fiber (SMF), (b) solid core PCF, and (c) hollow-core PCF[39]

Through the fabrication process (depending on the type of fiber to the produced) the physical parameters to be controlled: in an SMF the only the diameter of the core has to consider, while there are three physical parameters in a PCF have to be controlled: the core diameter ρ, the diameter of the air holes d, and the pitch Λ. To enable different guidance mechanisms (such as Modified Total Internal Reflection (M-TIR) and/or Photonic Bandgap Guidance (FBG)) through the PCFs,with different geometry and materials will be used[34, 38] .

The classification of PCFs can be shown in Fig. (1.12) [40, 41] .

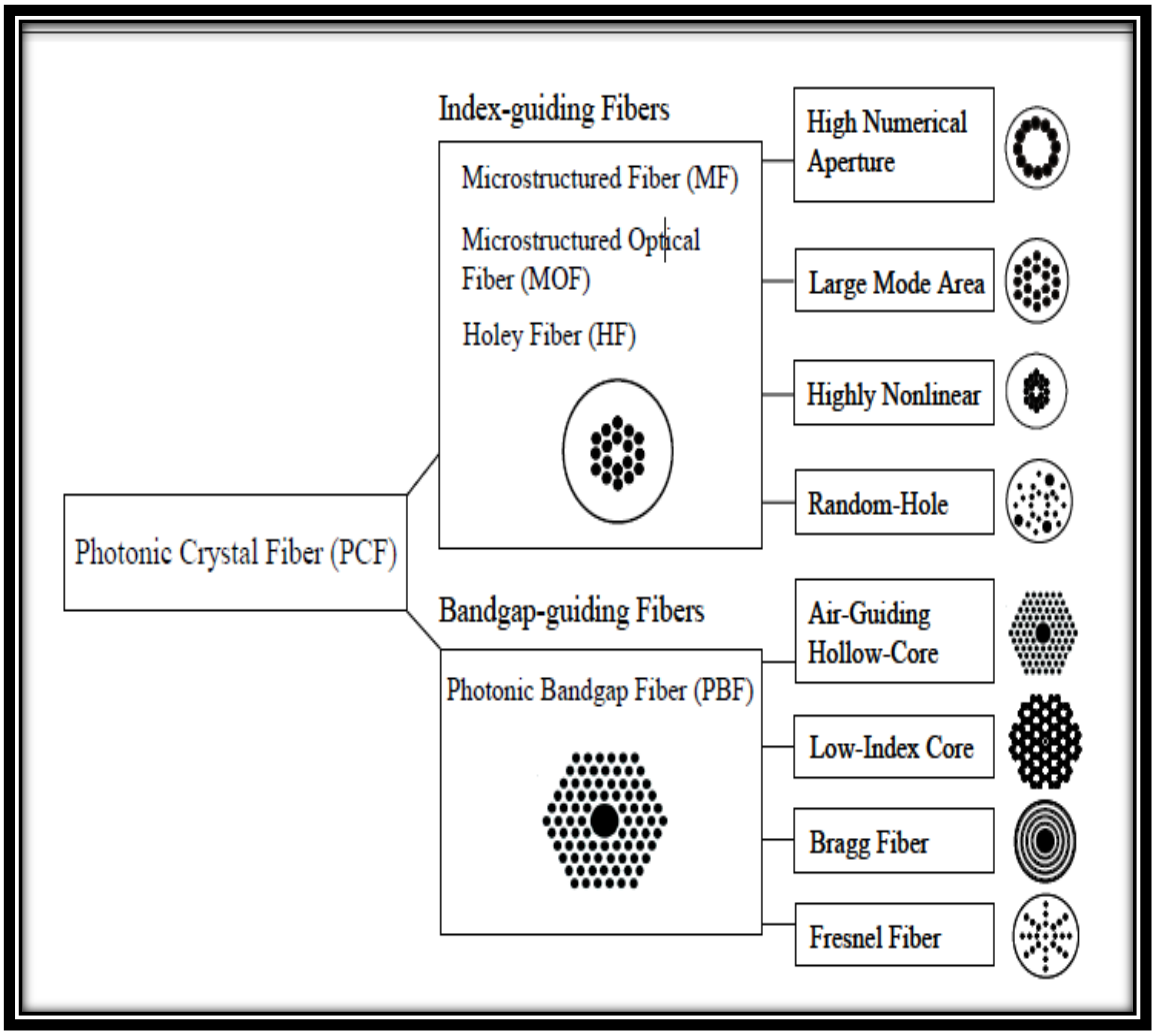

Fig.(1.12) Classification of PCFs[40]

The propagation of light in the PCF is control by structures of the air-hole, these arrays at the center of the PCF cause an index difference in the fiber and a periodical arrangement of holes influences the general optical properties of the PCF [42].If PCFs with a small silica core and large air-holes, high air-filling part in the transverse section, have better nonlinear properties, these kinds can be successfully utilized in super continuum generation. If PCFs fabricated with small air-holes and large hole-to-hole (pich^), in order to obtain a large modal area, this type advantageous for high power delivery [42]. The most important characteristics of PCFs, allowing the solution of a wide class of urgent problems and make PCFs particularly useful for a numerous practical applications, is the ability of these fibers to extremely expand the spectral range of single-mode wave guiding in comparison with

traditional fibers [43].In the case of traditional fibers, the spectral area of single-mode wave guiding is relatively not very vast [44]. As the frequency of optical radiation increases, a single-mode conventional fiber moves toward becoming multimode, while lowering the radiation frequency increases optical losses.

The situation radically changes in the case of PCFs which permit the spectral region of single-mode wave controlling to be significantly expanded [43], this property of PCFs relies upon the fact that the degree of light-filling of air holes in the cladding of PCFs changes as the radiation wavelength variations. Thus, the difference in the refractive indices of the core and the cladding becomes wavelength-dependent. When $d/\Lambda \leq 0.43$, the PCFs can be endlessly single mode, this feature was utilized in index-guiding PCF to perform an endlessly single-mode PCF can be relied upon to give an ultra-wide band of several hundred THz for future optical communication systems with an ultra-large capacity [45].

The development of PCFs opens the entryway for new possibilities in ultra-broadband transmission, high power optical fibers , amplifiers , lasers, optical fiber sensor and so forth.

1.٤.1.1Solid Core (Index-Guiding) PCFs:-

This type of PCF has a solid core. Because the refractive index of the pure silica core which is larger than the average index of the cladding which is made of pure silica and air holes, light is guided in a higher index core (solid core) by modified total internal reflection from a low effective index cladding, similar to conventional fibers. Solid Core (Index-Guiding) PCF represents the simplest kind of PCF[21, 38], its cross-section presents a solid core surrounded by a periodic array of air holes, which are expanded along the fiber length invariantly. The cross sectional configuration leads to a decreasing of the cladding's n_{eff} given that the solid core is fabricate of the same material, when using a single material in the

fiber fabricating. Cross section structure of a solid core PCF is presented in figure (1.13(a)), and its refractive index variety with the radial distance shown in figure (1.13(b)) .The refractive index in the cladding of solid core PCFs will change with the radial distance, according to its geometry and material. The n_{eff} will be lowered when compared with the core's refractive index, leading to the guidance mechanism to be (TIR), without the required to dope the core, leading to the capability to made the solid core PCFs with a single material. In solid core PCFs, the light guiding properties are from the arrangement of the tiny and closely spaced air holes, this guidance mechanism is called as M-TIR[39].

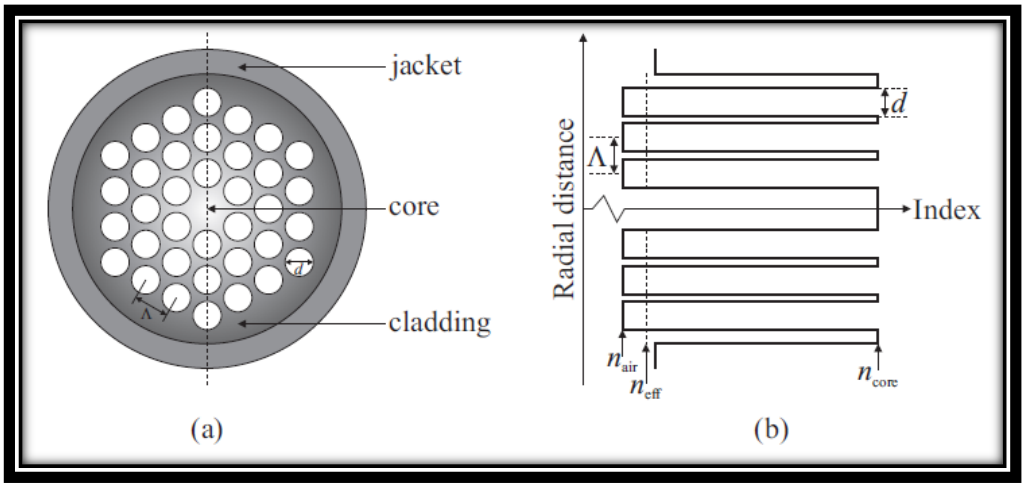

Fig. (1.13) Schematic illustration of (a) the cross-section and (b) the refractive index profile for an index-guiding photonic crystal fiber[21]

Fig. (1.14) shows that the solid core of PCF has embedded in a 2D-PC with a closely spaced array of air holes, traditionally arranged defect in the PC. The solid core has a higher refractive index compared with the cladding, because it has the same material as the PC background. Therefore, the mode index of cladding is lowered by having an array of air holes in it [21, 38].

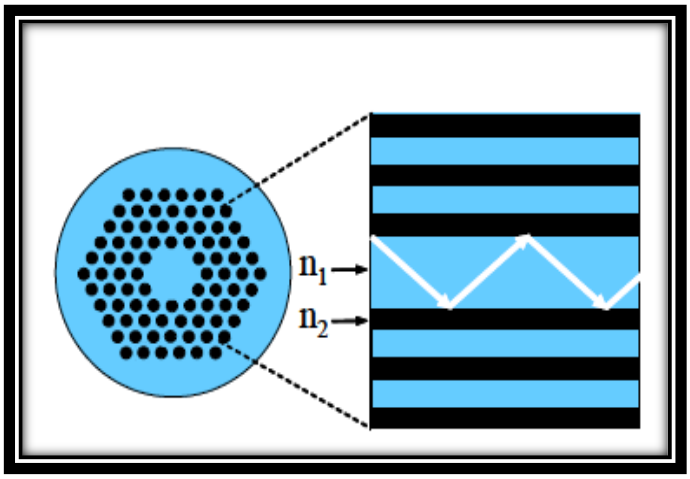

Fig. (1.14) Solid core (Index guidance)PCF ; n_1=1.45(silica) , n_2=1(air)[40]

Cylindrical shape of the cross section and huge length allows PCF to be similar to conventional fiber and it has been used analysis methods from the theory of propagation of optical radiation in dielectric cylindrical waveguides [46].

A conventional single mode fiber consist of core radius(ρ)and core and cladding indices (n_c)and(n_{cl}) respectively, there are propagation constants (β) associated with specific modes in the core which do not propagate in the cladding. It satisfies [46]:

$$kn_{cl}<\beta<kn_{co} \qquad (1.6)$$

Where k=2π/ λ, wave number in the vacuum, and λ is the free-space wavelength. In a standard step-index fiber with core radius ρ and core and cladding indices n_c and n_{cl}, the number of guided modes is determined by the V [46]:

$$V = \frac{2\pi}{\lambda}\sqrt{n_c^2 - n_{cl}^2(\lambda)} \qquad (1.7)$$

Which should be lower than 2.405 for the fiber to be single mode. Consequently single-mode fibers are in actuality multimode for light of sufficiently short wavelength.

Also the fibers have another advantageous feature of is that they can be made endlessly single mode. One mode only should have a propagation constant between the effective propagation constants for the cladding and the core [47].

The limitation corresponds to one solution only to Maxwell's equations propagating in the core and evanescent in the cladding. The effective frequency parameter is given by relation (1.7) [47]

As λ decreases, the n_{cl} increases, due to the more intensity of light will be confined to the silica part of the cladding. *V* can be kept below (2.405) for the extensive variety of wavelengths, and the fiber is said to be endlessly single mode. Even with a very large core, the fiber can be made endlessly single mode [47].

1.4.1.1.1Large Mode Area (LMA):-

The unique characteristic of PCFs is the cross-section geometrical feature. It's possible to fabricate PCFs with large effective area by changing these characteristics, this kind know as Large Mode Area (LMA) PCFs, Ultra-LMA single-mode PCF can be obtained by keeping the small hole size and large pitch in a suitable range [48].

Due to Ultra-LMA, high laser power operation in PCF can have a low energy density in the core. It has no limitation of intensity dependent nonlinear effects, and can bypass material damage in high-power fiber lasers[49, 50]. So, it can be utilized for propagating and generating high power laser. Because of LMA-PCFs ability to be single mode over a wide wavelength range with large mode area , it have a special feature for high quality beam and broadband applications [49] .

1.4.1.2Hollow- Core Photonic Crystal Fiber (HC-PCF):-

Hollow-Core PCFs (HC-PCFs) or (PBG) composed of a hollow core surrounded by air-holes cladding with a periodic arrangement of micro structured in glass as fabricated by removing some fibers around the center, in this case total internal reflection conditions are not fulfilled since the air core has a lesser refractive index than the cladding. Light can propagate along the fiber only with photonic bandgap mechanism, the microstructure periodic cladding results in a PBG that confines light inside the hollow core or in the core that made of material with a refractive index lower than that of the n_{eff} of the cladding. So, light can be guided in a gas-filled core, or even in a solid core. The multiple Bragg reflections causes the bandgap, which leads to light transmission wavelength dependence, as shows in Fig.(1.15) [40, 50].

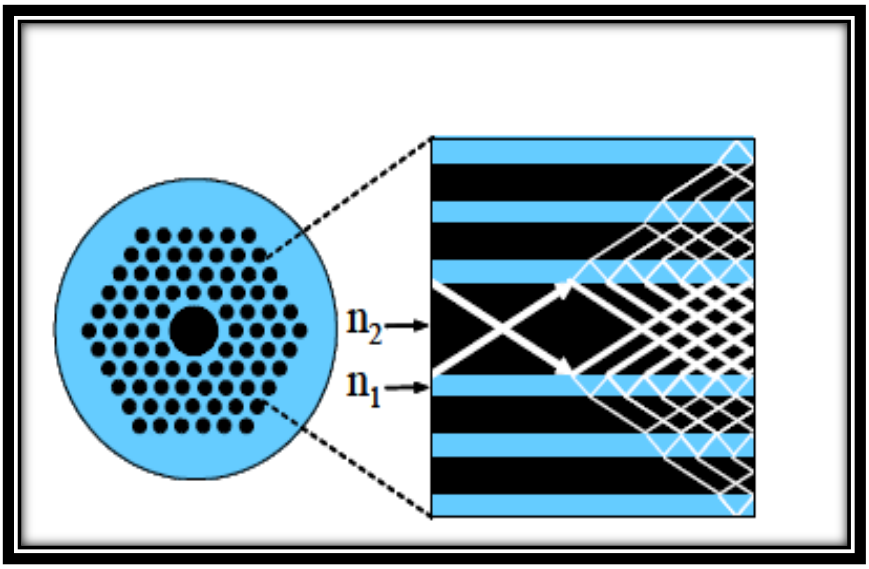

Fig. (1.15) HC- PCF ; n_1=1.45(silica) , n_2=1(air)[40]

Hollow-Core PCF despite supporting multiple optical modes, it presents quasi single-mode operation. Furthermore, usually higher-order modes have scattering losses and much higher confinement compared to the fundamental mode, leading to achieve single-mode output practically at

the desirable wavelength by utilizing fiber with long length or by bending the fiber. Finally, HC-PCFs ease the delivery of light over kilometer length scales with low attenuation. In HC-PCF the losses, as low as 1.2 dB/km, has been gotten by expanding the core from 7 to 19 unit cells to reduce the fundamental core mode overlap with the glass-air surface modes [21] .

1.5 Optical Properties of PCFs:-

Photonic Crystal Fibers (PCFs) undergo important consideration because of their optical properties, such fibers can supply special dispersion properties, higher birefringence and enhanced nonlinearity compared with traditional optical fibers. The PCFs become more attractive for many sensing applications due to the possibility of guiding light in air. The major optical characteristics of PCFs are described below[40].

1.5.1Dispersion:-

The relation of dispersion (in a homogeneous medium) between frequency*(ω)*of the propagating light and wave vector (k) is given through the refractive index of the material(n), can be given from the relation (1.8) [47] *:*

$$\omega = {c|k|}/{n} \dots\dots\dots (1.8)$$

The combined effect of the material dispersion and the band structure arising from the 2D-PC is the PCFs dispersion that determines the dispersion characteristics of the fiber. The interesting parameter for propagation in fibers is the dispersion or the wave vector part along the z-direction(k_z) [47].

k_z is referred to as the propagation constant β in the fiber optics. It is then reasonable to define an effective refractive index n_{eff} as in relation (1.9) [47]:

$$n_{eff} = \frac{\beta c}{\omega_{fund.}} \dots\dots\dots (1.9)$$

Where $\omega_{fund.}$ denotes the frequencies of the lowest lying mode in the fiber.

The higher derivatives of the propagation constant are given as in relation (1.10) [47]:

$$\beta_n(\omega) = \frac{\partial^n \beta}{\partial \omega^n} \dots\dots\dots (1.10)$$

And the second order dispersion, as in relation (1.11) [50]:

$$D = -\frac{2\pi c}{\lambda^2}\beta_2 \dots\dots\dots (1.11)$$

Equation (1.11) is just another way of expressing β_2.The zero-dispersion wavelength (λ_{ZD}) is defined as the free space wavelength (1.12) [47]:

$$\lambda_{ZD} = \frac{2\pi c}{\omega} \dots\dots\dots (1.12)$$

Whereβ_2= 0.

The dispersion can be tuned by a proper choice of the air holes size, the size of the central defect and the distance between the holes (pitch). The zero dispersion wavelength (at a shorter wavelength) is found when the central defect is decreased and the fraction of air filling is increased.

It is possible to fabricate fibers with zero dispersion wavelengths (between500 and 1500 nm). When decreasing either the hole-size or the pitch leads to a higher curvature of the dispersion profile, causing the two closely laying zero dispersion wavelengths.

1.5.2 The Nonlinearity:-

Photonic Crystal Fiber (PCF) fabrication process allows for the manufacturing of fibers with a high air-filling portion and too small core diameter (∼1-2) μm and So, the propagating modes can exhibit very small effective mode areas compared with traditional fibers. Narrow-core PCFs can exhibit high nonlinearities as the magnitude of the nonlinear coefficient is inversely proportional to the mode area. The nonlinearity combined with the PCFs special dispersion properties provides new possibilities in nonlinear optics. So, the PCFs mode area can be wavelength dependent. This can be employ in the fulfillment of wavelength dependent nonlinear effects [40].

1.٥.3. The Losses:-

For any optical fiber technology the most important factor is loss. The most common reasons of loss in conventional optical fiber were due to material absorption and Rayleigh scattering [52]. The minimum loss in fused silica is slightly less than 0.2 dB/km at ($\lambda = 1550\text{nm}$). In PCFs, loss mechanisms are described in details in the following**[**36**] :**

a-Confinement Losses:-

Confinement losses (or leakage) are contributed in the losses in both solid-core and hollow-core PCFs. Because of the limited number of air-holes which can be made in the fiber cross section. In this way, all the PCF

guided modes are leaky .Many analyses can be performed recently, in order to determine the guidelines for designing both solid-core PCFs and PBG-based fibers with insignificant losses of the leakage. It has been shown a strong dependence of the confinement losses on the air-hole rings number, particularly for fibers with high air-filling fraction. By increasing the ring number , the leakage losses can be reduced[36]**.**

b-Bending Losses:-

PCF at long wavelength exhibit a bend loss edge because of the way that the modes extends further into cladding, causes more weakly guided mode that will suffer more disruption in response to bending. PCF at short wavelength also possess an additional bend loss edge as a direct consequence of their novel cladding structure. Fig. (1.16) describes a guided mode propagating in the z direction around a bend in the x plane that has a radius of curvature R_0 [53].

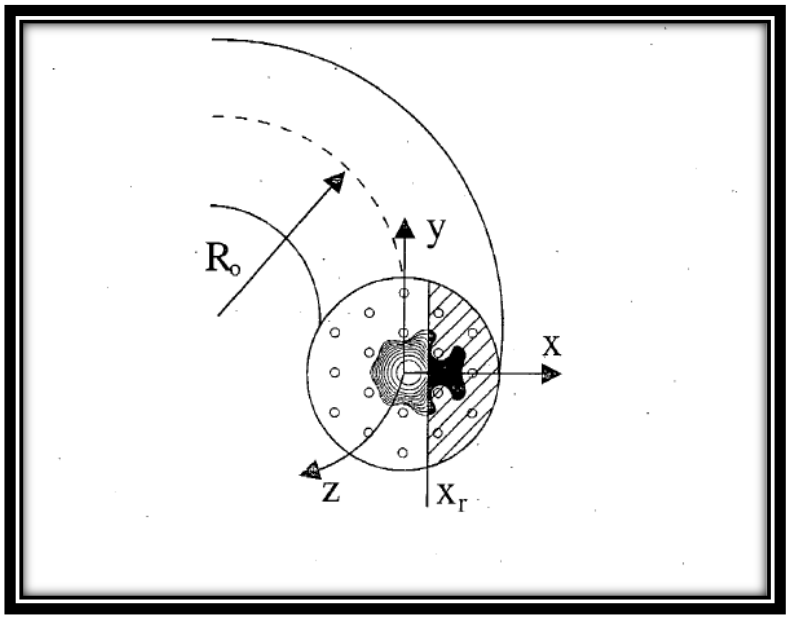

Fig (1.16): Schematic of the bending of the PCF

1.6 Photonic Crystal Fiber Interferometer (PCFI):-

There are a different kinds of fiber interferometers used for sensing, such as a Michelson interferometer [54], Fabry-Perot interferometer [55], micro-ring interferometer [56],modal interferometer [57],and Sagnac interferometer configurations [22].

The use of fiber optic technology provides some advantages like mechanical stability, compactness, and absence of moving parts for the construction of interferometers.

The two common ways to build of a fiber optic interferometer are: two-arm interferometer and modal interferometer in Mach-Zehnder interferometer (MZI). In two-arm interferometer, the first coupler splits the input signal into reference arm and sensing arm, Another fiber coupler is used to recombine the signal as shown in Fig. (1.17). The recombined light has the interference component according to the optical path difference between the two arms, the two-arm interferometer includes splitting and recombining two optical beams that propagate indifferent fibers, which needs several meters of optical fiber and one or two couplers [58].

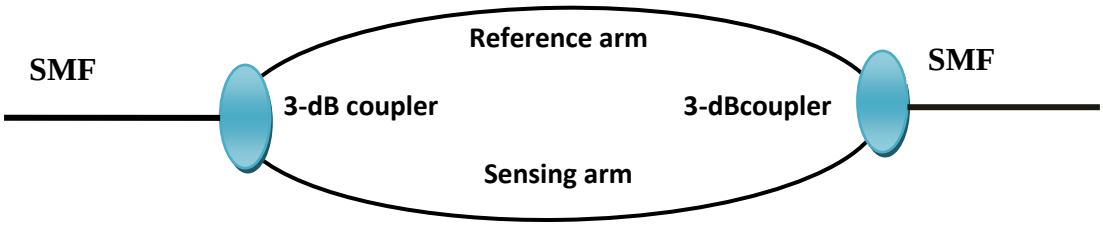

Fig. (1.17): the schematic of an MZI. Two couplers are used to split and recombine the signals[39]

The modal interferometer take advantage of the relative phase shifting between two modes of the similar fiber. When the modal interferometers compared to their two-arm peers, found that its sensibility

to environmental fluctuations is lowered because the modes propagate in the same fiber.

Photonic crystal fiber (PCF) has unique properties offer many interesting possibilities for the build of fiber interferometers, and as a result have attracted much interest from the optical fiber sensor community. The PCF design based interferometers is interesting for their high sensitivity and wide range of utilizations[58].

Some photonic crystal fiber (PCF) based modal interferometers contain PCFs in a fiber loop mirror, interferometers structure with tapered PCFs, interferometer based on long period gratings, and interferometers manufactured via micro-hole collapse [58].

A latter technique involves cleaving and splicing only. The different configurations are a PCF with two collapsed regions separated by a few centimeters, a short PCF section sandwiched longitudinally between standard SMFs by fusion splicing (transmission type) [59], and a stub of PCF with cleaved end fusion spliced to SMF (reflection type) [60] .

The feature of the last two configurations is that the PCF modal properties are exploited but the interrogation is carried out with SMF, which leading to more cost-effective interferometers. The two configurations shown in Figs.(1.17)and (1.18) [58].

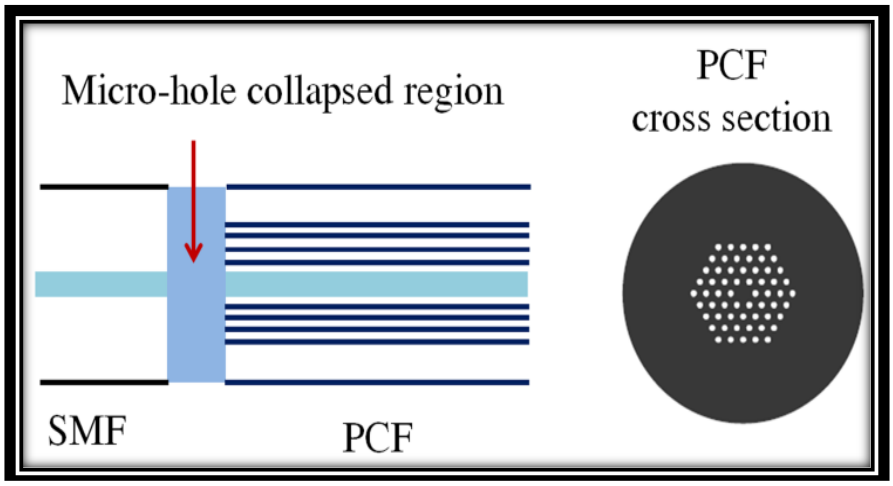

Fig (1.1^): Reflection type PCF interferometer [58]

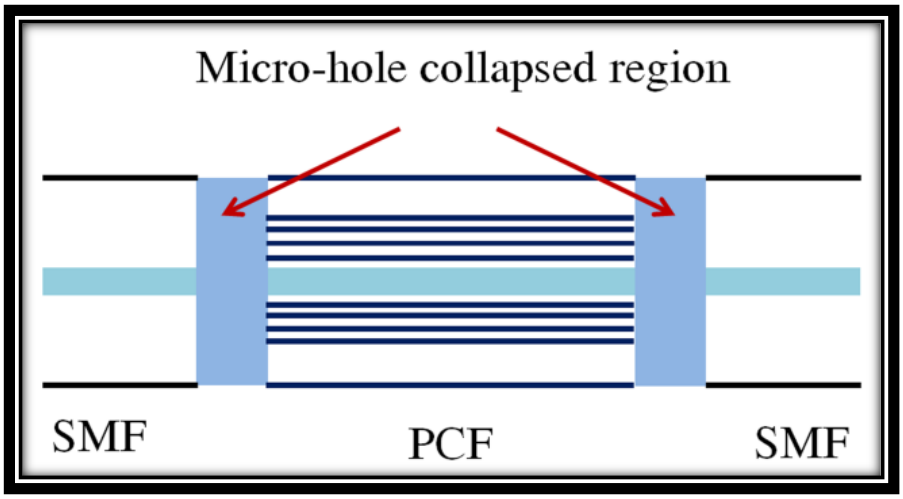

Fig (1.18): Transmission type interferometer PCFI[58]

The interferometers fabricated through microholes collapsing show actually sinusoidal and stabilized interference spectra which are observed over a broad wavelength range (~800 nm).The period or fringe spacing (Δλ) of the interferometer is calculated approximately as[60].

$$\Delta\lambda = \frac{\lambda^2}{\Delta nL} \quad (1.13)$$

Where Δn is the effective refractive index deference between the modes contributing in the interference, L is the PCF length .

The fringe spacing or period in these interferometers can be controlled easily with the between the two splices.

As the reflection type PCFI where the light is passing through the PCF twice the period or fringe spacing in these interferometers as in relation (1.14) [58] :

$$\Delta\lambda = \frac{\lambda^2}{2\Delta nL} \quad (1.14)$$

Collapsing techniques have some important properties that are significant for optical sensing,. In interferometers which built via collapsing, the excitation and recombination of modes are achieved with stable splices. These don't degrade after some time or with temperature, thus, interferometers with high stability are achievable [60].

All these structures can supply humidity information by either measurements of spectral, or measurements of intensity/power variations of the transmitted/reflected light. The sensors based on PCFI demonstrated have a fast response compared to other mechanical/electronic humidity sensors and can be used as a breath monitor for example in medical applications and in many other chemical, biological and industrial applications[58].

1.7 Humidity sensing

The term moisture refers to water in liquid form that is suspended in air or gas in form of small droplets. The term humidity means the concentration of water vapor in the air, where the water is in a vaporous phase. Humidity is a physical amount that has significant importance in a various areas extending from life sciences [61,62] to building automation [63]. Subsequently humidity control, sensing and monitoring are important in a various areas. Fast humidity sensors are required for the diagnosis of pulmonary diseases [64] and for mapping the human respiratory framework [65] by monitoring the water vapor substance of exhaled breath. For meteorological applications. Humidity measurements play an ever increasing role in various industries such as semiconductor, bio-medical, agricultural, food processing, automotive and meteorological industries as illustrated in Fig.(1.19). These measurements are important to allow improvements in the quality of products and reduction of costs. Humidity measurements can be expressed in a different of terms and units. The three

normally utilized terms are absolute humidity, dew/frost point and relative humidity (RH). Absolute humidity is the ratio of the mass of water vapor to the volume of air or gas in which the water vapor resides. It is commonly expressed in grams per cubic meter. Dew point is the temperature (above $0^{O}C$) at which the water vapor in a gas condenses to form liquid water. Frost point is the temperature (below $0^{O}C$) at which the vapor condenses to ice. Dew/Frost point is expressed in °C or °F and is a function of the pressure of the gas but is independent of temperature, therefore it provides a better absolute measurement of water vapor content. The percentage ratio of water vapor show in air at a particular temperature and pressure to the maximum amount of water vapor the air can hold at that temperature and pressure is called relative humidity (RH). It is often expressed as a percentage using the following expression,

$$RH = \frac{P_w}{P_{ws}} \times 100\% \dots\dots\dots (1.15)$$

Where P_w is the partial pressure of the water vapor and P_{ws} is the saturation water vapor pressure. RH is a relative measurement because it is a function of temperature.

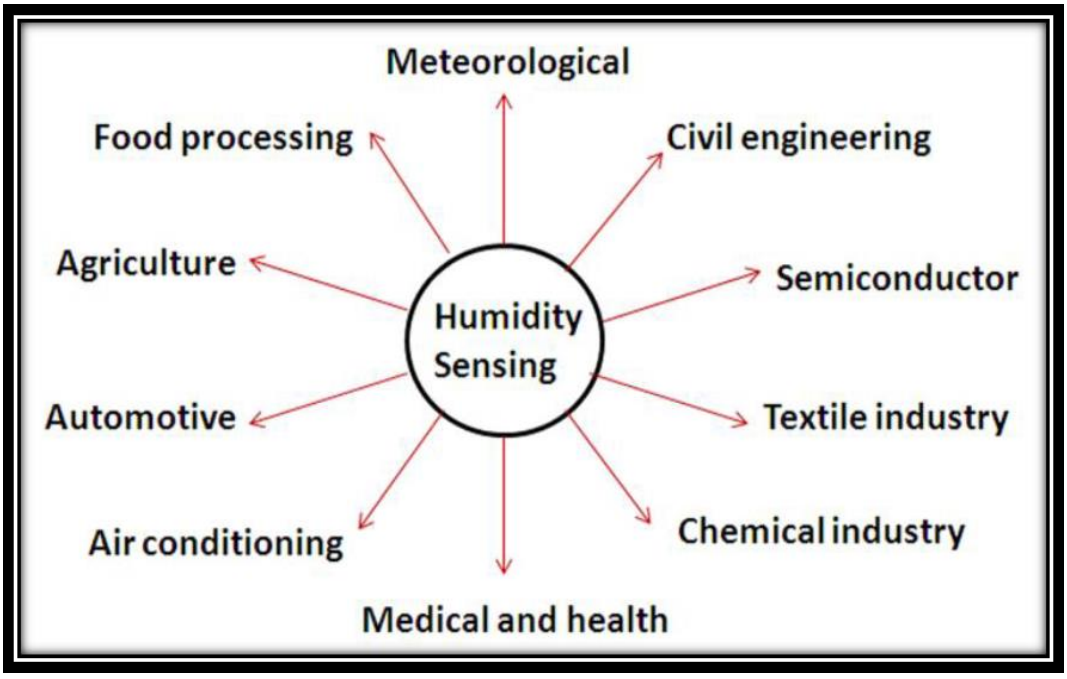

Fig. 1.19 Examples of applications of humidity sensors in different areas.

The most important parameters of a humidity sensor are its precision, repeatability, ability to recover from condensation, resistance to chemical and physical contaminants، size, cost effectiveness, operating RH range, temperature dependence and response time. Given the wide range of industrial humidity measurement sensors available it is clear that no single measurement technique is suitable for all applications.[66]

1.7.1 Fiber optic humidity sensor

Optical fiber humidity sensors supply specific features by comparison to their traditional electronic counterparts. They are :

1- Immune to electro-magnetic interference and radio frequency interference.
2- Remote operation possible.
3- No explosion risk in volatile atmospheres.
4- Response time is fast.
5- Minimized size and weight.
6- Great corrosion protection.
7- High precision conceivable.

There is broad range of optical fiber humidity sensors, and they divided by the technique used for sensing into: direct spectroscopic, in-fiber grating , evanescent wave, and interferometric types. To avoid the limitation of using the conventional optical fiber for humidity sensing, can using PCFI where infiltrated and coated a small region of the PCFI with hygroscopic material which provide a good RH sensitivity and fast response time. [67].

1.7.1.1Operating Principle of The RH Sensor Based on PCFI:-

Photonic crystal fiber (PCF) is used for the PCFI fabrication, its surface (silica) is hydrophilic and therefore when it is presented to moist air, the water vapor adsorption on the surface exists[58].

Two kinds of water-vapor adsorption mechanisms happen in sequence at the SiO_2-airinterface. The water vapor chemisorption first modifies the SiO_2 surface, leading to a surface with silanol groups(Si-OH). Physisorption is the second type of adsorption, exists on these silanol groups. A schematic shows the adsorption of water-vapor is given in Fig. (1.20) [58].

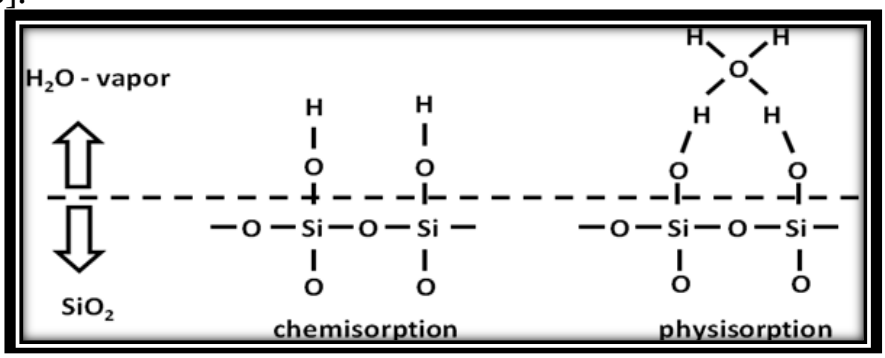

Fig.(1.20): Water vapor adsorption mechanisms on an SiO_2 surface[58]

The physisorption at room temperature is a reversible function of the surrounding air relative humidity, while the chemisorption appears to be irreversible. So, only the physisorption process is considered. The adsorbed water amount measured as a function of the partial vapor pressure (at a constant temperature). It appeared that adsorption isotherm can be described very well by the BET (Brunauer-Emmett- Teller) adsorption theory [58].

David and **Seong** specified the configuration of water molecular adsorbed on a hydrophilic SiO_2 surface at room temperature as a function of RH using Attenuated Total Reflection (ATR)- Infrared Spectroscopy.

The water hydrogen-bonded ice like network grows up as the RH increases from 0% to 30%. In the RH from 30% to 60%,the fluid water design shows up, while the structure of ice-like carries on increasing to saturation. Above 60% RH, the structure of the liquid water develops over the ice like layer. This structural evolution shows that the outer layer of the adsorbed water molecules suffers transitions in equilibrium behavior as

humidity varies. Also it was shown that the adsorbed layer thickness (at room temperature) starts increasing exponentially above 60% RH [58].

For an interferometric type fiber optic RH sensor, the sensing mechanism relies on the perturbation of the light signal phase properties that propagating in the optical fiber introduced by the humidity change. The phase change detection is realized by mixing the signal of interest with a reference signal, then converting the phase difference into wavelength shift or an optical intensity change [58].

In photonic crystal fiber interferometer (PCFI),the excitation and recombination of modes can be achieved by the hole collapsed region of the PCF. The fundamental single mode fiber (SMF) mode starts to diffract when it gets in the collapsed area of the PCF. As result of diffraction, the mode broadens; depending on the modal characteristics of the PCF and the nature of the hole collapsed section, the power in the input beam can be coupled to the fundamental core mode and to higher order core modes, or to cladding modes of the PCF[55].The modes propagate through the PCF at various phase velocities, in a specific length of PCF the modes accumulate a differential phase shift. The phase velocities and phase difference are wavelength dependent; [55].

At the end of the PCF, the modes reach another solid glass section, i.e., the other collapsed end of the PCF (transmission type) ,also in (reflection type) the modes propagate through the PCF till they reach the cleaved end from where they are reflected and reenter the collapsed region, the modes will further diffract, and because the mode field of the SMF is smaller, the core acts as a spatial filter and picks up only a part of the resultant intensity distribution of the interference pattern in the PCF. Therefore, the optical power reflected or transmitted by the device will be maximum at certain wavelengths and minimum at others.

The adsorption of water vapor changes the n_{eff} of the interfering cladding mode propagating in the PCF[58].The adsorption/physisorption is a reversible process, therefore a modulation of the n_{eff} occurs with respect to the ambient humidity values which accordingly prompt change the position of the wavelength shift. The rise in humidity causes the PCFI wavelength shift toward longer wavelengths, and the value of this wavelength peak shift is exponential with respect to RH. This wavelength peak shift is due to the adsorption and desorption of H_2O molecules along the holes surface within the PCF (at the interface between air and silica glass).The adsorption on the PCF end face causes a shift in the overall power level of the interference pattern [58].

In order to provide a good RH sensitivity to the device, it have infiltrated and coated a small region of the PCFI with hygroscopic material. A microscopic image of the PCFI and a schematic of the excitation and recombination of modes in the PCFI reflection and transmission types are shown in the inset of Figs. (1.21)and (1.22) respectively.

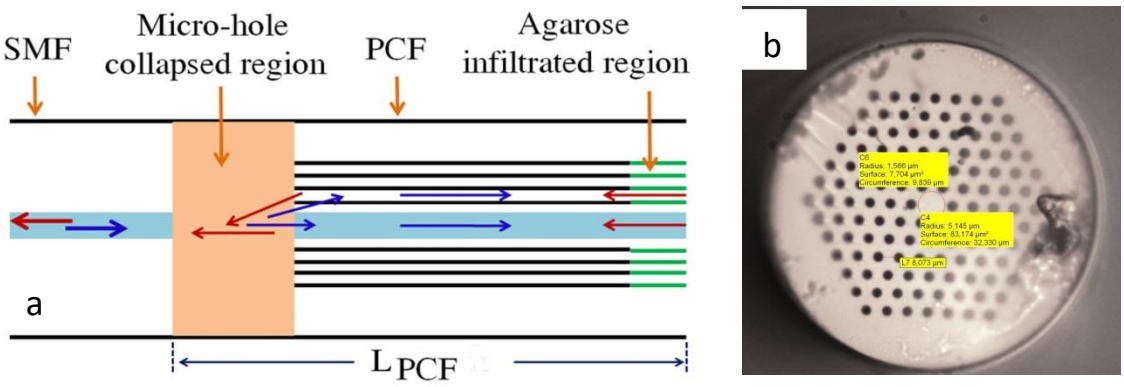

Fig.(1.21)a) drawing of the reflection type PCF interferometer and b)a diagram of the cross section of the PCF employed.

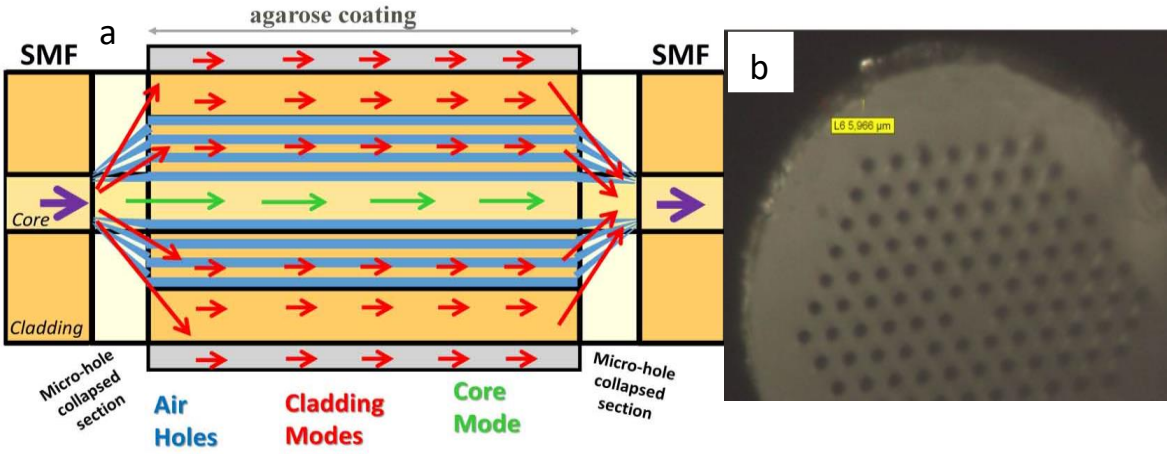

Fig.(1.22)a) drawing of the transmission type PCF interferometer and b) a diagram of the cross section of the PCF employed.

The effective RI of the cladding mode depends on the RI of the hygroscopic material. The hygroscopic material which used in this research is agarose.

Agarose is an unbranched polysaccharide acquired from the cell walls of some species of red algae or seaweed. Chemically, Agarose is a polymer made up of subunits of the sugar galactose with Molecular Formula ($C_{24}H_{38}O_{19}$)[68]. Agarose has an added advantage of low material degradation compared with the materials used in. Since Agarose is soluble in hot water, it polymerizes to form hydrogel when it cools down and reaches room temperature ,Agarose solutions exhibit hysteresis in the liquid-to-gel transition - that is, their gel point is not the same as their melting temperature(90-95)°C[68]. the preparation coating, infiltration and procedures are simple. Agarose also has a good adhesion to silica and easily forms a thin coating film on silica fiber[69]. All these factors make it a suitable choice as a coating or infiltration for the fiber optic humidity sensor considered here.

The RI of the agarose increases with an increase in the ambient RH, which in turn changes the modal propagation constant of the cladding mode[70]. As a result, a phase change is induced between the interfering

core and cladding modes, which in turn causes the shift of the interference pattern.

The development of PCFIs by coating or infiltrating microholes of PCF lead to improve sensitivity and fast in response time which opens the entryway for new applications and possibilities , breathing sensor is the one application based on PCFI as shown in Fig. (1.23).

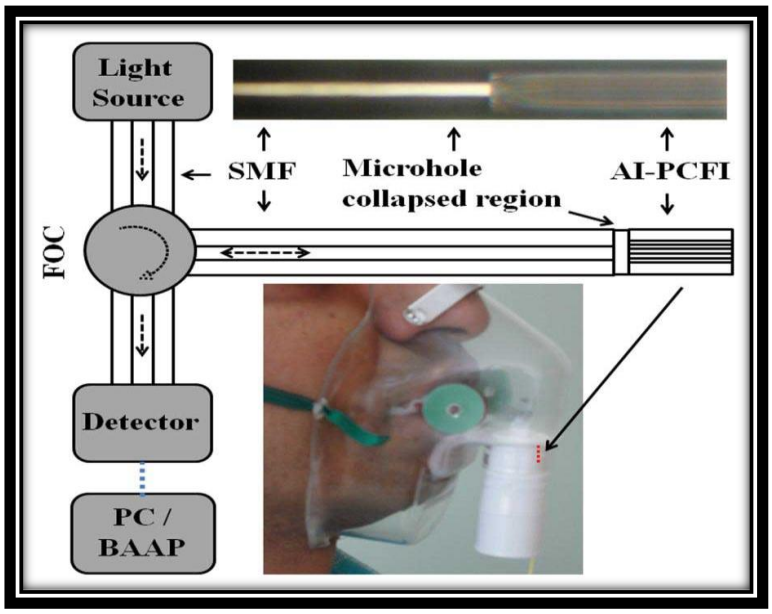

Fig.(1.23)Schematic diagram of a fiber optic breath sensor system, (upper) microscope image of an AI-PCFI and (lower) a photograph of the mask placed on the volunteer's face showing the position of the sensor inside the mask (dotted line). FOC- Fiber optic circulator, SMF-Single mode fiber, AI-PCFI-Agarose infiltrated-photonic crystal fiber interferometer, PC/BAAP-Personal computer/Breath analysis application program[58]

1.٧.١.2 Evanescent wave sensing method based RH sensors

The sensing method of evanescent wave (EW) based humidity sensors allows the optical fiber to be utilized as an intrinsic sensor where the EW field generated at the fiber interface interacts with the humidity sensing material surrounding the fiber which in turn allows for the detection of the attenuation/insertion loss [71,72] or the resonant wavelength shift of the fiber structure due to the change in refractive index, optical absorption, or scattering of the sensing material with respect to the ambient RH[73,74].

An evanescent wave is created whenever light undergoes TIR at the core cladding interface. The evanescent wave penetrating a small distance into the cladding of optical fiber. Fig. (1.24) is shown the evanescent wave which decays exponentially from the interface of core and clad and travelling parallel to it.

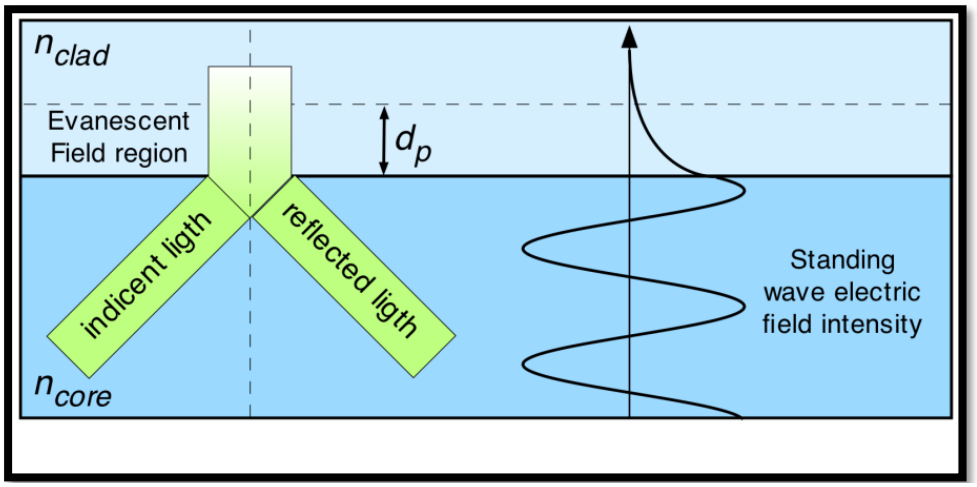

Fig. (1-24) Evanescent wave in the optical fiber cladding[72].

Design of evanescent field absorption based sensor devices requires a knowledge about certain parameters. These design parameters play a crucial role in determining the sensitivity, dynamic range etc. of optical fiber sensors such as the penetration depth d_p of the evanescent field [75].

This is defined as the perpendicular distance from the interface of core and clad at which the electric field amplitude has become $1/e$ of its value at the waveguide interface. If I_0 represents the intensity at the interface ($z = 0$), after a distance d_p , it decay exponentially with perpendicular distance z from the surface and is given by the equation:

$$\mathbf{I_Z = I_0 e^{(-z/d_p)}} \dots\dots\dots (\mathbf{1-16})$$

The magnitude of the penetration depth is:

$$\mathbf{dp} = \frac{\boldsymbol{\lambda}}{\mathbf{2\pi n_c}\left[\mathbf{\sin^2\theta - \frac{n_{cl}^2}{n_c^2}}\right]^{1/2}} \dots\dots\dots (\mathbf{1-17})$$

where(λ) is the wavelength of the transmitted light, θ is internal incident ray angle with the normal to the core-cladding interface and $n_c$and $n_{cl}$are the refractive index of the core and clad of the optical fiber respectively [75].Equation (1-17) shows that the penetration depth is larger with closer index matching (i.e. as$n_{cl}/n_c \rightarrow 1$) and increases with increasing wavelength.

1.^ Literature Survey:-

Photonic Crystal Fiber (PCF) sensors have played an important role in both fundamental and applied researches.

Many research groups have investigated different schemes in RH sensing field which exploit the properties or structures of PCFs with a view to developing new optical sensors, the most significant published work which related to the RH sensors is resumed in the table (1.1).

This table is focused on work submitted between 2007 to 2017, and presented a different RH optical fiber based sensing schemes with different type, extrinsic and intrinsic.

Table (1-1)*:*Summary of the published works in RH sensor

Year	Title of paper	Author	Sensing material and Sensing mechanism	Sensitivity and Response time	Ref.
2007	A Comparative Study of Fiber Optic Humidity Sensors Based on Chitosan and Agarose	Jinesh Mathew et al.	fiber preparation and deposition of the Agarose/ Chitosan film _ changes in refractive index and modulates the intensity of light propagating through a fiber due to swell of the film	For Chitosan Sensitivity 0.001 dB/RH _ response time 2sec for Agarose Sensitivity 0.001 dB/RH _ response time 3sec	[76]
2009	Sensitivity Improvement of a Humidity Sensor Based on Silica Nanospheres on a Long-Period Fiber Grating	Diana Viegas et al.	Coated long-period fiber grating with a SiO_2-nanospheres film _ blue shift in the peak of resonant wavelength	In the relative humidity level of 70% , sensitivity is≈ 0.13 nm/%*RH* for the PAH/SM30 coating and ≈ 0.48 nm/%*RH* for PDDA/PolyR + PAH/SM30 structures _ Response time in range of 100–200 ms	[77]

Year	Title of paper	Author	Sensing material and Sensing mechanism	Sensitivity and Response time	Ref.
2009	Optical fiber humidity sensor based on lossy mode resonances	M. Hernaez et al.	Indium Tin Oxide coating onto an optical fiber core Shifts in maximum absorption peak	Sensitivity for RH range 20% - 40% is 0.25 nm/%RH and the sensitivity for the RH range 40%-80% is 1.5 nm/%RH	[78]
2010	Tunable humidity sensor based on ITO-coated optical fiber	C.R. Zamarre noet al.	Optical fiber coated with ITO – monitored the transmitted spectra	Sensitivity from 5.4 to 1.2 nm/ %RH	[79]
2010	Humidity Sensor Based on a Photonic Crystal Fiber Interferometer	Jinesh Mathew et al.	photonic crystal fiber interferometer-reflection mode	region from 40% to 70%RH the PCFI shows a sensitivity of ~ 5.6 pm/%RH above 70% RH shows a sensitivity of ~24 pm/%RH	[55]
2011	Humidity sensor based on a single-mode hetero-core fiber structure	Qiang Wu et al.	small-core single-mode fiber (coated with poly ethylene oxide) spliced at both end to SMF28 _ shift in central wavelength	sensitivity 430nm / %RH in range 80% - 83% RH and a sensitivity 50nm /%RH in range 83% - 95% RH	[80]

Year	Title of paper	Author	Sensing material and Sensing mechanism	Sensitivity and Response time	Ref.
2011	Improving the sensitivity of a humidity sensor based on fiber bend coated with a hygroscopic coating	Jinesh Mathew et al.	polyethylene oxide (PEO) coated fiber bend measurement of power at optimized wavelength and bend radius	Highly sensitivity between 85% and 90% Response of sensor is suitable to use as human breath rate monitor	[81]
2012	Optical Humidity Sensor Based on Air Guided Photonic Crystal Fiber	M. Y. Mohd Noor et al.	sensor based on the Air Guided Photonic Crystal Fiber (AGPCF) using the direct absorption spectroscopic method	humidity detection resolution of around 0.2% RH over the range 0 to 90% RH	[٨٢]
2012	Optical Fiber Relative Humidity Sensor Based on a FBG with a Di-Ureasil Coating	Sandra F. H. Correia et al.	Bragg grating written in optical fiber and coated with organo-silica hybrid Material change in Bragg wavelength	sensitivity 22.2 pm/%RH in range of 5–95 %RH	[٨٣]

Year	Title of paper	Author	Sensing material and Sensing mechanism	Sensitivity and Response time	Ref.
2013	Fiber Optic Hybrid Device for Simultaneous Measurement of Humidity and Temperature	Jinesh Mathew et al.	Fiber Bragg grating and photonic crystal fiber interferometer (PCFI) infiltrated with Agarose _ monitoring the change in optical power of the reflected spectrum	Optical power variation of >7 dB for an RH change of 75 %	[8٤]
2013	An investigation into relative humidity measurement using an alumino silicate sol–gel thin film as the active layer in an integrated optical Bragg grating refractometer	Dominic J. Wales et al.	planar integrated optical Bragg grating sensor chip modified with Using a simple mesoporous silica thin film shift in Bragg wavelengths	Sensitivity in range 0 – 65%RH, was 2.47 ± 0.18 pm/%RH	[8٥]
2013	Fiber humidity sensors with high sensitivity and selectivity based on interior nanofilm-coated photonic crystal fiber long-period gratings	ShijieZheng et al.	photonic crystal fiber long-period grating coated with two types of nanofilms_ change in transmission intensity and shift in transmission spectra	Sensitivity of 0.00022%/10−3 dBm from relative humidity 38% - 39% and 0.0007%/pm for a relative humidity 22% - 29%	[8٦]

Year	Title of paper	Author	Sensing material and Sensing mechanism	Sensitivity and Response time	Ref.
2014	Highly Hygroscopic Polymer Microcavity Fiber Fizeau Interferometer for Humidity Sensing	Yan-Wun You et al.	uses a single-mode fiber tip with very little polymer coating shift in reflection spectra	linear humidity sensitivity 0.211nm/%RH	[87]
2014	Optical fiber relative-humidity sensor with evaporated dielectric coatings on fiber end-face	WeijingXie et al.	optical fiber with evaporated dielectric coatings composed of multilayers of Ti_3O_5 and SiO_2_ shift of interference fringe	average sensitivity is 0.43 nm/% RH in RH range 1.8% RH - 74.7% RH_ Determined cycling time of 5s for a rise/fall time	[89]
2014	A Mach–Zehnder interferometric humidity sensor based on waist-enlarged tapers	Min Shao et al.	Sensor head is formed by a single-mode–multimode–single-mode _ excite multiple modes and cause intermodal interference	Sensitivity of 0.119dB/%RH in the range of 35–90%RH	[90]

Year	Title of paper	Author	Sensing material and Sensing mechanism	Sensitivity and Response time	Ref.
2015	Intensity-modulated relative humidity sensing with polyvinyl alcohol coating and optical fiber gratings	Jingyi Yang et al.	Coating Tilted-Fiber Bragg Grating (TFBG) cascaded with polyvinyl alcohol _ reflected optical signal is modulated by the TFBG	sensitivity of ~1.80 μW/% RH in the range 20% - 85% RH	[91]
2015	Relative Humidity Sensor Based on S-Taper Fiber Coated With SiO_2 Nanoparticles	Haifeng Liu et al.	S-taper fiber coated with SiO_2 nanoparticles shift in the transmission spectrum	sensitivities of 1.17nm/% RH and 0.441 dB/%RH achieved for RH range of 83.8% - 95.2%RH	[92]
2016	Performance of humidity sensor based on photonic crystal fiber interferometer	Suaad Sahib Hindal, Hanan J. Taher	a relative humidity sensor based on Mach- Zehnder Interferometer (MZI), in reflection mode ,used different PCF length (0.5,1.5,3.5,4.5,6) cm	maximum humidity sensitivity of (5.86 pm / %RH) is achieved with (4.5cm) PCF length, and the rise time of (8sec)	[93]

Year	Title of paper	Author	Sensing material and Sensing mechanism	Sensitivity and Response time	Ref.
2016	Effective Enhancement of Humidity Sensing Characteristics of Novel Thermally Treated MWCNTs/Poly vinyl pyrrolidone Film Caused by Interfacial Effect	Xing long Pan et al.	MWCNTs/hydrophilic poly(vinyl pyrrolidone) (PVP) films are prepared by a simple spin-coating method shows the response of the thermally treated MWCNTs/PVP film sensor as a function of time when sensor was exposed to different RHs at 27 ± 0.5 °C	linear response to humidity with enhanced sensitivity of 0.06 dBm·(%RH) in the humidity range of 11%~94%RH fast response time(less than 15 s) and ultrafast recovery time (less than 1.8 s)	[94]
2016	Photonic crystal fiber interferometer coated with a PAH/PAA nanolayer as humidity sensor	Diego Lopez-Torres et al.	(PCF) spliced (SMFs), forming PCFI with two collapsed region , nanocoating of poly (acrylic acid) (PAA) deposited on the PCF by the well-established layer-by-layer nano assembly (LbL) technique	The sensitivity of 0.074% of (RH) in the 20–95% RH range. response time is 0.3 s	[95]

2017	Optical Humidity Sensor Based on Tapered Fiber with Multi-walled Carbon Nanotubes Slurry	Habibah Mohamed et al.	(MWCNTs) slurry coated tapered optical fiber , acrylonitrile butadiene styrene (ABS was dissolved using acetone to produce MWCNTs-acetone suspension. then drop-casted on the tapered fiber to produce MWCNTs slurry by evaporation process at room temperature, which acts as the cladding for humidity changes measurement.	improvement of sensitivity from 3.811 μW/% of bare tapered fiber to 5.17 μW/% for the coated tapered fiber with MWCNTs slurry when the humidity varied from 45% to 80%	[96]
2017	Sensitivity optimization of ZnO clad-modified optical fiber humidity sensor by means of tuning the optical fiber waist diameter	Saeed Azad et al.	different fiber waist diameter with long length of 15 mm	enhanced more than 10 times compare to bare fiber at the proposed optimum fiber diameter of 28 μm. Also, high linearity and fast recovery time about 7 s	[97]
2017	Humidity Sensor Based on Bragg Gratings Developed on the End Facet of an Optical Fiber by Sputtering of One Single Material	Joaquin Ascorbe et al.	altered The refractive index of sputtered indium oxide nanocoatings by changing the sputtering parameters, such as pressure	A sensitivity of 150 pm/%RH was obtained for relative humidity changes from 20% to 60%.	[98]

Year	Title of paper	Author	Sensing material and Sensing mechanism	Sensitivity and Response time	Ref.
2017	: A carboxy-methyl cellulose coated humidity sensor based on Mach-Zehnder interferometer with waist-enlarged bi-tapers	Qifei Ma · et al.	A fiber-optic Mach-Zehnder interferometer (MZI) humidity sensor is comprised a pair of waist-enlarged bi-tapers and carboxy-methyl cellulose (CMC) coating interference between the core mode and cladding modes varies with surrounding humidity	sensor is linearly responsive to relative humidity (RH) within the humidity range from 70% RH to 85% RH, with maximum sensitivity of −0.8578 dB/% RH.	[99]
2017	A chitosan-coated humidity sensor based on Mach-Zehnder interferometer with waist-enlarged fusion bi tapers	Kai Ni et al.	splicing of a segment between the two SMF with waist-enlarged fusion bi tapers and deposition of chitosan on the cladding	The sensitivity of 119.6 pm/RH within the range from 10% to 90%	[100]
2017	Enhancing sensitivity of photonic crystal fiber interferometric humidity sensor by the thickness of SnO2 thin films	Diego Lopez-Torreset al	Sensors with coatings of different thickness were performed by applying distinct sputtering times in order to obtain an optimal thickness: the resulting nanofilms ranged from 470 to 1800 nm	humidity resolution of 0.067 %HR within the range from 20% to 90%	[101]

.1.9 The Motivation , aims and objectives of the research

The motivation for this research is to investigate a number of approaches to humidity sensing using optical fiber which both enhancement and overcome the disadvantages of existing fiber optics sensors then which also allow fiber humidity sensors to be applied in new application areas. The specific objectives of the research are as follows:

a- Sensor enhancement of humidity sensor based an Agarose infiltrated reflection type PCFI

b- Sensor enhancement of humidity sensor based an Agarose coating transmission type PCFI .

c- Comparison of the RH sensors performance .

Chapter Two

Experimental set up and Procedures

2-1 Introduction

This chapter characterizes the experimental works. The design and structure of the fabrication of RH sensors based on the reflection and transmission type by coating or infiltration of Photonic Crystal Fiber interferometer (PCFI). The sensors under investigation were based on Mach-Zehnder Interferometer (MZI) based on collapsing technique which was used in this work as modal interferometer. This was done by splicing specific length of Large-Mode Area -Photonic Crystal Fibers (LMA-PCFs) with Single Mode Fiber (SMF-28), which was allow the excitation and recombination of two (or more) core modes to detect. Sensor sensitivity was improved by infiltrating the micro holes or coated of the PCF with a hygroscopic material . In this chapter, two types of sensors have been designed and constructed ,The schematic block diagram summarizes the experimental work as shown in Fig. (2.1).

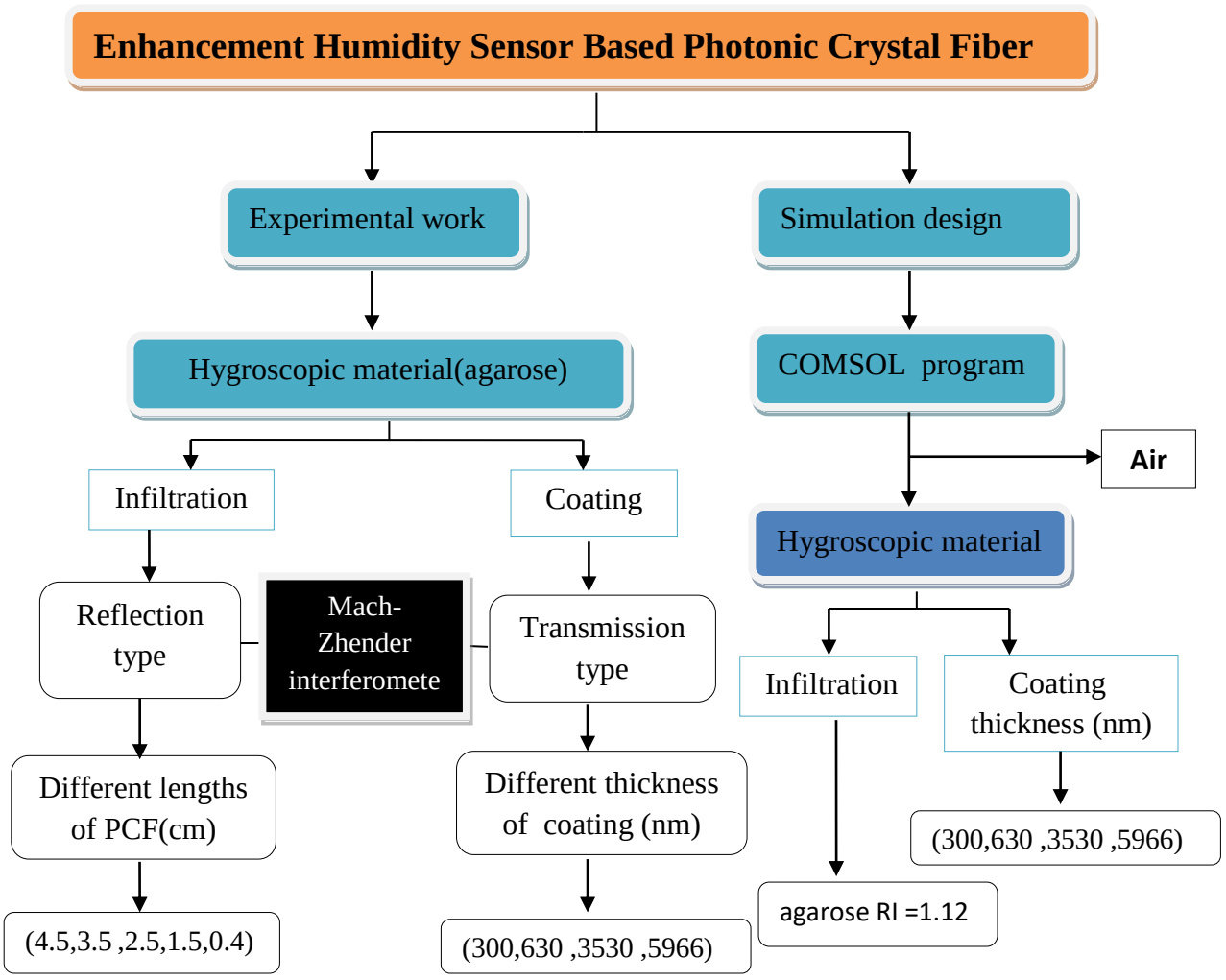

Fig. (2-1): Schematic diagram for the structural work of the study.

2.2 PCFs cleaving:

PCFs are easy to break because it special structures, therefore a special procedure should be done to cut these fibers.PCF(LMA-10) and SMF (Corning-28) has been used in this experiments. PCFs (supplied by NKT Company) were all equipped with a standard coating, which was more smooth and brittle.

The coating can readily be removed, using a mechanical stripping, a sharp blade was used as mechanical stripping by applying controlled strain to

remove the coating. Mechanical methods support the small risk of the fiber surface damage, which can lead to precision problems.

For stripping fibers, Fiber Optics Stripper(JIC – 375 Tri – Hole, Fujikura) has been used.

The second step was cleaving the PCF and SMF, which was done by fiber cleaver (CT-30) from Fujikura Company (Japan), as shown in Fig. (2. 2), the cleaver cut the fiber in 90^{o} angle.

Fig. (2. 2) Fiber cleaver (CT-30)

After cleaving, SMF had to be cleaned by alcohol land wipes. To prevent infiltration in PCF, any solvent had not been used for cleaning the PCFs after cleaving, because this will lead to solvent infiltration inside the holes of fiber and may cause a failure of connecting and sensing process. A dry wipes had been used to remove remains coating after cleaving. Top view of PCF under a microscope shown in Fig. (2. 3), which shows the quality of the cleaved end of PCF.

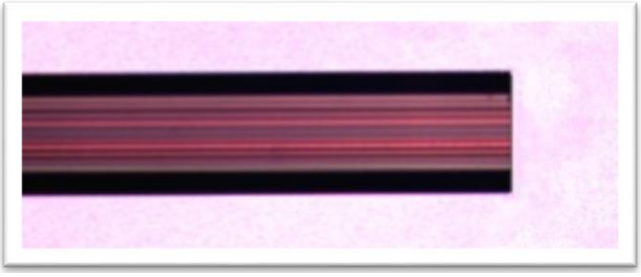

Fig (2. 3): Microscope images of PCFs (LMA-10) end after cleaving

2.3 PCF-SMF fusion splicing:

Fusion splicing is act to join two optical fibers end-to-end using heat. PCF (LMA-10) connected from one side with a conventional optical fiber (Corning SMF-28) by using an arc fusion splicing machine. It is very simple and inexpensive technique for splicing different types of fibers. In all experiments splicing procedure was done by trial and error method to get optimal parameters of fusion splicer.

Photonic Crystal Fiber – Single Mode Fiber (PCF-SMF) splicing needs a special machine setting and care, because is different from splicing of two conventional optical fibers, due to the MFD of the PCF and SMF are different.

First, manual modes have been selected of the fusion splicer. And the most common parameters of the fusion splicer are fusion power and fusion time, and it changed during splicing to get optimal splicing. After stripping and cleaving the fibers, the typical steps to be performed were:

1. Clamping of fibers in supports with V-grooves.
2. Visual inspection of fiber tips for proper cleave and cleanliness.
3. Alignment of fibers for lowest transmission loss. Leave only a small gap between the fibers.
4-Began the electric arc and push the fiber ends together.
5- Check the quality of the obtained splice, ideally by measuring the transmission, since the process may not always work as expected.

The fusion splicer (FSM-60S) used in the experiments, shown in Fig. (2. 4),it is supported by Fujikura. Its specifications are shown in the appendix (**A**).

Fig (2. 4): Arc fusion splicer (FSM-60S*)*

2.4 Fabrication of a PCFI:

A required length of PCF with its protection coating removed and both ends cleaved was taken. The cleaved end of the input SMF and the input end of the PCF were fusion spliced together to form a reflection type PCFI. The transmission type PCFI can be formed by again fusion splicing the output end of the PCF section to the cleaved end of the output SMF.

As shown in Fig. (2. 5) the PCF (LMA-10) was designed for an endless single –mode operation was utilized it had six layers of air holes organized in a hexagonal pattern around a silica core , the fiber had a core diameter(C4) of 10.2μm , voids with diameter(C6) 3.2 μm , pitch (L7) of 8.07 μm and the outer diameter of 125 μm and the optical properties of this fiber are shown in appendix **(B)**.

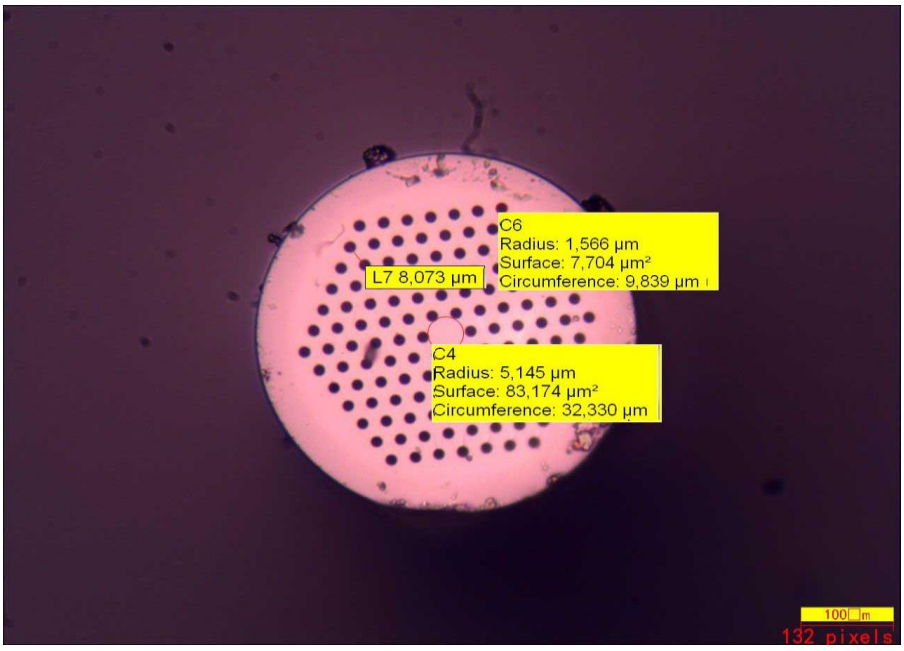

Fig (2.5): Scanning electron microscope image of the cross section of the PCF that has been used for the experiment

These dimensions of the PCF aligned and spliced with SMF by splicing machine and due to mismatch of mode- field diameter (MFD) compared to other PCFs, the loss was minimized . during the splicing process and due to surface tension , the voids of the PCF collapsed within a microscopic region (~ 248 µm) near the splice point , as shown in the Fig. (2.6) .

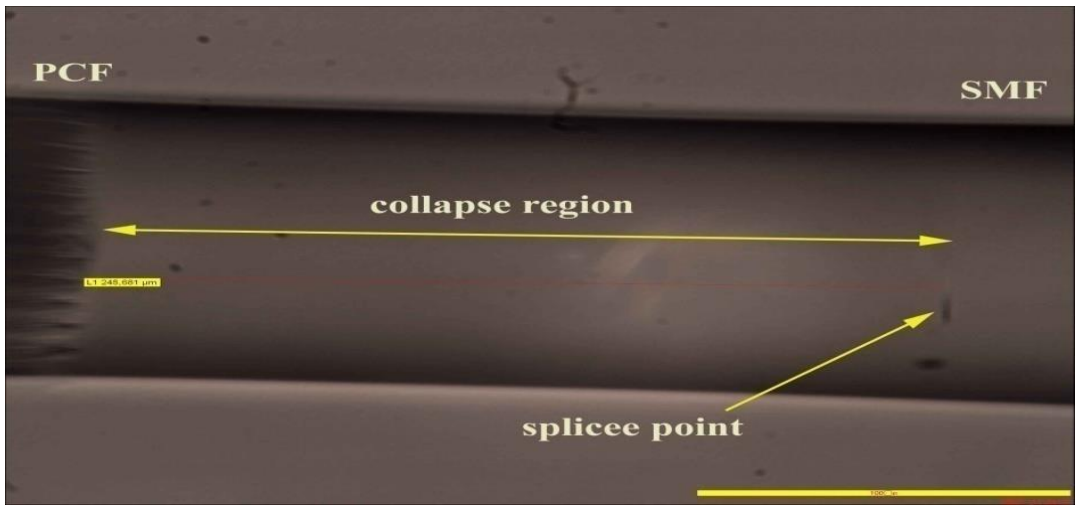

Fig (2.6): Microscope image of the PCF collapsing interferometer

2.5 PCF Humidity Sensors Based on Modal Interferometer Setup:-

To characterise sensors the generic experimental setup took one of two forms, depending on the sensor type. The generic setup for transmission type sensors was composed of a light source, sensor head and a light detector as shown in Fig. 2.7.

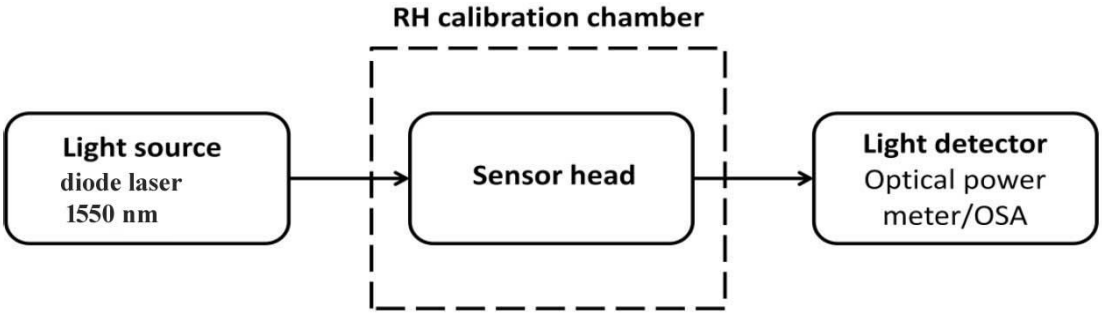

Fig. 2.7 Block diagram of the generic experimental set-up to study the RH response of the transmission type sensor

For an end type sensor head such as open ended PCFI, a fiber optic coupler/circulator was used to couple the light between source, sensor head and the detector as shown in Fig. 2.8.

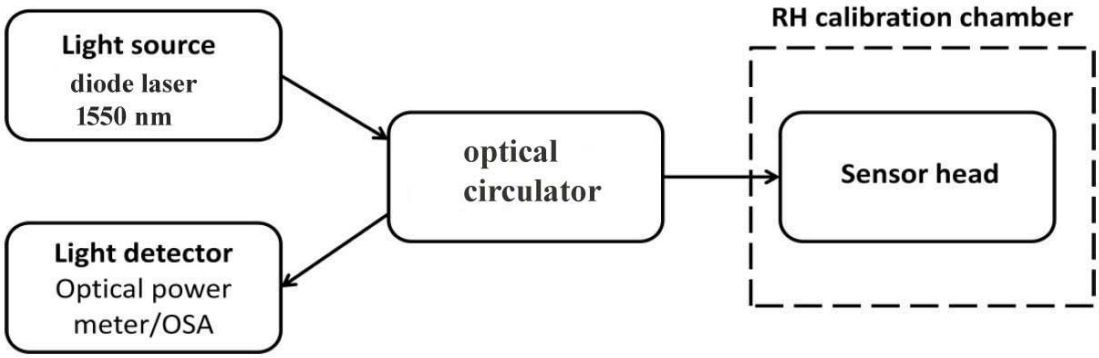

Fig. 2.8 Block diagram of the generic experimental set-up to study the RH response of reflection type

The optical circulator allows light to propagate in only one direction. A signal entering to (**port1**) will exit (**port2**) with low loss, whilst a signal entering (**port2**) will exit (**port3**) with low loss. Light entering (**port2**)undergo a large amount of loss at (**port1**), and light entering (**port3**) undergo a large amount of loss at **ports 2 and 1,** as shown in Fig. (2.9) .The specifications and data sheet are shown in appendix (C).

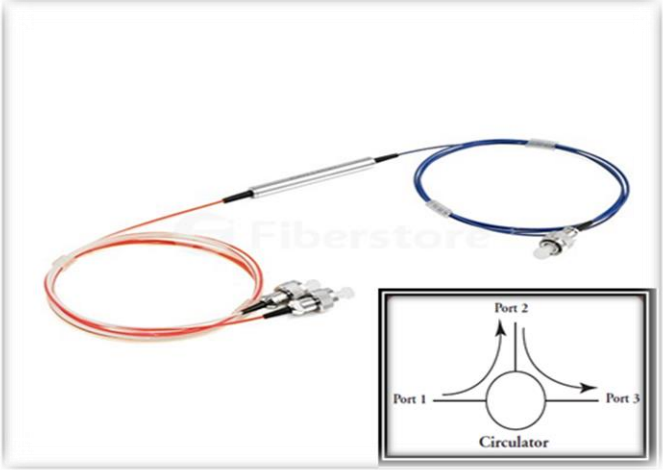

Fig.(2.9)Fiber Optic Circulator

The light sources used were either a diode laser. Thor labs Bench top Fiber Pigtailed Laser Sources were ideal for fiber based applications has been used in this work, as shown in Figure (2.10). Our Series came with a pigtailed Fabry Perot Laser diode with single mode fiber behind an FC/PC bulkhead connector. To reduce reflections back into the laser diode , the fiber pigtailed lasers used an angled fiber ferrule at the internal laser/fiber launch point, that way increasing the overall stability. The specifications of the light source as shown in appendix **(D)**.,

Fig. (2.10) Light source (S1FC1550)

The light detector used to monitor the response of the sensor was an optical power meter (FPM-300, EXFO Company, China) or an Optical spectrum analyzer OSA (YOKOKAWA, Ando AQ6370) with resolution of 0.02 nm was used to monitor the interference spectra of the sensors. Fig. (2.11) shows the photograph of OSA and Fig. (2.12) optical power meter used in the experiments. The specifications of the power meter are indicated in the appendix (E).

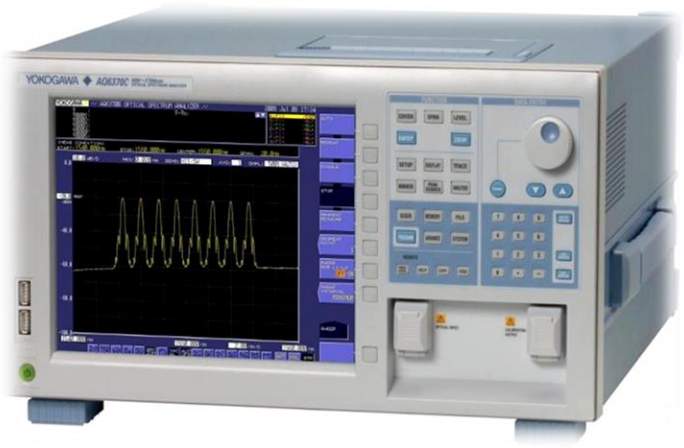

Fig (2.11): photograph of optical spectrum analyzer (OSA).

Fig. (2.12) Power meter

A transmission Microscope from (Euromex Company) was used in this experiment, as shown in Fig. (2.13), to view all the tested samples. It has many lenses (4 X, 10 X, 40 X and 50 X) to magnification the picture of samples to see cross section and side view of SMF-28, cross section and side view of PCF before and after the experiments, length of collapse region , length of infiltration region and coating thickness of agarose of PCF.

Fig.(2.13) The Transmission Microscope

2.6 Controlling the humidity environment

The humidity response of the sensors was studied by placing the sensor in a controlled environment chamber which was a cuboid -shape sealed chamber, fabricated from Polyvinyl chloride (PVC) plastic with dimensions (length =40cm, height= 27cm, and width=17cm). It consists of dry/wet air flow system that can vary the internal humidity in the chamber (27%RH - 95%RH).There are three fans in this chamber, the first fan(1) pumps a wet air from container containing distilled water and heater (70watt), the second fan (2) pumps a dry air form container containing a silica gel, and the last fan(3) is in the surface of chamber to expel the air as illustrates in the Fig. (2.14). A calibrated electronic humidity(XMT9007-8 temperature & humidity control instrument) was used for monitoring the humidity and temperature inside the chamber as shown in Fig. (2.15) .

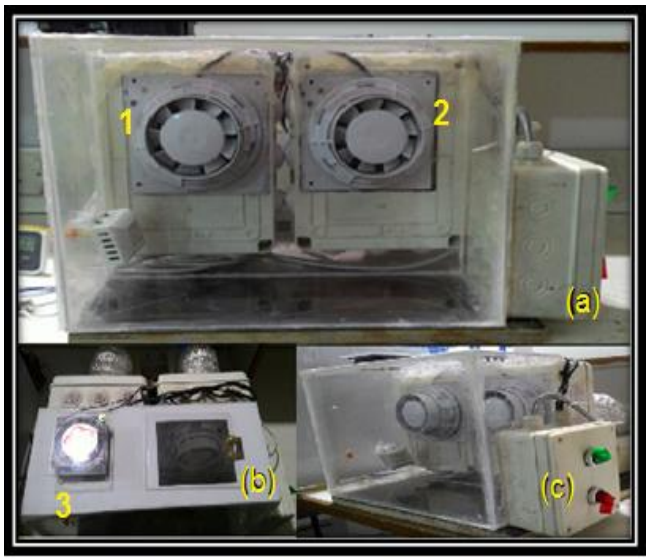

Fig.(2.14) Humidity chamber a) front view, b) top view, and c) side view

Fig. (2.15) Temperature and Humidity Controller

2.7 Chemical processes:

It involved the preparation of a hygroscopic material solution for developing techniques to allow coating or infiltration. The solution has been prepared by dissolving a convenient quantity of Agarose in distilled water. The Agarose infiltrated PCFI was fabricated by infiltrating the microholes of the reflection type PCFI with hot Agarose solution via capillary action. The Agarose coated PCFI was fabricated by passing the transmission type PCFI through a hot Agarose solution. The UV/Visible Spectrophotometer SP-3000 from Optima Company has been used to investigate the absorption and the transmission characteristics of the proportions that had been used. The Fig. (2.16) shows the photograph Spectrometer.

Fig.(2. 16)The Spectrophotometer sp-3000 from optima Company

2.8 RH sensor based on Agarose infiltrated photonic crystal fiber interferometer (AI-PCFI)

2.8.1 System Layout:-

Photonic crystal fiber interferometer (PCFI) operated in reflection mode for relative humidity (RH) sensing , the sensor of the humidity based on an agarose infiltrated (AI-PCFI) photographic picture is shown in Figs. (2.1ᵛ), the whole sensor system was composed of a laser diode 1550 nm, a fiber coupler/circulator (FOC), the Agarose infiltrated PCF interferometer as a sensor head, and a photo detector (PD)/optical spectrum analyzer (OSA) / power meter.

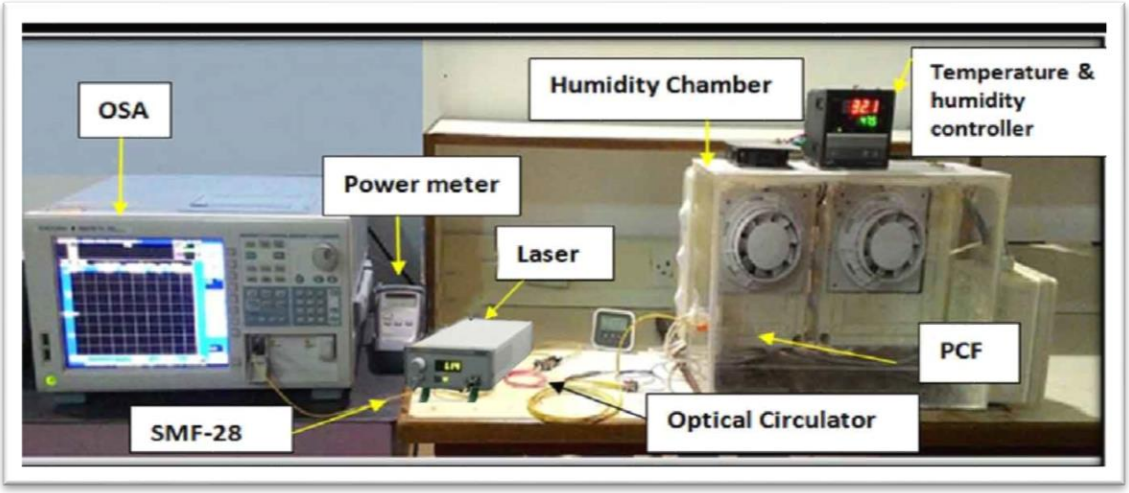

Fig. (2.1ᵛ) The photographic picture for the PCFI humidity sensor set up (reflection type)

2.8.2 Experimental Procedures

Humidity sensor based on reflection type of the PCFI has been proposed. First, the coating of a stub of PCF (LM A-10) and conventional optical fiber (Corning, SMF-28) were removed by using a mechanical stripping. Then, the second step was cleaved the PCF and SMF, which was done by fiber cleaver, and third step was cleaning the fibers. Then, the stub of

PCF (LM A-10) was spliced to the conventional optical fiber by a conventional splicing machine. After fusion splicing, the PCF was cleaved using a standard fiber cleaving machine so that the PCF end behaved as a reflecting surface, then the tip of the PCF was immersed in a hot agarose solution to infiltrate the PCF microholes with agarose. The preparation of solution was made by dissolving (1wt%) agarose in distilled water. In order to dissolve the agarose in distilled water, the mixture in the beaker was placed on a heater merged with a magnetic stirrer. The heater was set at (65 ◦C) and in the same time the agarose material and water inside the beaker was stirred until the agarose was wholly dissolved. Then kept the solution in the same temperature, the open end of the PCF was immersed in this solution for around 30 s. The external part of the fiber was wiped by using a dry cleaning tissue directly after the fiber was pulled out from the solution. When the infiltrated solution was cooled, the gel polymerized, and once the gelling point was come to (<30 ◦C) the mixture assumed its hydrogel form and won't take a liquid form again unless it is heated and reaches its melting point (>60 ◦C).

2.9 RH sensor based on Agarose coated photonic crystal fiber interferometer (AC-PCFI)

2.9.1 System Layout:-

A transmission type PCFI in which the two ends of a PCF were fusion spliced to lead-in and lead-out single mode fibers has already been demonstrated, the humidity sensor based on an agarose coated PCFI. Schematic system of the humidity sensor and photographic picture is shown in Fig. (2.١٨), the whole sensor system was composed of a laser diode 1550 nm, the agarose coated PCF interferometer as a sensor head, and a photo

detector (PD)/optical spectrum analyzer (OSA) / power meter. it does not require the use of a fiber optic circulator.

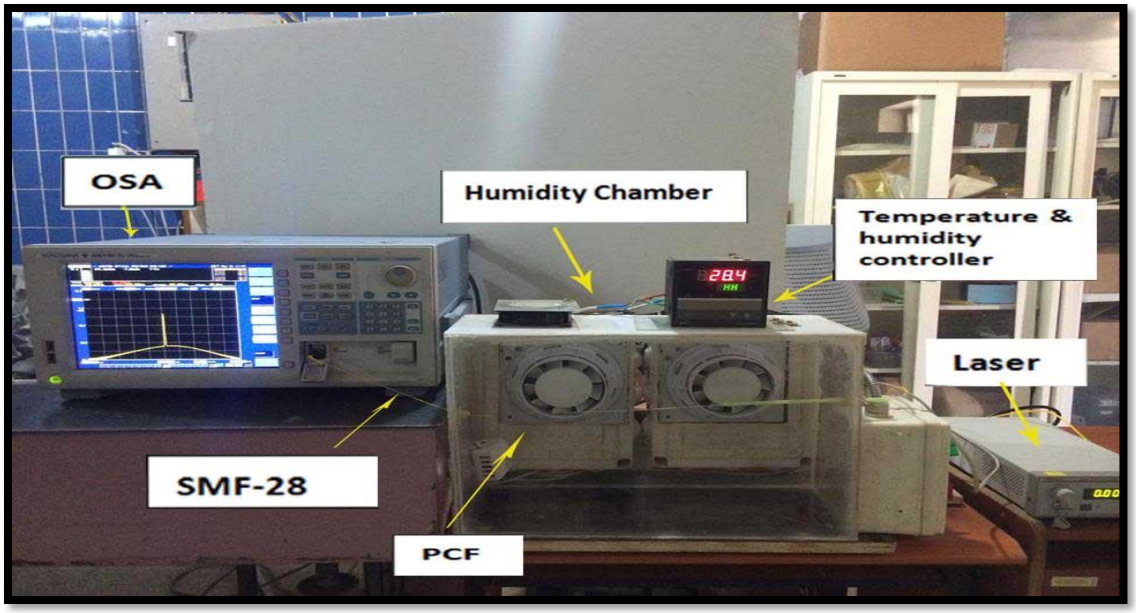

Fig.(2.١٨)The photographic picture for the PCFI humidity sensor set up (transmission type)

2.9.2 Experimental Procedures

Humidity sensor based on transmission type of the PCFI has been proposed. First, the coating of a stub of PCF (LM A-10) and conventional optical fiber (Corning, SMF-28) were removed by using a mechanical stripping. Then, the second step was cleaving the PCF and SMF, which was done by fiber cleaver, third step was cleaning the fibers. Then, the stub of a (10 mm) long of commercial PCF was fusion spliced between two SMFs (Corning SMF-28) by a conventional splicing machine. After fusion splicing, was coating with Agarose, it was carried out by drawing the interferometer through a hot (65 ^{O}C) Agarose solution, which prepared by dissolving (1 wt%) Agarose in distilled water. In order to undertake the coating process the

fiber was fixed straight and horizontally above a translation stage (TS). Below the PCF a heater was fixed on a (TS). A small container placed at the top of the heater was filled to the top with hot Agarose solution as shown in Fig. (2.١٩) and the experimental schematic diagram setup for Agarose coating shown in Fig. (2.٢٠).

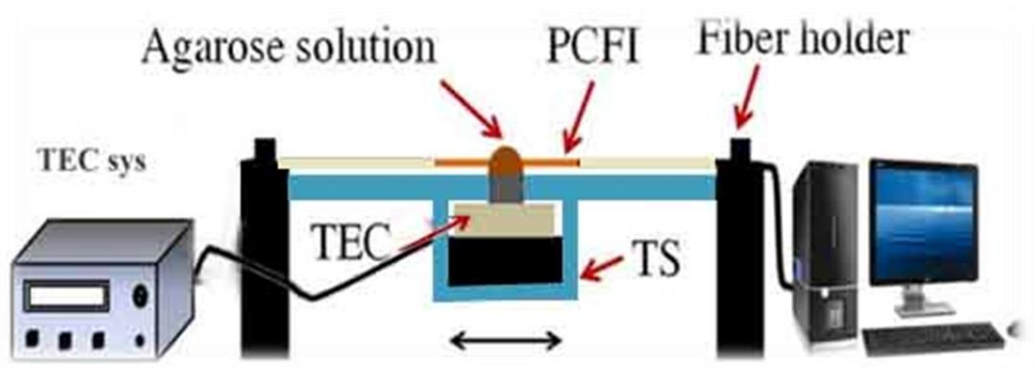

Fig. (2.١٩) Schematic diagram of the experimental setup for Agarose coating

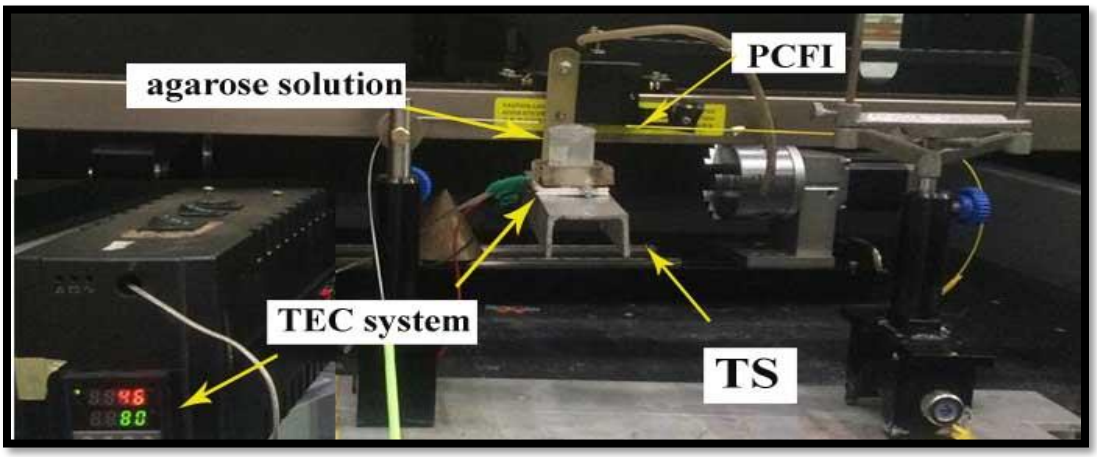

Fig. (2.2٠) The photographic picture for setup of Agarose coating

The surface of the solution formed a dome like shape which projected slightly above the rim of the container because of surface tension. The container position can be adjusted to allow the fiber to pass through this dome

of Agarose solution. The temperature of the heater was set at 65 ^{O}C by temperature electrical controller system (TEC sys.) . The PCF is drawn through the hot Agarose solution by a (TS) which was controlled in software using a computer. This arrangement allowed for good repeatability of the coating parameters.

2.10 Simulation Design:

COMSOL multphysics program has been used to design the photonic crystal fiber large-mode area with infiltration and coating of agarose solution then find the guiding of laser 1550 nm diode laser at this fiber.

There are many steps followed to design PCF with COMSOL illustrated in Fig. (2.21):

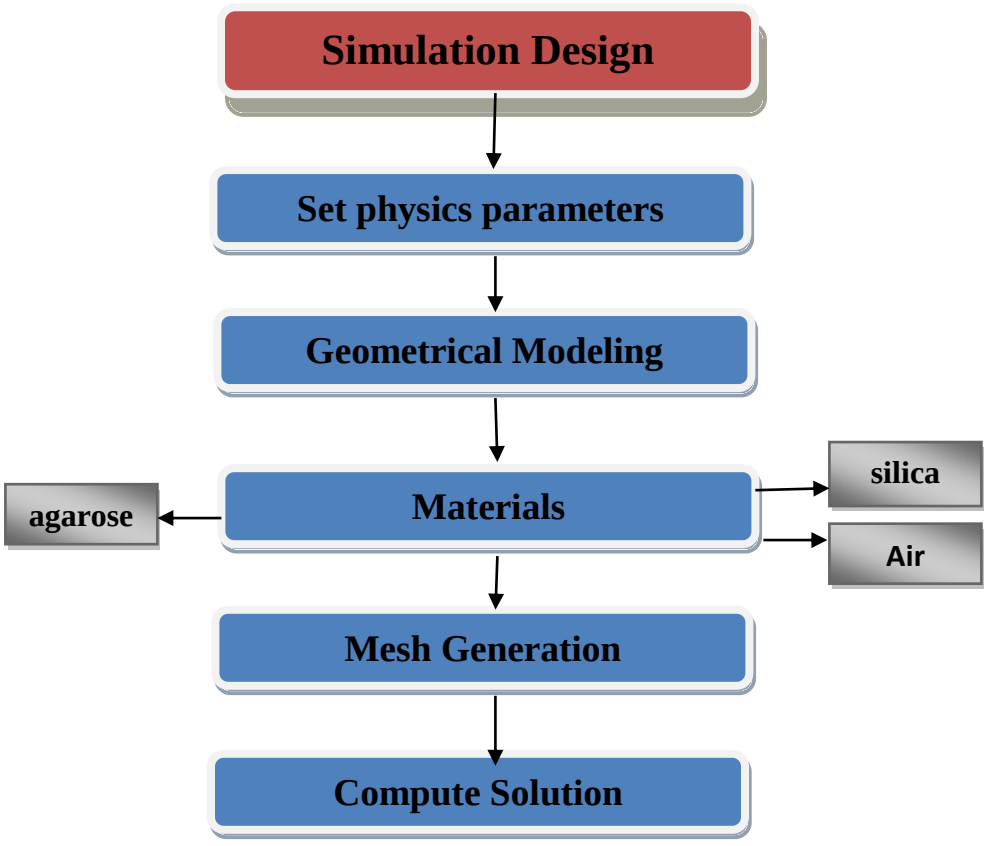

Fig.(2.21) procedures of design the PCFI in the COMSOL multphysics.

Chapter Three

Results and discussion

3.1 Introduction:-

This chapter presented the results of the fabricated reflection and transmission type MZI sensors test, conclusion, comparison of the two RH sensors performance and the future work .The response of the PCFIs is observed for a different humidity values. The shift in wavelength of the interference fringes was observed and recorded.

The sensors sensitivity has been calculated by dividing the experimentally measured PCFI response to the relative humidity. Also the rise time of sensors has been calculated for the sensors.

The experiments were carried out under the 0.02 nm resolution of the optical spectrum analyzer (OSA) and light source (1550 nm) with optical power (1.79mW). All the results were taken under laboratory conditions (at room temperature and normal atmospheric pressure).

3.2The interferometer fabrication:-

The optimum parameters of fusion splicer (FSM-60S) used in sensors have set to obtain optimized low splice loss. These parameters have been epitomize in the table (3.1).

Table (3.1): The optimized parameters of arc fusion splicer (FSM-60S) for splicing SMF-28 with PCF (LMA-10)

Splice parameters	Perfusion time (ms)	Perfusion power STD (bit)	Gap (µm)	Overlap (µm)	Arc 1 power STD+(bit)	Arc1 time (ms)
SMF-28/ PCF(LMA-10)	180	STANDARD	15	10	40	3600

The PCF (LMA-10) was designed with core diameter ρ(10.2μm) , void diameter (d) was 3.17 μm and the pitch (Λ) (hole-to-hole distance) was about(8.073μm) , d/Λ is 0.347712, when d/Λ ≤ 0.43, the PCF can be endlessly single mode. The PCF dimensions simplified the aligning and splicing to SMF-28 when these fibers splice by a standard splicing machine.

The splicing loss was due to two reasons; the first one was the mode field mismatch between PCF (LMA-10) and SMF, the other one was that PCF's air holes may completely collapsed near the joint of splicing, thus caused destroying the light directing structure close to the joint interface, therefore increased the coupling loss. The PCF (LMA-10) had similar MFD as the SMFs, so a low-loss splicing was achieved. Fig. (3.1) shows the splicing process; (1)the alignment of SMF-28 with PCF(LMA-10), and (2, 3, 4) some splice loss resulting from splicing process.

Fig.(3.1): The splicing process and the loss obtained in (dB)

Under these splicing conditions, the PCF voids collapsed wholly over a microscopic region, and the total length of collapse region was typically less than (300µm) as agree with [17], and it shown in Fig. (3.2). Because of the disappearance of the difference between refractive indices of the core and the cladding so the light will expand and causing a splice loss.

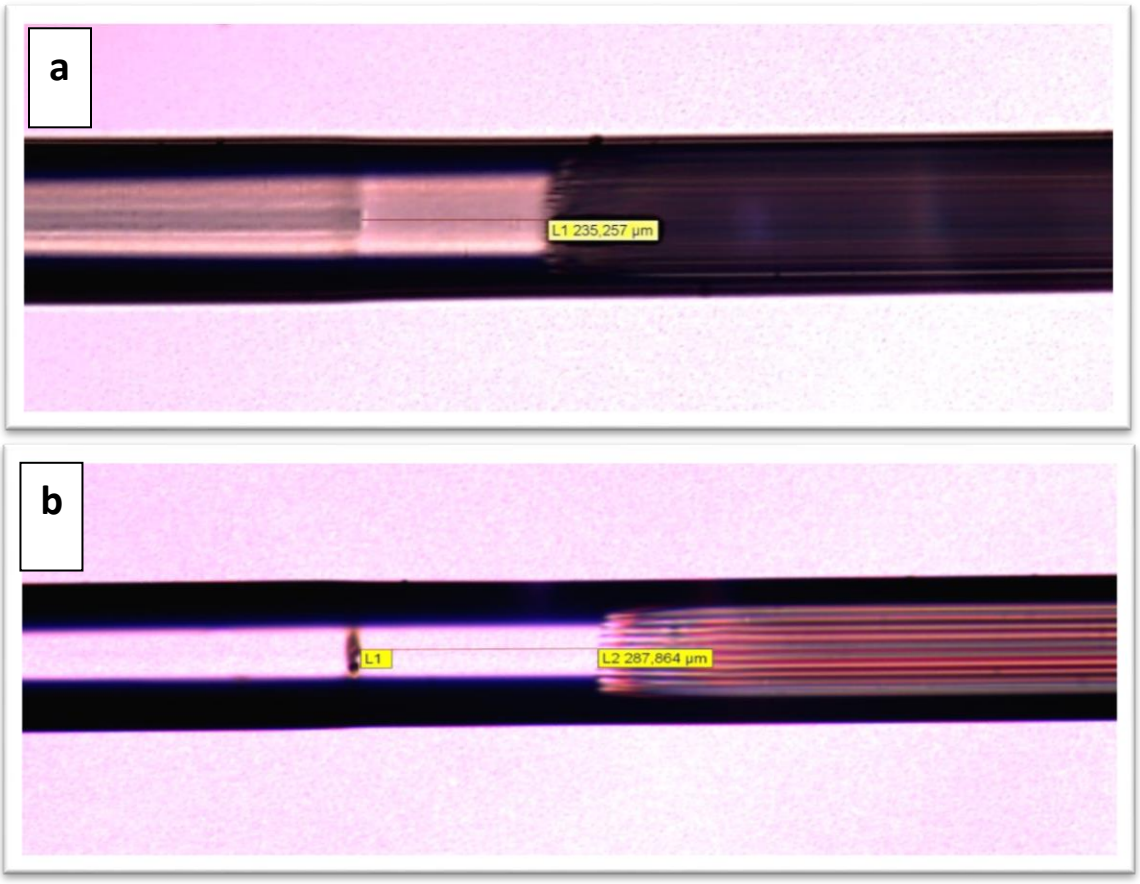

Fig.(3.2): Microscope images of the splice regions, between PCF (LMA-10) and the SMF-28, a)the collapsed length is ~235.2 µm, and b)the collapsed length is ~287.8µm, when the magnification power of the transmission microscope is (10X)

The long collapsed region leads to excitation of many cladding modes and then increases the splice loss. So, excitation of single cladding mode was preferred to improve the sensor performance, due to its simple interference with the core mode.

Photonic crystal fiber interferometer (PCFI) after fabricating process, has been checked the stability of the laser diode 1550 nm which was used as a light source in the experiment, This was done after half –one hour with power set 1.79 mw of operation. Fig. (3.3) illustrated the output spectrum of diode laser (1550 nm).

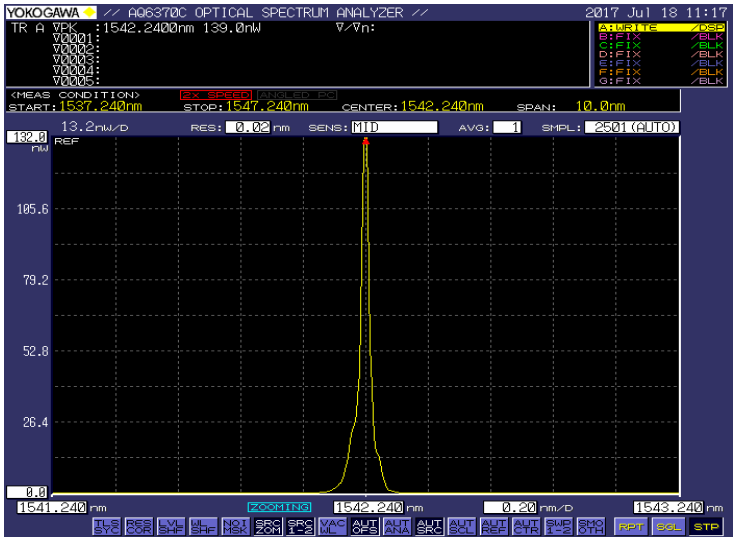

Fig.(3.3): Output Spectrum of laser diode 1550 nm

3.3 Physical properties of Agarose gel

Agarose was sold in a form of white powder, soluble in water at 34-38°C. In this experiment Agarose powder was dissolved in distilled water in proportions of 1, 2,3and 4 wt./vol.%. The solutions were heated up to 65°C to dissolve the Agarose in distilled water, the beaker containing the mixture was placed on a heater combined with a magnetic stirrer. When the Agarose solution cooled down and reached room temperature, it polymerized to form hydrogel and will not assume a liquid form again unless it is heated above the melting point (90-95)°C. Agarose solutions exhibit hysteresis in the liquid to

gel transition [68] , that is their gel point is not the same as their melting temperature.

In order to find the refractive indices and absorbance of four proportions was had tested by UV/Visible Spectrophotometer. The SP-3000 from Optima Company has been used to investigate the absorption and the transmission characteristics of the proportions that had been used. The absorbance peak illustrate in Fig. (3.4)and Table (3.2) it is obvious some parameters.

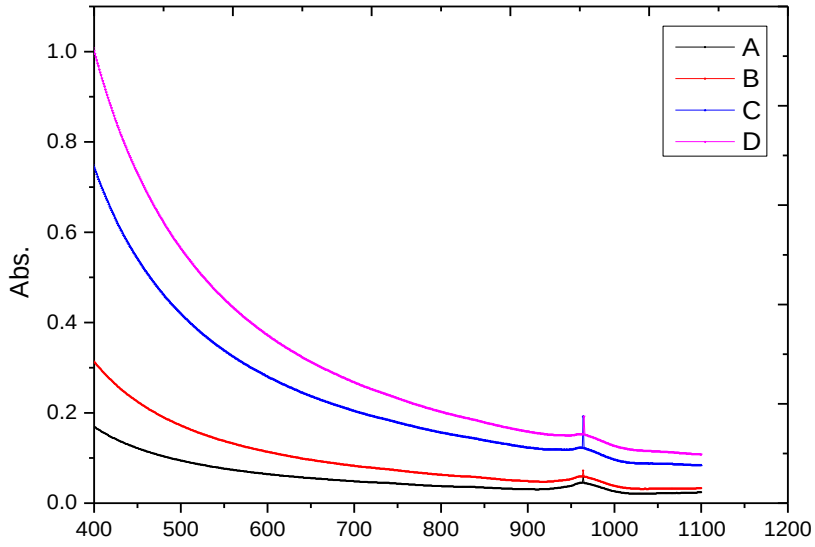

Fig.(3.4) spectrophotometer UV/visible absorption spectrum of (A,B,C,D)proportions.

Table.(3.2) parameters of (A,B,C,D)proportions.

Agaros proportions in d. water	A	B	C	D
W/V % (g/ml)	1	2	3	4
Absorbance	0.085	0.11	0.194	0.25
Transmittance	0.9456	0.93017	0.88247	0.8483
Refractive index	1.12611	1.16289	1.27912	1.36425

3.4 Experimental investigationand discussion of RH sensor based on an agarose infiltration reflection-type photonic crystal fiber interferometer (AI-PCF)

It have been studied an uninfiltrated PCFI that be observed PCF with length (4.5cm)which show the higher sensitivity (4.6033 pm/RH%) for range (27%-85%) RH as agree with [93] , for wider range (27%-95%) RH, the higher sensitivity was calculated about(1.926 pm/RH%), the sensitivity calculated from the linear fitting versus wavelength curve to RH values as shown in Fig.(3.5) .

In this experiment demonstrated that there was no wavelength shift and no decreasing in reflection power when increase the RH >88 % as shown in Figs.(3.5(a ,b)), this was because water has a hydrogen-bonded network (ice-like), which grows up as the relative humidity increases from 0%to30%. The liquid water structure starts appearing in the RH range of 30-60 %,while the structure of ice-like continues growing to saturation .

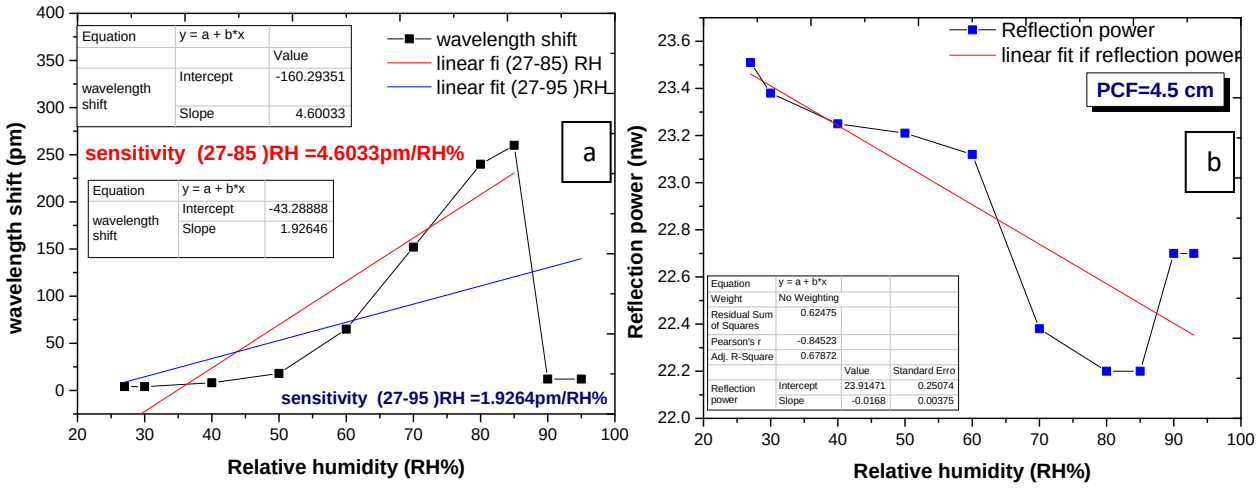

Fig.(3.5)a Change in the reflection spectrum of a PCFI with length 4.5 cm with respect to different ambient relative humidity values. b) Change in the reflection power of a PCFI with length 4.5 cm with respect to different ambient relative humidity values.

The agarose-infiltrated in order to improve the humidity sensitivity of PCFI, all the concentrates was tested , it found 1wt% proportion of agarose less viscosity and get in the holes of PCF smoothly which was Convenient choice for infiltration .

3.4.1. The Effect of the PCF length on the infiltration region

The Agarose solution in this study was prepared by dissolving 1 wt% Agarose in distilled water at a temperature of 65 ^{O}C. Then keeping the solution at the same temperature, the open end of the PCF is immersed in this solution for about 30 seconds, after that , the fiber was pulled out from the infiltrated mixture, the gel polymerized at once ,when gelling point was reached (<30 ^{O}C) the mixture assumed its hydro-gel form and will not take a liquid form again unless it was heated and reaches its melting point (> 60 ^{O}C), initial infiltration length depends on capillary forces, the length of the PCFI and the temperature. Fig.(3.7) illustrate the change in infiltration length for all AI-PCFIs .At a constant temperature it is the balance between the capillary forces and the forces exerted by the pressure of the air inside the silica holes. In this case the air inside the micro holes compressed as a result of the sudden cooling from 65 ^{O}C to room temperature of 23 ^{O}C after the fiber was taken out of the solution and this results in an increase in the infiltration length inside the microholes of the PCFI. The experiments were carried out using infiltrated PCFIs with different PCF lengths (*4.5 cm ,3.5cm ,2.5 cm,1.5 cm and 4 mm*). For the sensor presented here the infiltration length was estimated using a polarizing microscopeas shown in Fig (3.6).

Fig.(3.6) Microscope image show a)length of infiltration region in PCF
b) cross section of agarose infiltration in PCF (AI-PCF)

The Agarose infiltrated fiber was kept for one –two hours at room temperature until it was partially dehydrated and reached the equilibrium with the ambient environment. the length includes both the 248µm hole collapsed region and Agarose infiltrated region.

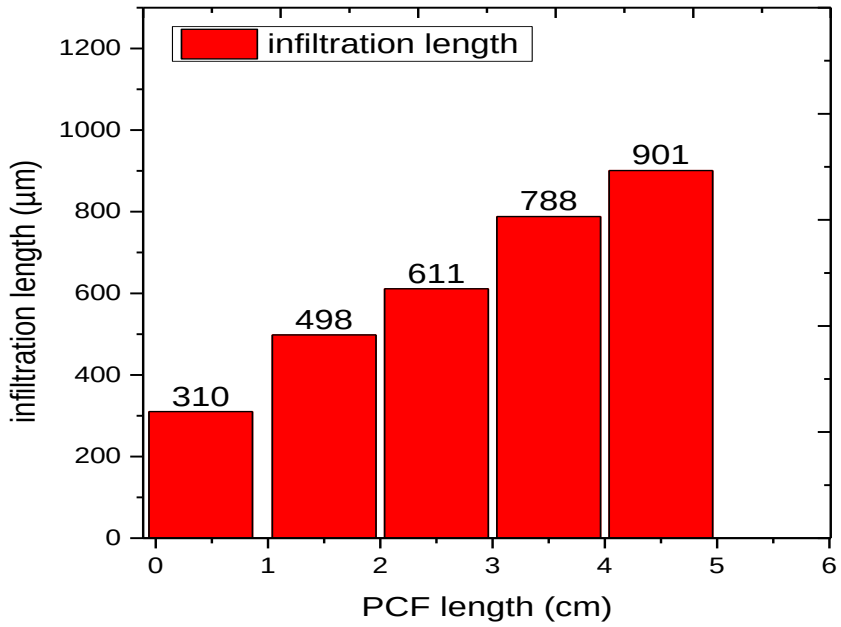

Fig. (3.7) The infiltration lengths of the five different AI-PCFI devices at R.T.

3.4. 2 Performance Analysis of the RH Sensor Based on AI-PCFI

The PCFI response was observed for a range of humidity values (27%, 30%, 40%, 50%, 60%, 70%, 80%, 85%,90% and 95%)RH.

The sensitivity of the sensor was calculated by dividing the experimentally measured PCFI response to the relative humidity.

An increase in the RH level increased the RI of the agarose and this change in RI changed the propagation constant of the cladding mode. The result changing phase between the interfering modes thus shifted of the interference pattern as a function of ambient RH. When humidity increased, the interference pattern shifted to higher wavelengths(red shift). Therefore, the reflected power decreased for the sensor in the observed wavelength region, experiments were carried out using infiltrated PCFIs with different PCF lengths (*4.5 cm ,3.5cm ,2.5 cm,1.5 cm ,4 mm*) the figures below shows the shifting of the interference peaks of reflection power and wavelength shift respectively to relative humidity of the PCFIs submitted sensors.

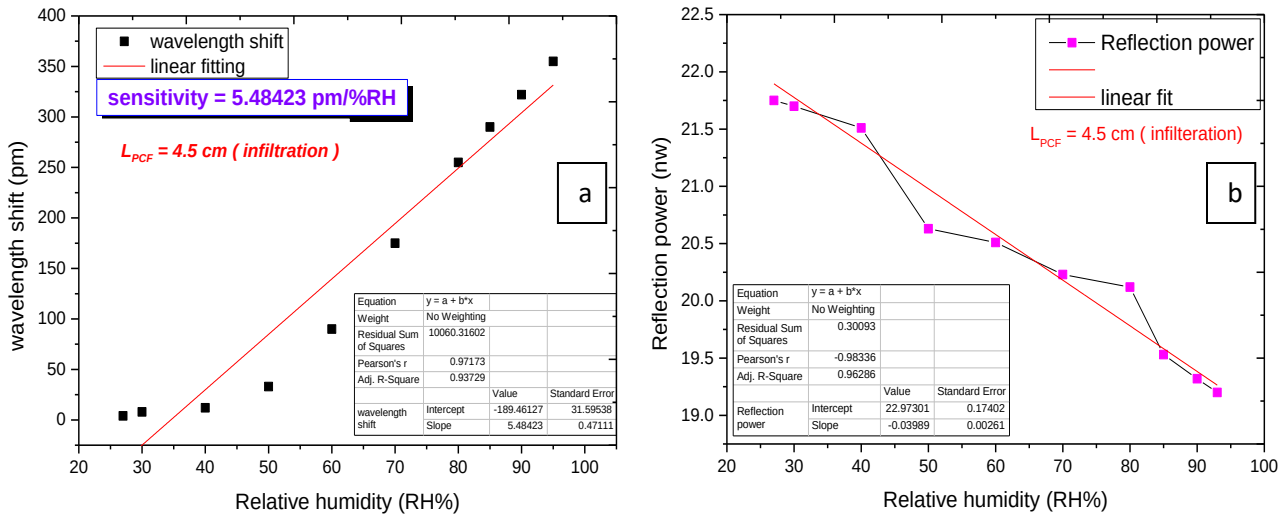

Fig.(3.^)a) Interference peaks shift of wavelength shift with RH for length(4.5) cm of PCF b) Interference peaks shift of reflection power with RH for length(4.5) cm of PCF

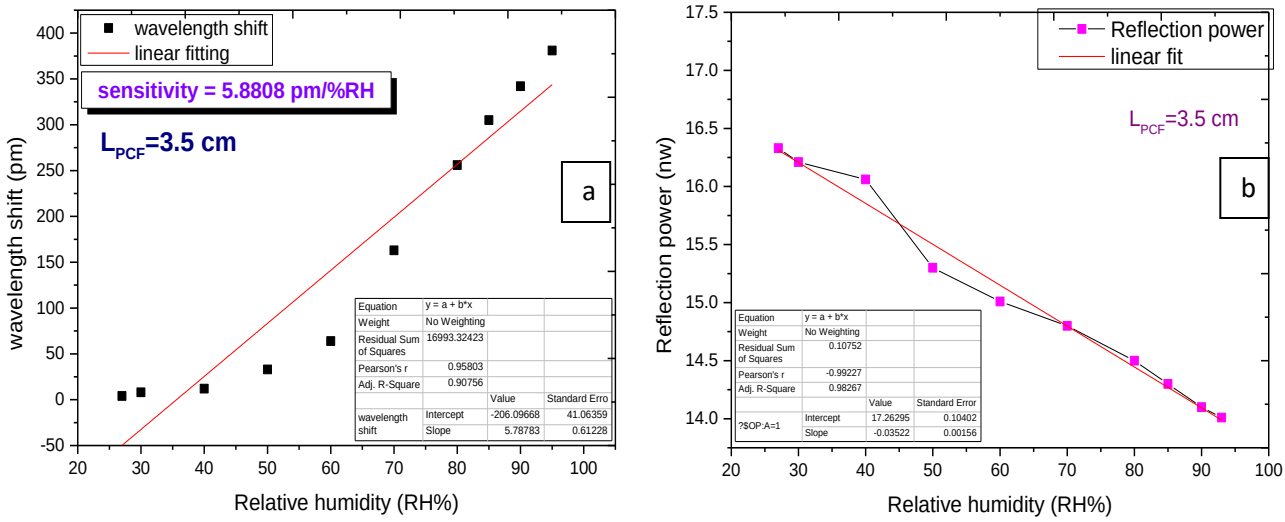

Fig.(3.9a) Interference peaks shift of wavelength shift with RH for length(3.5)cm of PCF. b) Interference peaks shift of reflection power with RH for length (3.5) cm of PCF

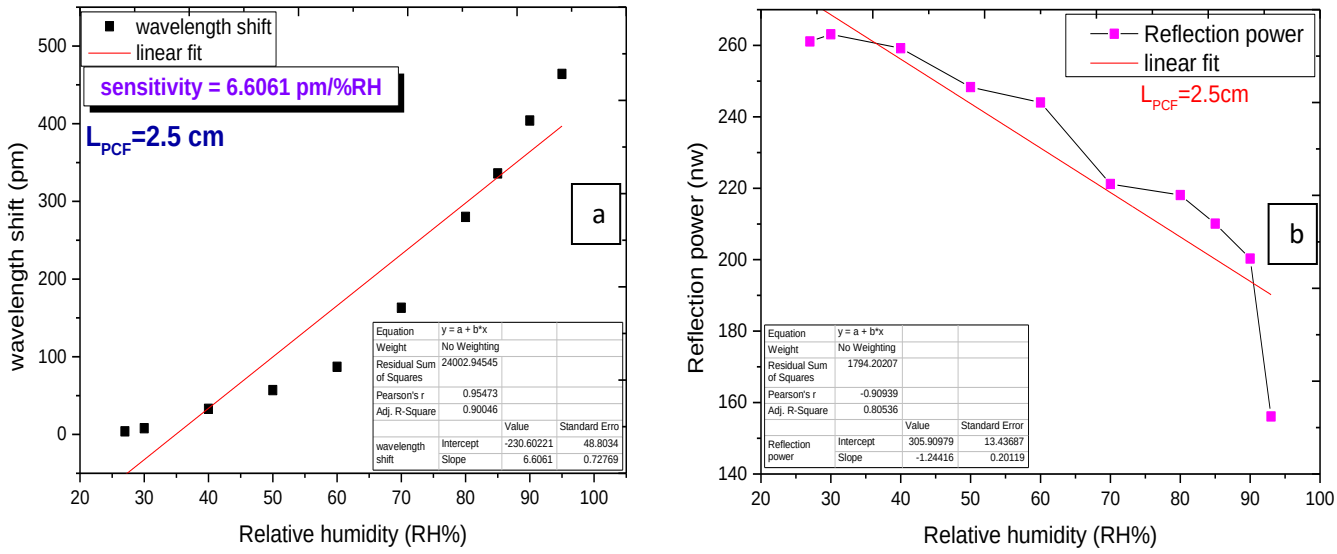

Fig.(3.10)a) Interference peaks shift of wavelength shift with RH for length(2.5)cm of PCF b) Interference peaks shift of reflection power with RH for length(2.5)cm of PCF

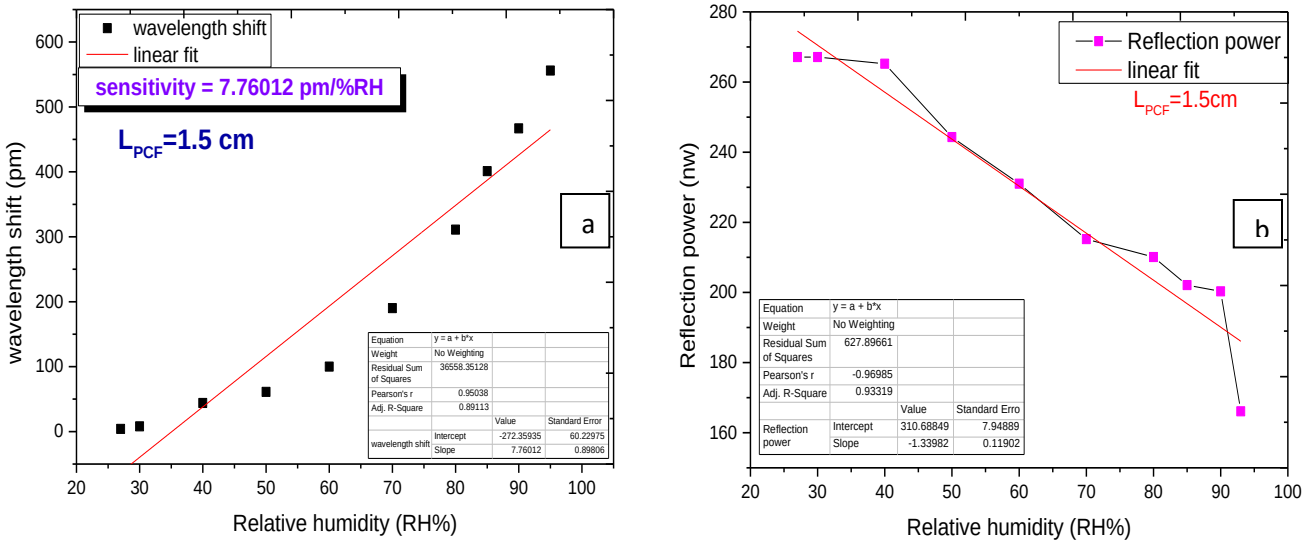

Fig.(3.11)a) Interference peaks shift of wavelength shift with RH for length(1.5)cm of PCF
b) Interference peaks shift of reflection power with RH for length(1.5)cm of PCF

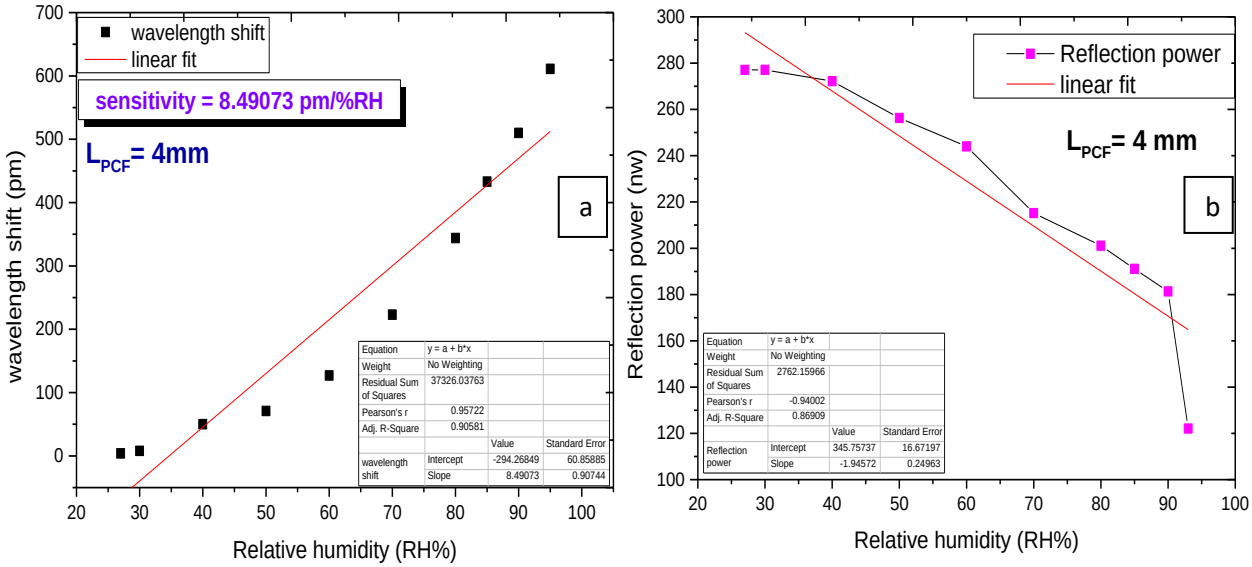

Fig.(3.12)a) Interference peaks shift of wavelength shift with RH for length(0.4)cm of PCF
b) Interference peaks shift of reflection power with RH for length(0.4)cm of PCF

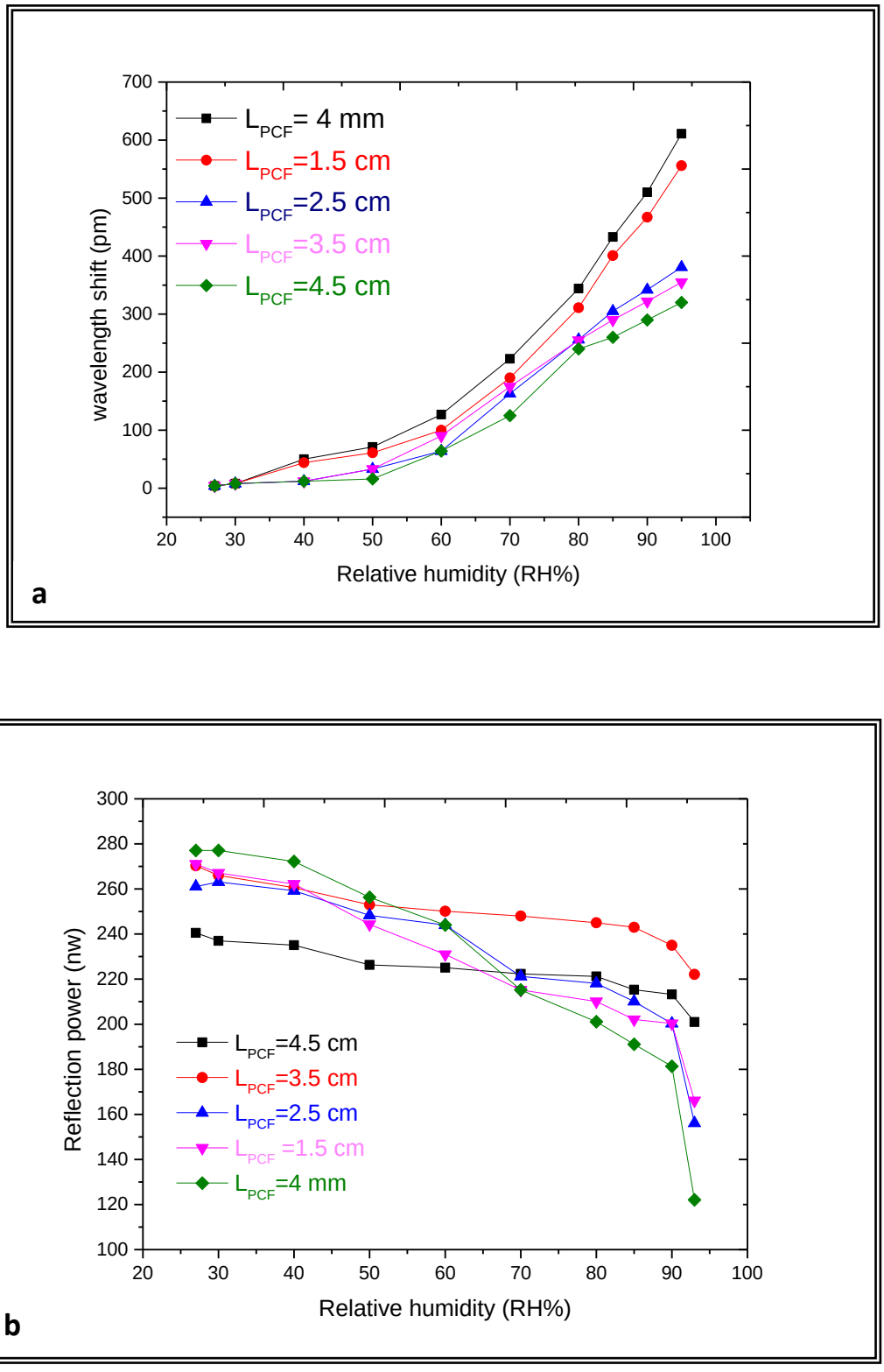

Fig. (3.13 a) : behavior of all lengths for wavelength shift with RH .

b)behavior of all lengths for reflection power with RH

As seen in Figs. (3.13(a,b)), it is observed that there are no any shift in interference peak and no decreasing in reflection power for lengths (4.5 , 3.5 and 2.5) cm between (27%-40%) RH region, the shift being to appear from relative humidity value 40% RH while the shift is observed in wide range (30% -95%) for lengths 1.5cm and 4mm .

The sensitivity values observed for the different PCF length in the region between (30%-95%) RH, summarized in the Fig.(3.14)

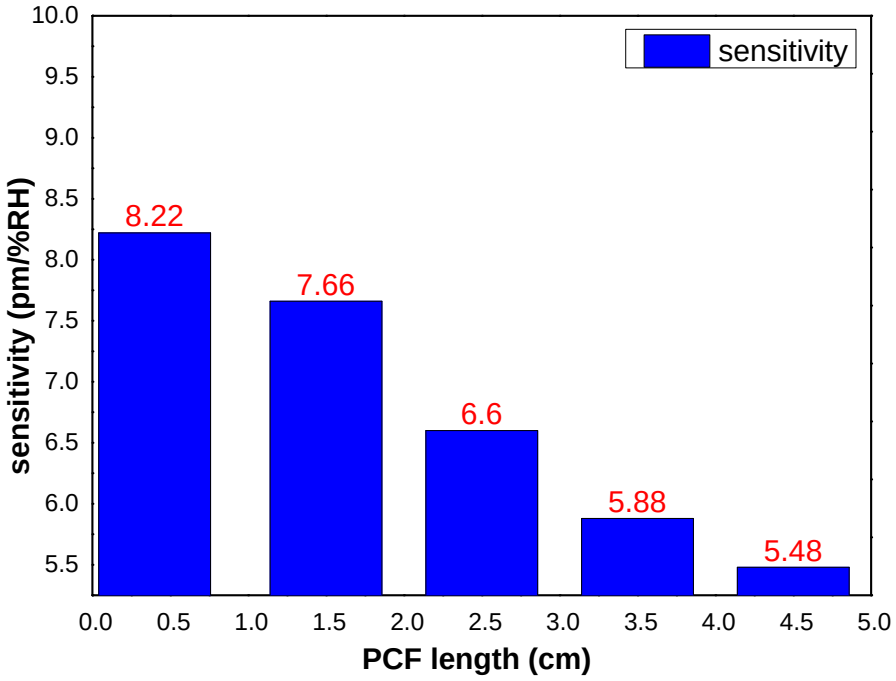

Fig (3.14) The sensitivity values obtained from different PCF lengths

3.4.3 The Effect ofthe PCF Length on The Sensor Sensitivity:-

It is clear that by using equation (1.14) when the length of the PCF is less than 5 mm the fringes spacing will be greater than 100 nm. Therefore for a small sensor length only a narrow sub-periodic part of the interference pattern with a 10 nm span can be observed.As seen in Fig. (3.14) it observed that PCFI with length 4mm show the higher sensitivity(8.49073 pm/RH%)

compared with the other PCFI lengths,in this experiment a length of 4 mm for the sensor head was selected. The fringe spacing of a PCFI with a (4mm) length calculated using the equation (1.14) was about 390.016nm.The fringe spacing for a longer PCFI will be shorter which limited the measurement range of the PCFI, the fringe visibility will diminish when the length of the PCF increasing which leaded to increase the propagation loss of the interfering cladding mode as agree with [Mathew, J., et al, 58].

By using a multphysic's program, it calculated the effective refractive index of the PCF. The effective refractive index calculated of AI-PCF was 0.077011 at 1550 nm illustrate in Fig (3.1∘) ,if the refractive index of silica is 1.45 and for agaros gel is 1.12611.

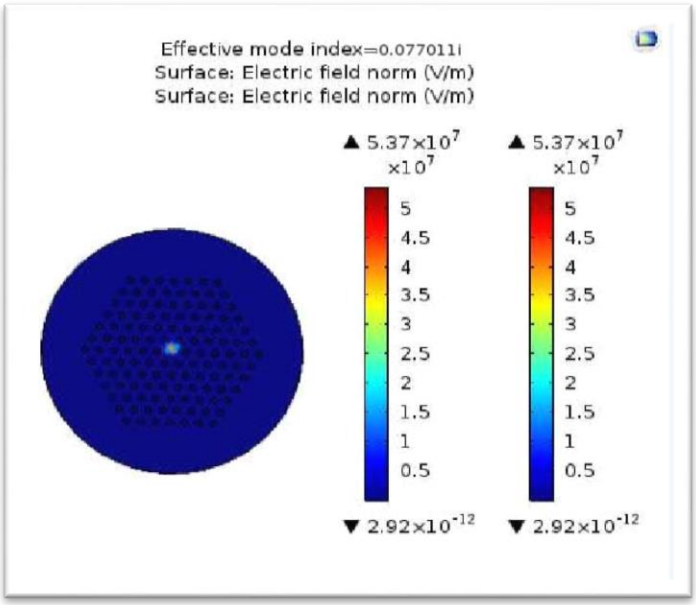

Fig.(3.15) COMSOL image snapshot of infiltrated PCF

Beside that if the length of the PCF section of the interferometer was relatively large the spectra observed may be unduly perturbed by mechanical vibrations and air flow currents. This was because bending or lateral strain of the PCFI may cause a shift in the interference pattern that was not related to

humidity and this phenomenon became more significant as the PCFI length increased. For a sensor head with a short length of 4 mm it was observed that the spectrum was very stable when subjected to vibrations and air flow shown in Fig. (3.16) , when each line represents humidity value. Fig. (3.17) shows the relation between the PCF lengths and sensitivity of the sensor .

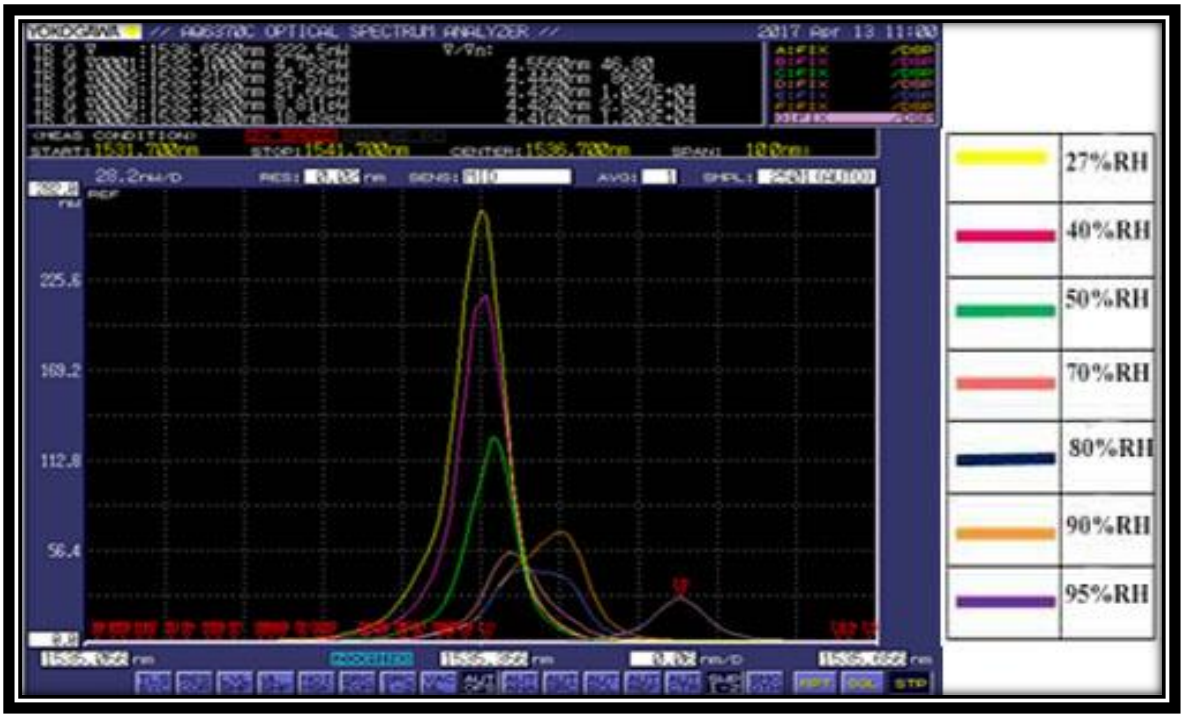

Fig. (3.16) OSA Graphics peaks shift of AI- PCFI with respect humidity of the length 4

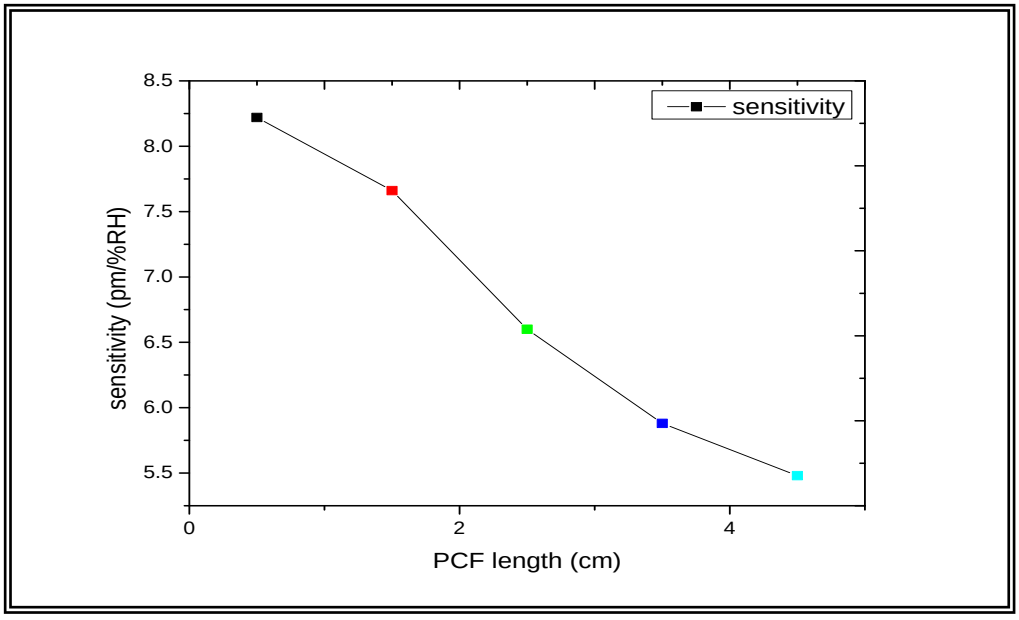

Fig. (3.17):The relationship between PCF lengths and sensitivity of the sensor

So as to confirm that the humidity sensitivity of the PCFI is mainly due to the RI change of the infiltrated hygroscopic material, it is useful to initially study the relative humidity response of a 4mm PCFI prior to infiltration with a hygroscopic material. Fig. (3.13b) shows the changes in the reflection power with respect to ambient relative humidity for a PCFI with length 4 mm. A small change in the reflected signal power (276nW) for a humidity change of(27-40 %RH) the change was observed at higher relative humidity values. Therefore it was concluded that an uninfiltrated PCFI with a compact length had only a weak sensitivity to relative humidity changes. Also this is in agreement with [93] , that when the length of PCF decreases the RH sensitivity of the PCFI increases.

3.4. 4The Rise Timeof RH Sensor Based on AI-PCFI:-

To calculate the rise time of the sensor, PCFI (withcompact length 4mm which was the length that show the higher sensitivity to relative humidity variations)was exposed to an environment with rapid changes of the RH. First, kept the RH in the chamber at 50% RH, and then rapidly increased the humidity of the chamber to>90% (at room temperature and normal atmospheric pressure).

The measured rise time of the sensor is shown in Fig. (3.1^). The sensor had a fast response to humidity variations and the estimated response time from was about**(1.4 s)** when the RH changed from 40% to 90% at wavelength (λ =1550nm). The estimated recovery time of the sensor was 8 s, which depended on how fast the vapor was expelled from the sensor, which in turn was directly proportional to the air flow surrounding the RH sensor.

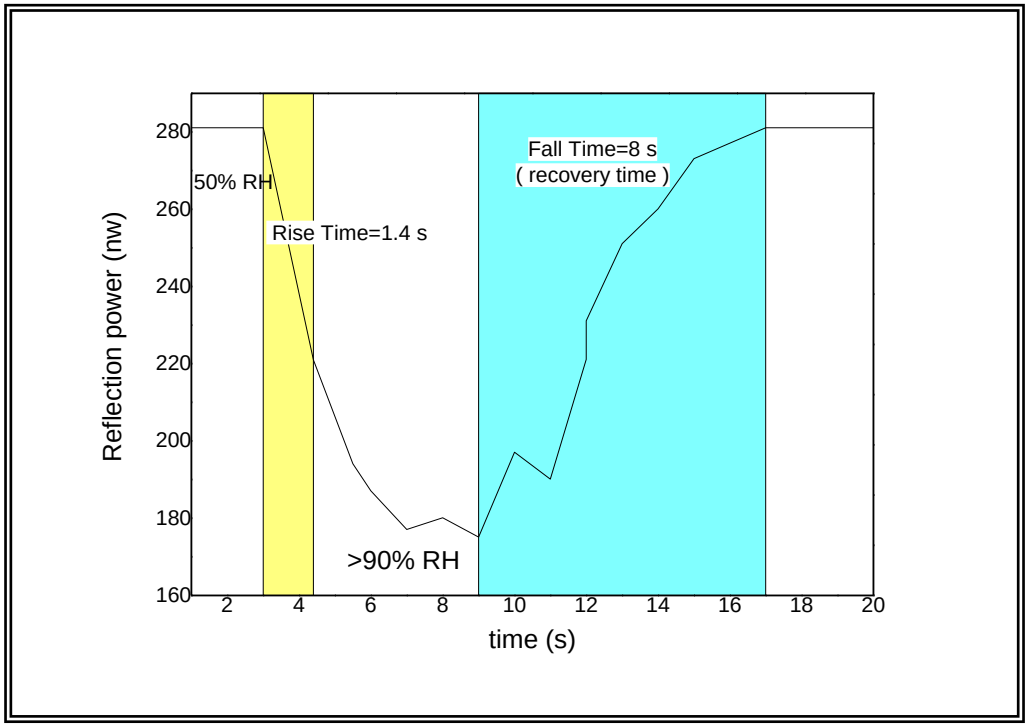

Fig. (3.1^):The rise time of the RH sensor with length (4mm)

3.4. 5 The Repeatability of the RH SensorBased on AI-PCFI:-

In order to make the sensor reusable,the sensor head had been protected to attach any materials to it and was kept in sealed box at room temperature (23 ^{0}C) to prevent any contamination (dust particles, organic pollutants and chemical vapors). The other way to remove the contaminants without damaging the sensor head was the ultrasonic cleaning with heating. The repeatability of the RH sensors over a large RH range (27%-95%)RH was demonstrated with a time gap of eight days ,and with (4mm) PCFI length, the sensor showed a good repeatability,as shown in Fig. (3.19).

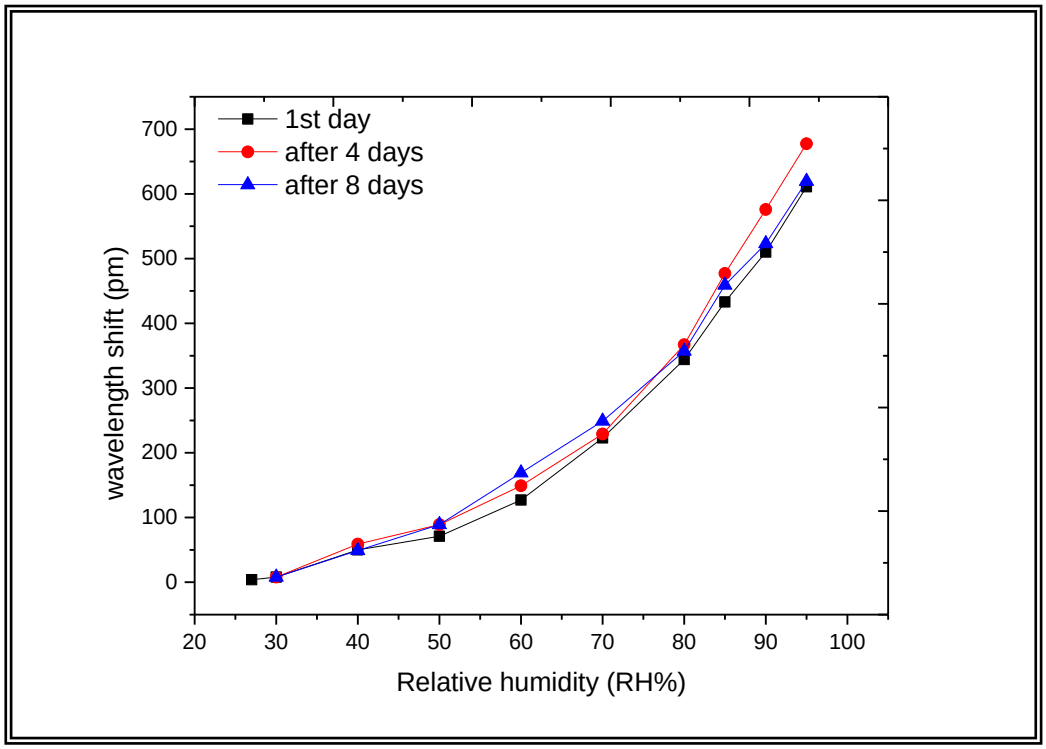

Fig. (3.19): The repeatability of the RH sensor with PCF length (4mm)

3.5 Experimental investigationand discussion of RH sensor based on an agarose coated transmission type photonic crystal fiber interferometer

It was studied an uncoated PCFI transmission type with a short (1 cm) length of (PCF) ,it found there was no wavelength shift based in Figs.(3.20) and Fig.(3.21(a)) and no decreasing in transmitted power when increased the RH <90 % as shown in Fig.(3.21(b)). This was because water has a hydrogen-bonded network (ice-like), which grew up as the relative humidity increased and continues growing to saturation [58].

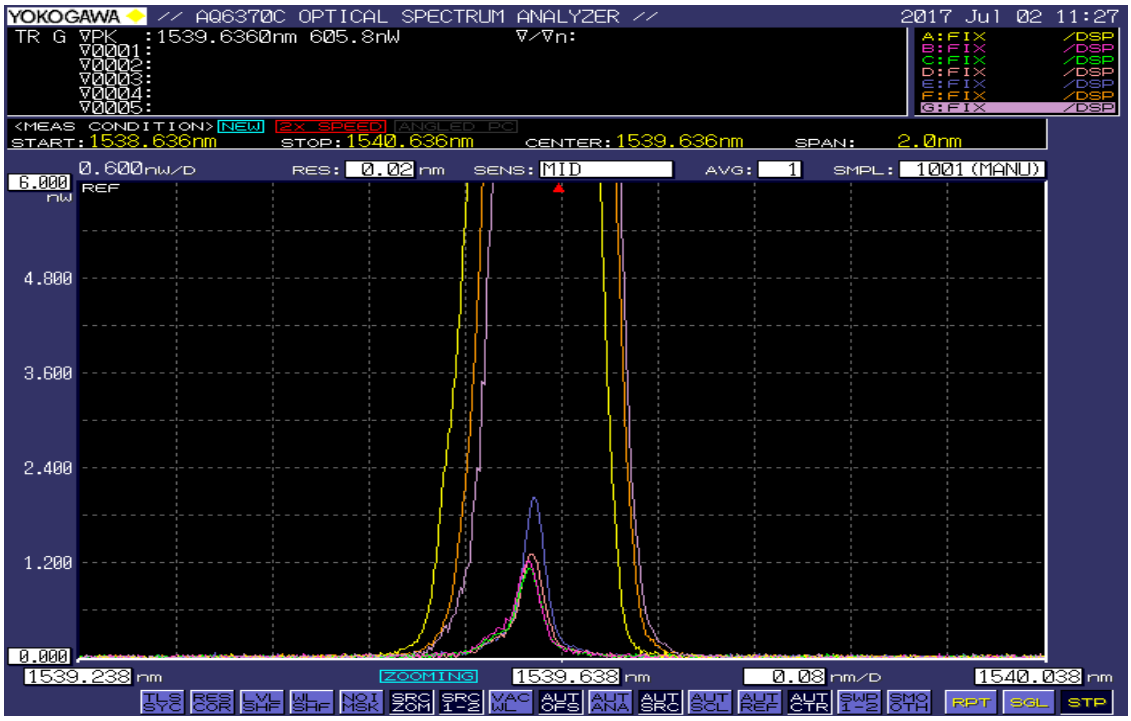

Fig.(3.20) The shift in Wavelength peak of PCFI without coating in humidity chamber

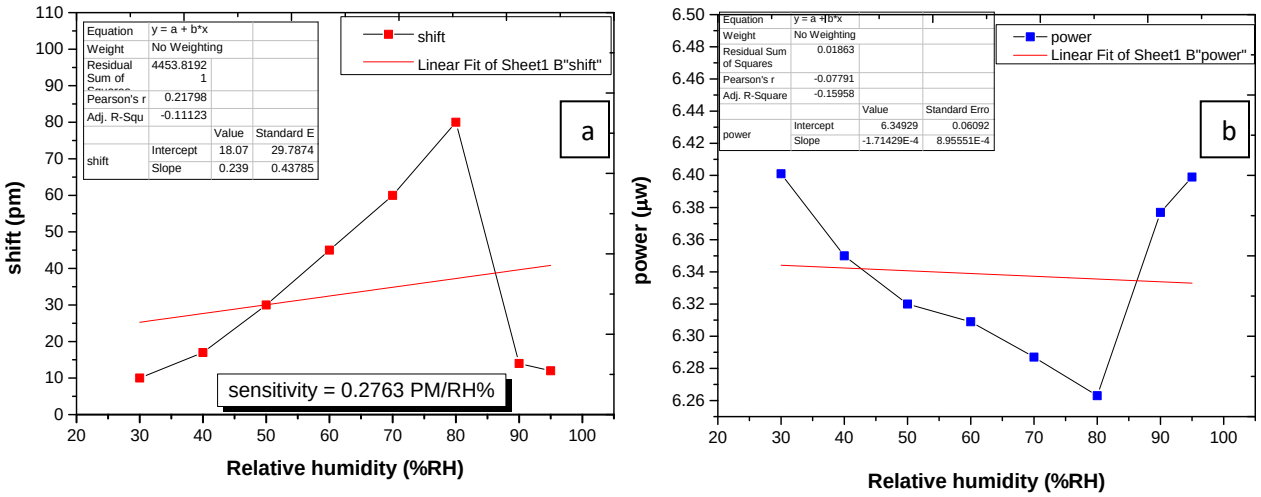

Fig.(3.21)a) Change in the transmission spectrum of a PCFI without coating of length 10mm with respect to different ambient RH values. b) Change in the transmission power of a PCFI without coating of length 10mm with respect to different ambient RH values.

The agarose was coated in order to improve the humidity sensitivity of PCFI. An uniform coating thickness can be accomplished by utilizing the setup as seen in chapter two in Fig. (2.19) by changing the drawing speed of

the fiber through the solution or passing the fiber multiple times through the hot solution. thus in this experiment, the PCFI was drawn through the solution with a fixed speed of 5 mm/s . In practice after passing the fiber through the solution the spectral red shift was observed in the transmission spectrum of the device compared with its initial spectrum that shows on Figs. (3.21(a,b)) .

Fig.(3.21)a) Wavelength peak of PCFI before coating. b) The shift in Wavelength peak of PCFI after coating is about 1.014 nm

3.5.1Effect of coating thickness on The Sensor Sensitivity:-

In order to study the influence of the Agarose film thickness on the properties of the PCFI the four PCFI devices (A, B, C, D) previously fabricated were coated with different thicknesses of Agarose film by passing the PCFI through the solution multiple times. The coated thickness of the device was estimated using an optical microscope at a room RH of 30±2%. Table (3.3) shows parameters of the different AC-PCFI Devices.

Table (3.3) Different Parameters of the AC-PCFI Devices

AC-PCFI	A	B	C	D
Red peak shift of the coated PCFI relative to the uncoated PCFI (nm)	0.284	1.014	1.186	1.238
No. of passes	1	2	3	4
The thickness of coating (nm)	300	630	3530	5966

The humidity responses of the AC-PCFI devices were studied by putting them inside a controlled environmental chamber. The ambient temperature during the experiment was 25°C at normal atmospheric pressure, the thickness changed of the Agarose coating for a changed of RH, the RI of the Agarose coating thickness changed and also increased when RH increased.

At the point when the RH level increased, more water molecules were diffused into the Agarose coating, resulting in the Agarose inflation and increased in the coating thickness, like to any other swelling polymer, an increasing in water content will decrease the bulk RI of the Agarose coating [72].

As the coating thickness increased lead to change optical path , resulting in a red shift of the interference spectrum for all RH values and this was the case with the devices A and B.

Fig. (3.22) illustrates the peak shift of the interference pattern of the AC-PCFI A and B with respect to RH. The AC-PCFI (A) showed a spectral red shift with an increased in RH and the observed shift was linear in the range from 27 to 95% RH with a slope of 5.25914 pm/%RH, as shown in OSA graphics in Fig.(3.23a).

As seen from Fig.(3.2٢)shows the AC-PCFI (B) shift to long wavelengths with a slope of 7.937 pm/%RH in the RH range 27 to 95% as illustrate in OSA graphics in Fig.(3.2٣b). It can be concluded that when the coating thickness increases the RH sensitivity of the AC-PCFI also increases.

This behavior had one possible reason that when the thickness of the coating increases, It is observed that when the thickness of coating is more than ~756 nm, which was the case with AC-PCFI devices C and D, the observed shift was blue for the interference spectrum of the AC-PCFI device when the RH increases.

For investigation that the penetration depth of the evanescent wave of device (C) was calculated at 40% RH using Eq. (1.15) by set the values of the RI of the fiber material silica n_{cl} = 1.44, the RI of the Agarose coating n_{ac} = 1.12611and assumed the angle of incidence at the fiber– coating interface θ= 90°. These values were used to calculate penetration depth was 756.09756 nm, verifying the observation that the wavelength shift changed from a red to a blue shift when the coating thickness was in the region of 756 nm.

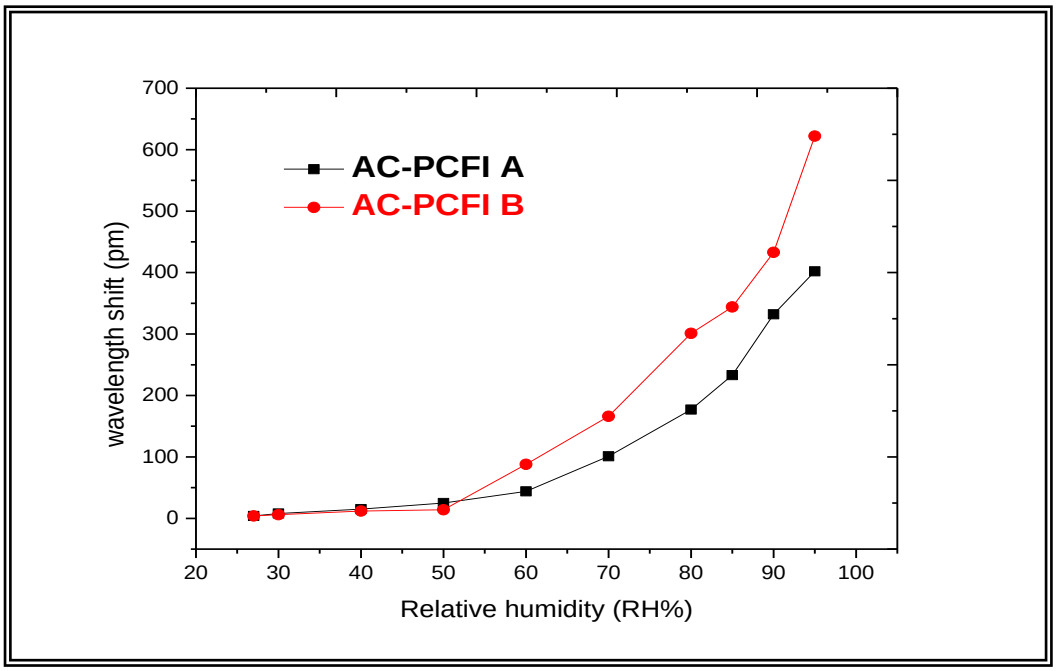

Fig. (3.2٢) The spectral peak shift of AC-PCFI A and B with respect to relative humidity.

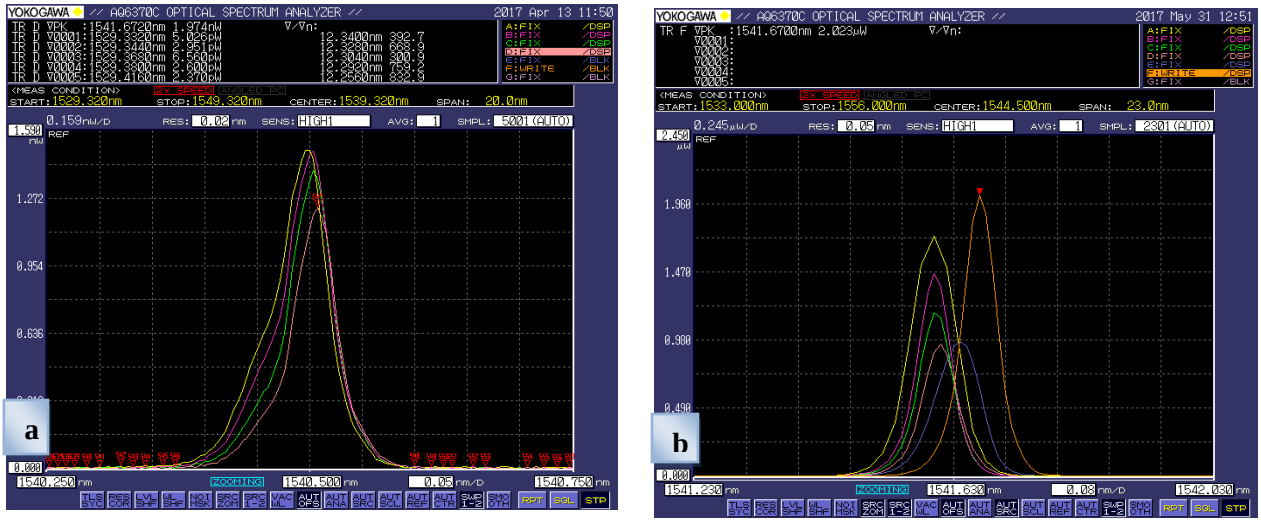

Fig. (3.2ᵛ) OSA Graphics peaks shift of AC- PCFI(A) with respect humidity. b) OSA Graphics peaks shift of AC- PCFI(B) with respect humidity

The RH responses of the AC-PCFI devices C and D are shown in Fig. (3.24).

The ACPCFI (C) showed no a spectral shift when humidity increased from 27% RH to 40% RH and then it showed a blue shift on a further increased of RH from 40% to 95% as seen from Fig.(3.25a). This was because below 40% RH the thickness changed factor dominated by comparison to the bulk RI change of the coating, and above 40% RH the coating thickness was more than the penetration depth of the evanescent wave part of the cladding mode interacting with the coating so that the effective RI of the cladding mode is chiefly dictated by the coating bulk RI.

For AC-PCFI (D) the peak wavelength phase changed point (RH at which the red shift changes to blue shift) of the RH response curve shifted to lower RH of 40% which was expected because here the coating was thicker than for AC-PCFI (C) that show in Fig (3.24) and OSA graphics Fig. (3.25b).

For AC-PCFI (D) the RI of the coating was in a greatest RI sensitive region of the PCFI and the RH sensitivity observed was also higher compared

to other devices with a smaller thickness of Agarose coating. The AC-PCFI (D) showed a sensitivity of -29.37394 pm/%RH in range (27-95)%RH.

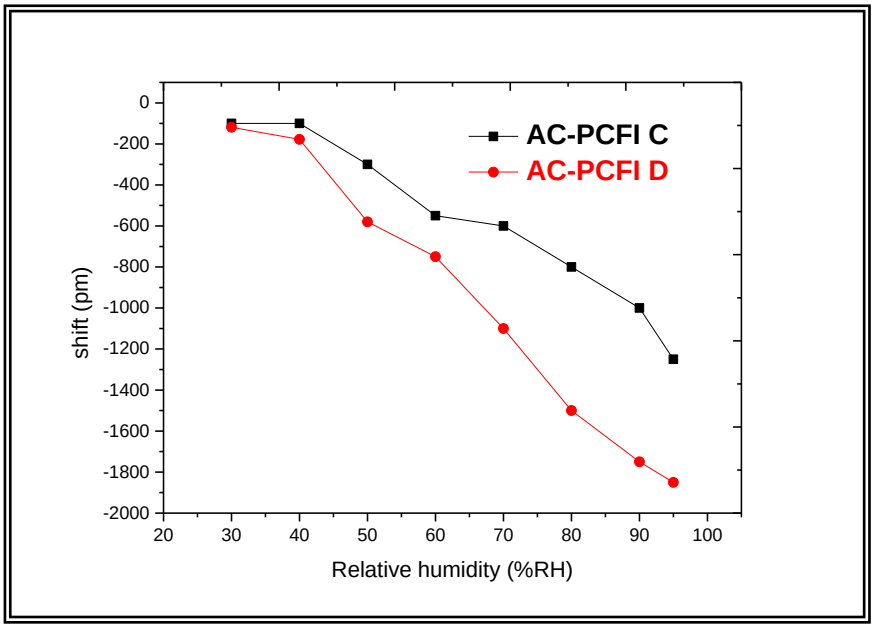

Fig. (3.24) The spectral peak shift of AC-PCFI C and D with respect to RH.

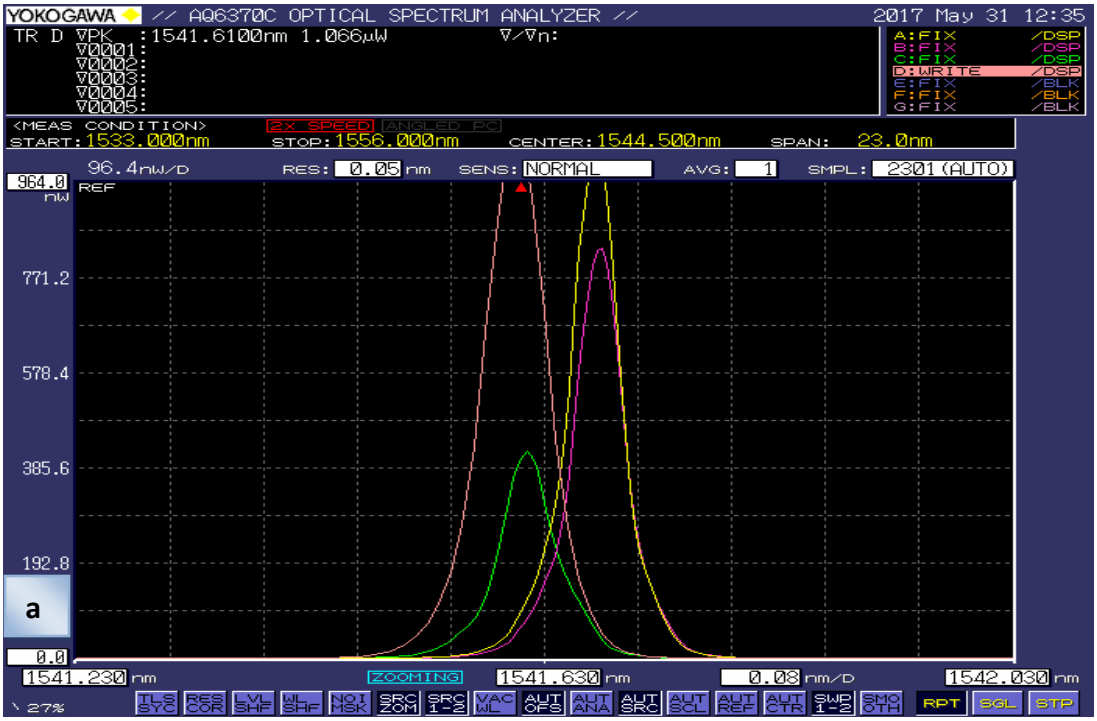

Fig. (3.25)a) OSA Graphics peaks shift of AC- PCFI(C) with respect RH .

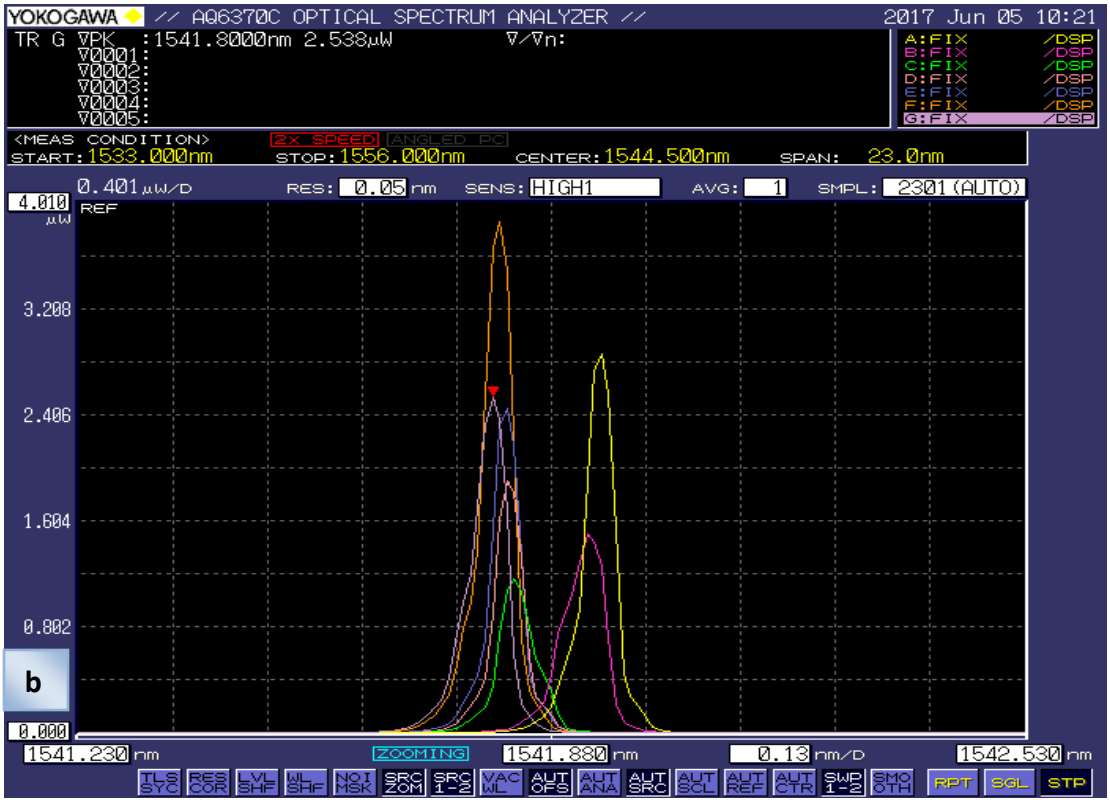

Fig. (3.25) b) OSA Graphics peaks shift of AC- PCFI(D) with respect RH.

The calculated RH sensitivities of the AC-PCFI devices in various linear RH values were recorded in Table(3.4) , where the positive sensitivity values represent spectral red shift and negative values represent a blue shift.

Table (3.4) RH Sensitivity of AC-PCFI Devices

AC-PCFI	A	B	C	D
Sensitivity (pm/%RH)	5.25914	7.93756	-17.3527	-29.37394

3.5. 2The Rise Time of RH Sensor Based on AI-PCFI:-

The response time was calculated of the sensor, (with AC-PCFI device(D) which showed the higher sensitivity to relative humidity variations(-29.37394 pm/%RH) was exposed to an environment with rapid

changes of the RH. A similar experimental conditionis maintained as AI-PCFI. The sensor measured rise time is shown in Fig.(3.26) , it had a fast response to humidity variations and the estimated response time from (10 % to 90% of the signal maximum) was about 0.8 s when the RH changed from (50% to 90 %) at wavelength 1550nm. The recovery time of a humidity sensor relies upon on how quick the water vapor is expelled from the sensor which is proportionate to the air flow surrounding the sensor. The estimated recovery time (90% signal maximum to 10% baseline) of the sensor is 7 s.

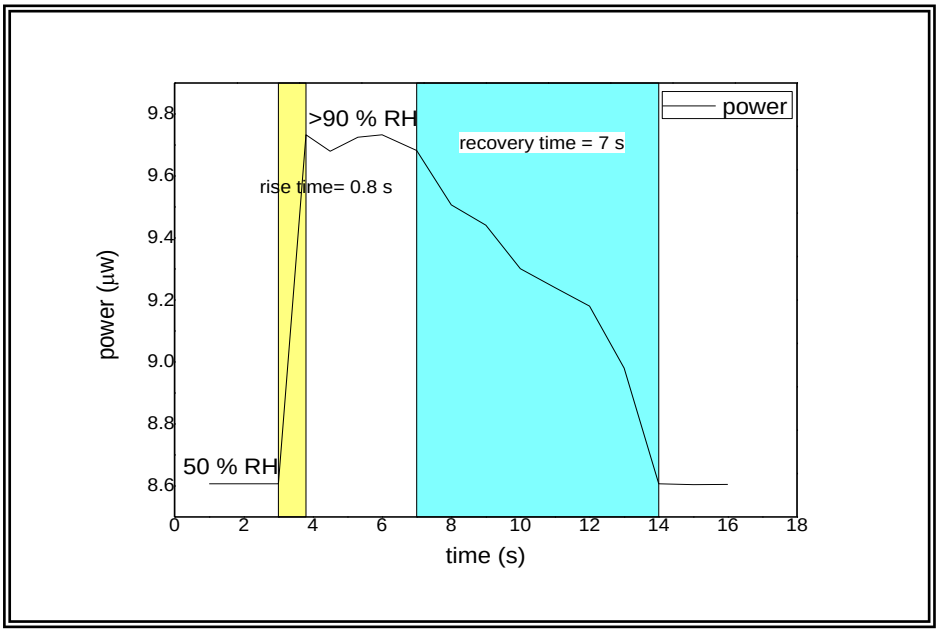

Fig.(3. ٢6). Response time of the sensor.

3.5. 3Long term stability of the RH SensorBased on AC-PCFI:-

The operation of RH sensor requires direct interaction with the environment, therefore its performance usually degrades over a period of time due to the different types of contamination, making any sensor unsuitable for long term humidity measurements without special protection. Possible contamination agents are dust particles, organic pollutants and chemical vapors thus protection of the sensor head using anti-contaminant filters,

another method to overcome contamination is ultrasonic cleaning and subsequent heating (which will remove the contaminants such as dust particles without damaging the sensor head.

In order to study the repeatability of the Agarose coated PCFI sensor (D), experiments were repeated one week after since the initial experiments.

A similar experimental condition was maintained for both sets of measurements. For comparison the averaged relative humidity responses obtained for the sensor during the two sets of measurements were plotted in Fig.(3.27) The relative humidity responses obtained were similar, confirming good long term stability for the sensor.

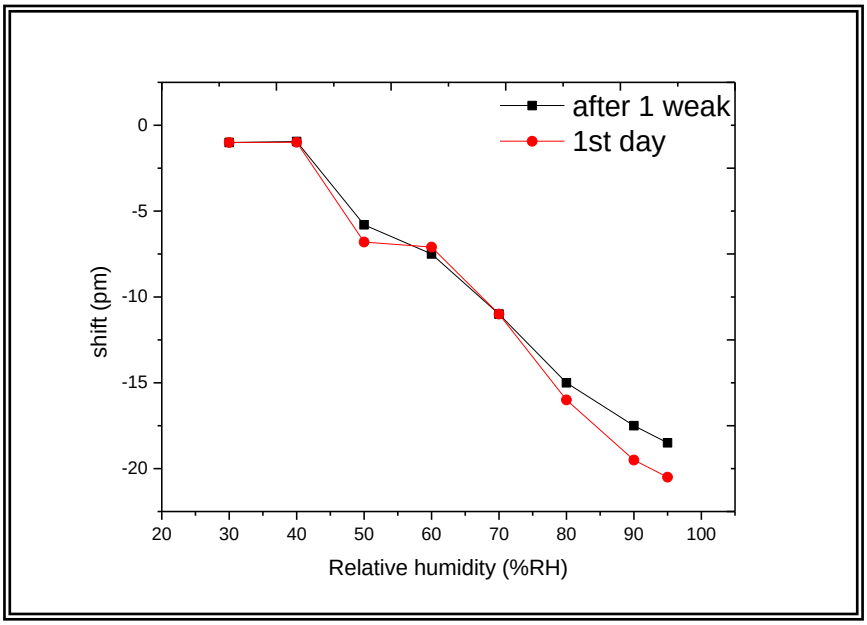

Fig. (3.27): The repeatability of the AC-PCFI sensor (D)

3.6 Performance comparison of the RH sensors:-

The performance comparison of the RH sensing devices Based on the parameters in RH range(27%-95 %), RH sensitivity, response time, sensor size, advantages and limitations of the sensor is presented in tables(3.5).

Table (3.5) Comparison of RH sensors

Comparative Criteria	RH Sensor	
	AI-PCFI	**AC-PCFI**
Higher sensitivity	(8.49073 pm/RH%)	(-29.37394 pm/%RH)
Size of sensor head	4mm	1 cm
Response time	1.4 s	0.8 s
Advantages of the sensor	• Wide linear response • Fast response time • Diminutive size • Improved sensitivity • Best Mechanical stability • The sensor is end type since it requires just single interconnection fiber. • Best sensor for breathing monitoring as shown in Fig. (1.23)	• Wide linear response • Fast response time • Can be tunable the RH sensitivity by changing the thickness of the coating • Sensitivity improvement • Simple fabrication, low cost • Suitable for high RH operation
Limitations of the sensor	• Only an approximate fabrication repeatability is possible because of the limitations in the fabrication accuracy	• Not an end type sensor because it requires an input and output fiber connected to the sensor • Sensor fabrication is costlier

As seen in table (3.5) the sensor based on an AC-PCFI shows the higher response time and sensitivity than the sensor based on an AI-PCFI while the last has the smaller size and good mechanical stability and suitable for breathing monitoring.

3.7 Simulation result for COMSOL Multiphsics Program for solid core PCF(LMA-10)

The solid core of the empty PCF(LMA-10) was interrogated by the transmission of laser with wave length (1550nm) was obtained simulation using COMSOL multiphysics program as show in Figs. (3.28).

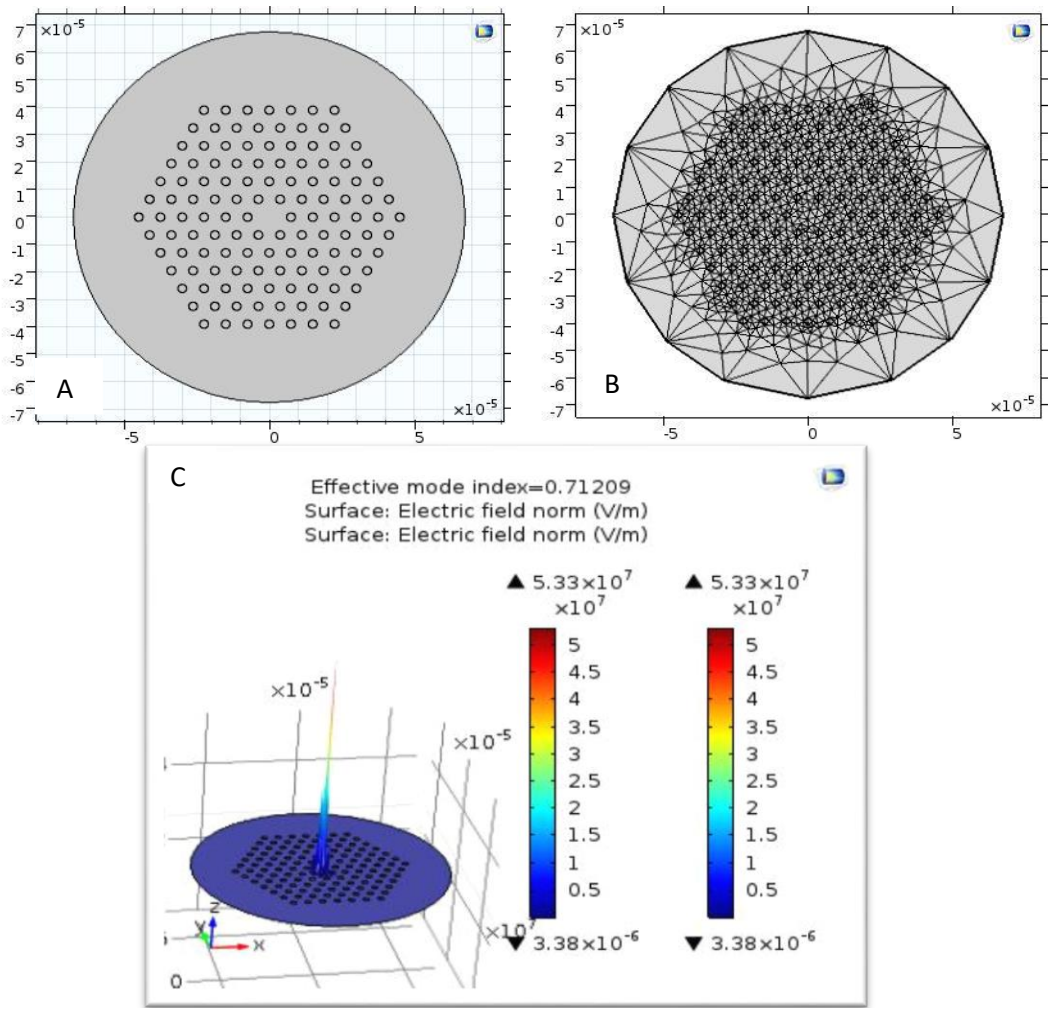

Fig. (3.28) (A) geometry of cladding PCF with refractive index of air =1(B) Mesh of PCF (C) Laser beam profile that exist from PCF(LMA-10) without infiltration

3.7.1 Infiltrated solid core PCF(LMA-10) with agarose solution:

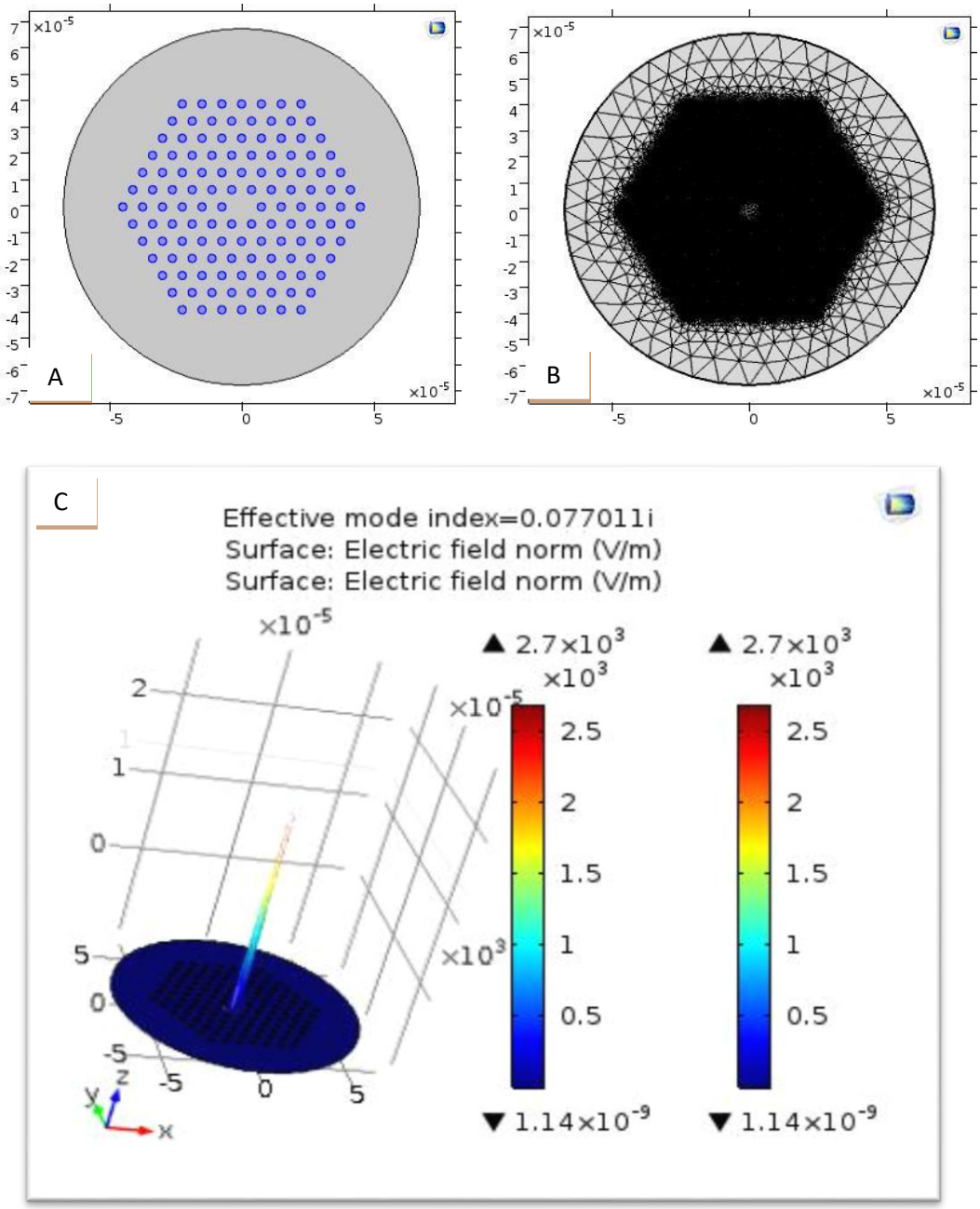

Fig. (3.29) (A) geometry of cladding PCF infiltrated agarose with refractive index =1.12 (B) Mesh of PCF (C) Laser beam profile that exist from PCF(LMA-10) with infiltration.

3.7.2Coated soild core PCF(LMA-10)with agarose solution at thickness 5996 nm:

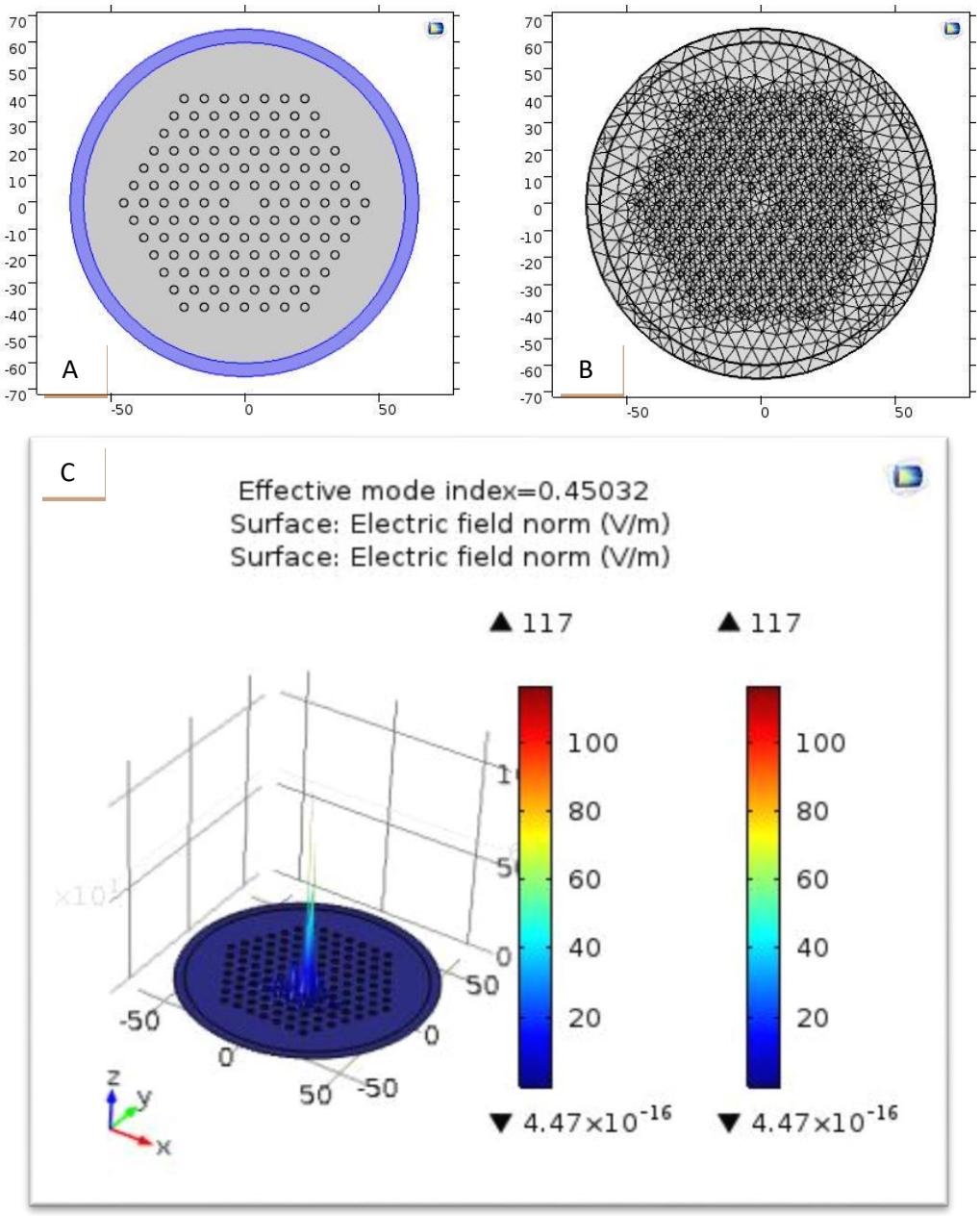

Fig. (3.30) (A) geometry of cladding PCF with coating of agarose thickness=5996nm (B) Mesh of PCF (C) Laser beam profile that exist from PCF(LMA-10) with PCF agaros coated.

3.7.3Coated soild core PCF(LMA-10)with agarose solution at thickness 3530 nm:

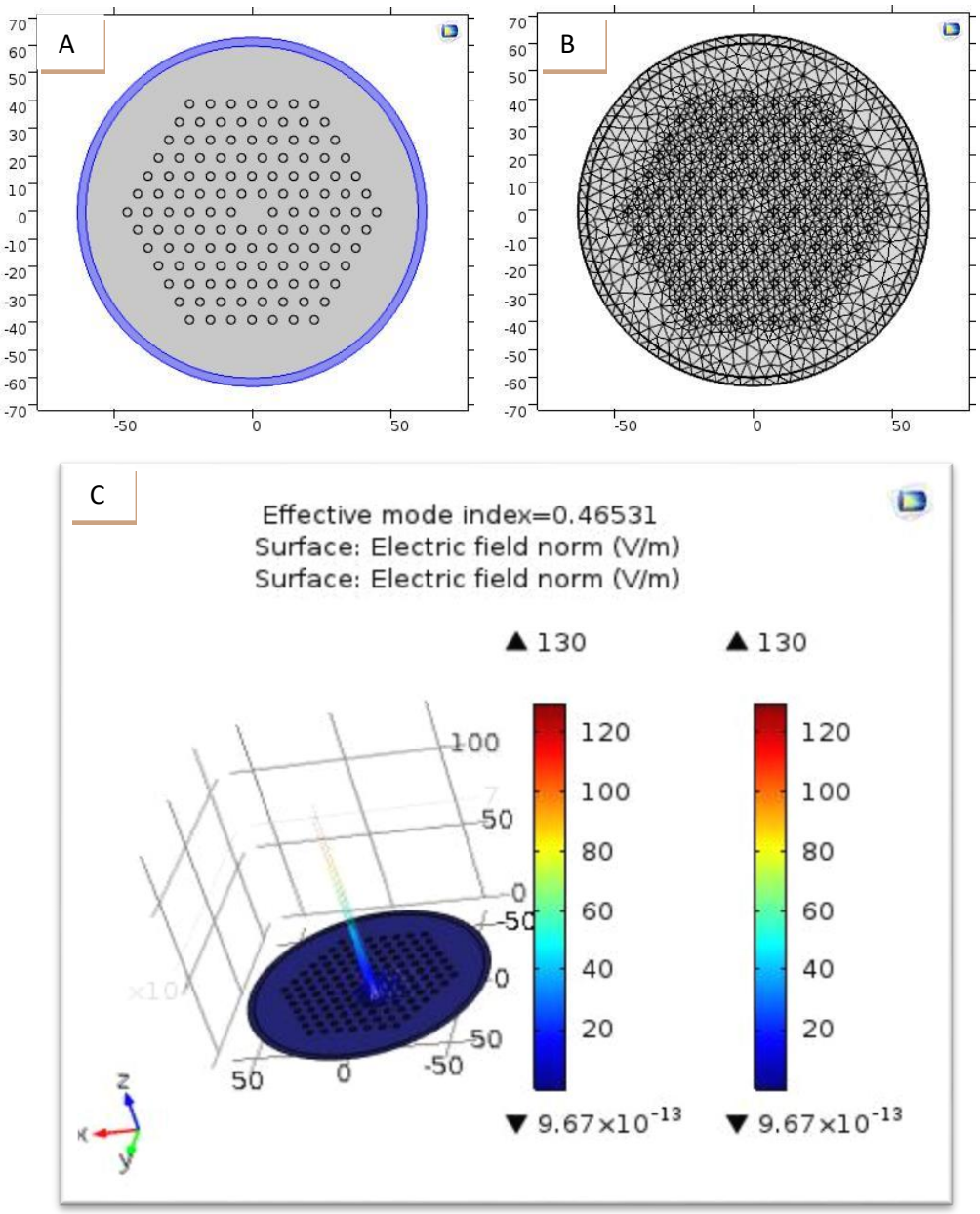

Fig. (3.31) (A) geometry of cladding PCF with coating of agarose thickness=٣٥٣٠nm (B) Mesh of PCF (C) Laser beam profile that exist from PCF(LMA-10) with PCF agaros coated.

3.7.4Coated soild core PCF(LMA-10)with agarose solution at thickness ٦30 nm:

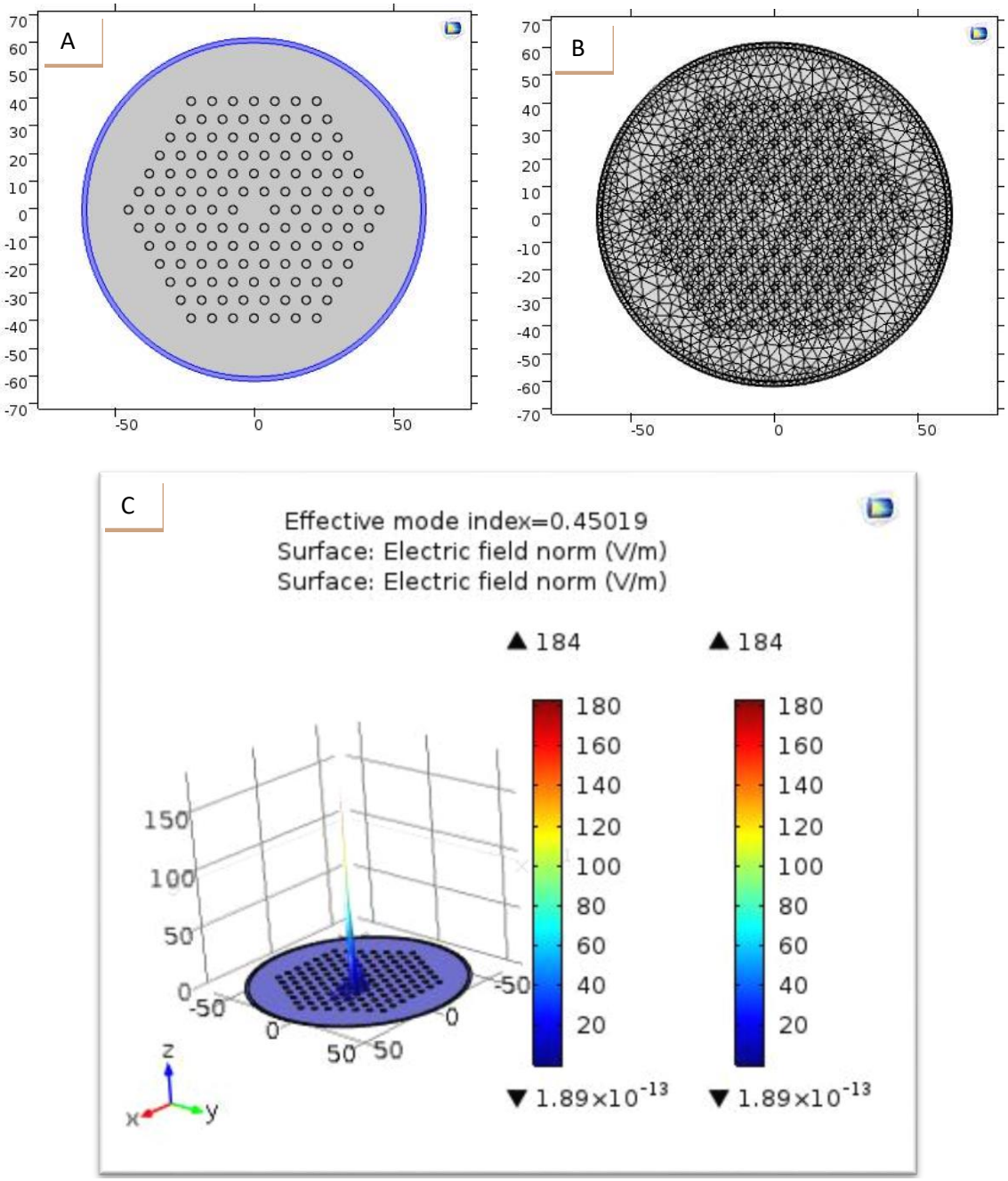

Fig. (3.32) (A) geometry of cladding PCF with coating of agarose thickness=٦٣٠nm (B) Mesh of PCF (C) Laser beam profile that exist from PCF(LMA-10) with PCF agaros coated.

3.7.5Coated soild core PCF(LMA-10)with agarose solution at thickness ٣٠0 nm:

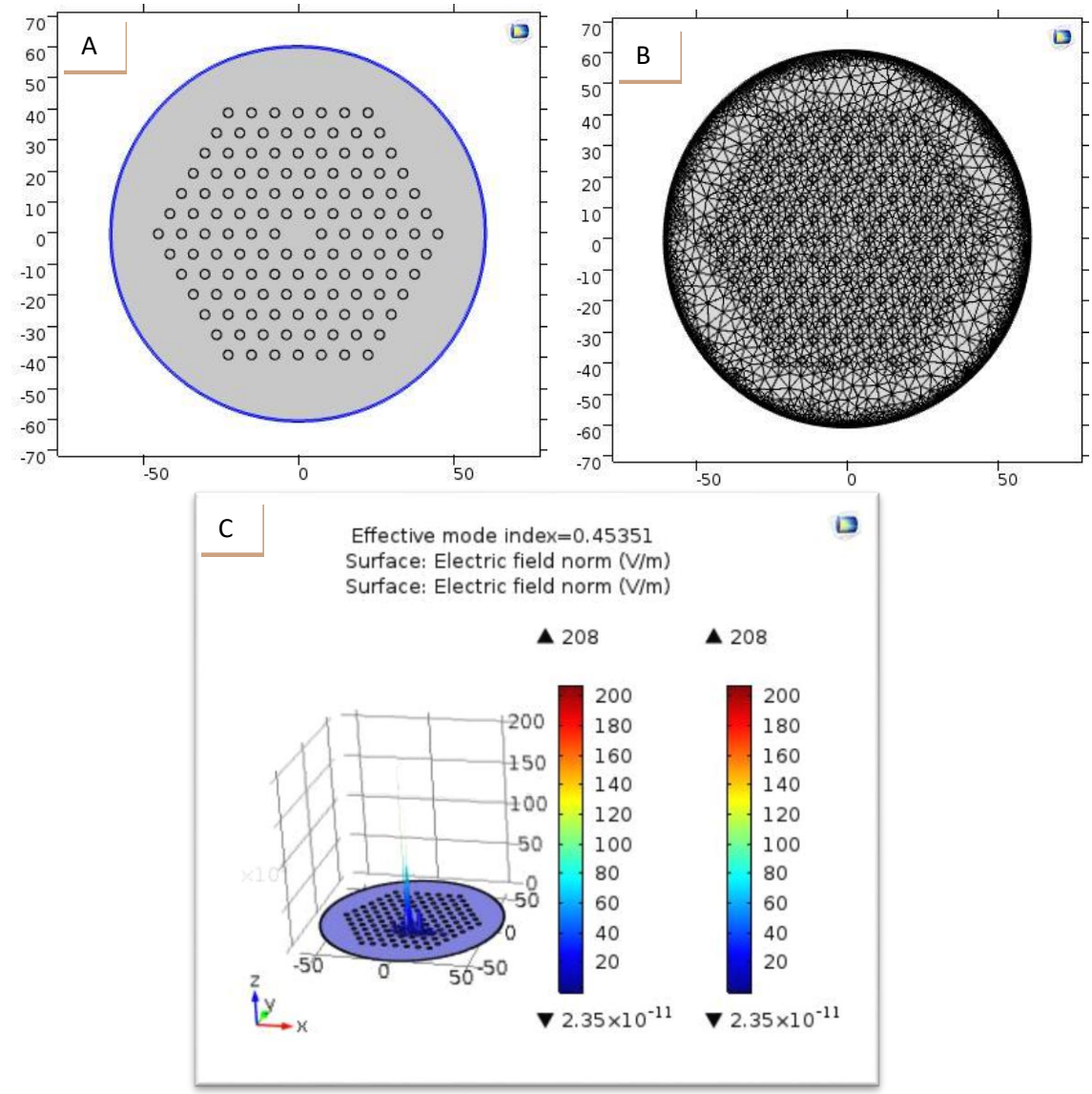

Fig. (3.33) (A) geometry of cladding PCF with coating of agarose thickness=٣٠٠nm (B) Mesh of PCF (C) Laser beam profile that exist from PCF(LMA-10) with PCF agaros coated.

As seen in Fig. (3.28) that show the light guidance for solid core PCF(LMA-10) at wavelength 1550 nm when the PCF was empty (air), the effective mode index is 0.71209 . The infiltration of the PCF microholes with agarose change the effective RI of the cladding mode, thus the effective RI of

the cladding mode depends on the RI of the Agarose material infiltrated into the PCF as shown in Fig (3.29). When humidity increased, the RI of Agarose increased and the effective index of the interfering cladding mode increased and as a result the interference pattern shifted to longer wavelengths (red shift) .

The Agarose coating changed the effective index of the cladding mode too with respect to RH and consequently the phase difference between the interfering cladding modes and the core mode produced a shift in the interference pattern. An increase in the effective RI of the cladding mode caused a red shift and a decreased in the effective RI caused a spectral blue shift. The peak of the laser was clear and very smooth. Figs.(2.28), (3.29) , (3.30),(3.31),(3.32) and (3.33) demonstrates the simulation result.

3.8Conclusions:-

3.8.1 RH sensor based on AI-PCFI

1- The sensor showed a shift to long wavelength (red shift) in its interference pattern due to the adsorption and desorption of water vapour with respect to ambient humidity.
2- The shorter PCF length is higher sensitivity.
3- Infiltration region depends on capillary forces, temperature and the length of the PCFI , infiltration length increase with increase of PCF length.
4- The maximum sensitivity of the sensoris 8.49 pm/RH% in the range 27–95 % RH has been obtained in 4mm, high resolution, low cost, wide humidity range , ease of fabrication , repeatable , shows good long term stability and Fast response time of 1.4 s.

5- An additional advantage of selecting a compact length for the sensor. is that such a sensor is more mechanically stable in the presence of vibrations and air flow currents.

3.8.2RH sensor based on AC-PCFI

1- The humidity response of an AC-PCFI sensor depended on both bulk RI change and the thickness change of the Agarose coating with respect to RH.

2- The sensor showed a linear response for an RH change in the RH ranges of 27–95 % RH which shifted to short wavelength (blue shift) .

3- The sensor showed maximum sensitivity was (-29.37394pm/%RH) at agarose coating thickness 5.966μm, Showed good repeatability , reversible , wide humidity range and Fast response time of 0.8 s.

3.9 Future Work:-

1- Sensing enhancement of relative humidity sensor with different concentrations of an agarose - coated photonic crystal fiber interferometer.

2- Sensitivity enhancement of relative humidity sensor based on an Agarose coated single mode fiber bend.

3- Enhancement the RH Sensor with a PVA-coated photonic crystal fiber Interferometer

4- Improvement the humidity sensor based on waist-enlarged tapers Mach–Zehnder interferometer

5- Sensing enhancement of relative humidity sensor based on single mode fiber bend.

6-study temperature effect of RH sensor based photonic crystal fiber interferometer.

References

References

[1] H. J. Patrick, G. M. Williams, A. D. Kersey, J. R. Pedrazzani, and A. M. Vengsarkar. "Hybrid fiber Bragg grating/long period fiber grating sensor for strain/temperature discrimination". IEEE Photonics Technology Letters. 8, 1223–1225. (1996).

[2] W. C. Goss, R. Goldstein, M. D. Nelson, H. T. Fearnehaugh, and O. G. Ramer. "Fiber-optic rotation sensor technology". Applied Optics, 19, 852-858 (1980).

[3] Yi-Ping Wang, Limin Xiao, D. N. Wang, and Wei Jin "Highly sensitive long-period fiber-grating strain sensor with low temperature sensitivity" Optics Letters, **31**(23) 3414-3416 (2006).

[4]Yoany Rodríguez García, Jesús M. Corres, and Javier Goicoechea "Vibration Detection Using Optical Fiber Sensors". Journal of Sensors. Article ID 936487 (2010).

[5] Minghong Yang, Jixiang Dai, Ciming Zhou, and Desheng Jiang. "Optical fiber magnetic field sensors with Tb DyFe magnetostrictive thin films as sensing materials". Optics Express, **17**(23) 20777-20782 (2009).

[6] Wenhui Wang, Nan Wu, Ye Tian, Christopher Niezrecki, and Xingwei Wang "Miniature all-silica optical fiber pressure sensor with an ultrathin uniform diaphragm" Optics Express, **18**(9) 9006-9014 (2010).

[7]. M. R. Layton and J. A. Bucaro "Optical fiber acoustic sensor utilizing mode-mode interference" Applied Optics, **18**(5) 666-670 (1979).

[8] LinaXu, Joseph C. Fanguy, KrunalSoni, and Shiquan Tao "Optical fiber humidity sensor based on evanescent-wave scattering'Optics Letters, **29**(11) 1191-1193 (2004).

[9]. Tian-Hao Xia , A. Ping Zhang , BoboGu and Jing-Jing Zhu "Fiber optic refractive-index sensors based on transmissive and reflective thin-core fiber modal interferometers" ,Optics Communications, **283**(10) ,(2010).

[10]Shuichi Tai, Kazuo Kyuma, and Masahiro Nunoshita "Fiber-optic acceleration sensor based on the photoelastic effect" Applied Optics, **22**(11), 1771-1774 (1983).

[11] S. C. Huang, W. W. Lin, M. T. Tsai, and M. H. Chen. "Fiber optic in-line distributed sensor detection and localization of the pipeline leaks". Sensors and Actuators A, **135**(13) 570–579, (2007).

[12] L. Zou and O. M. Sezerman. "Method and system for simultaneous measurement of strain and temperature". United States Patent, US 7,599,047 B2, (2009).

[13] M. E. Bosch, A. J. R. S´anchez, F. S. Rojas, and C. B. Ojeda. " Recent development in optical fiber biosensors ". Sensors journal, **7**,797–859, (2007).

[14] P. A. E. Piunno, U. J. Krull, R. H. E. Hudson, M. J. Damha, and H. Cohen. "Fiber optic biosensor for fluorimetric detection of DNA hybridization". Analytica Chimica Acta, **288**(3):205–214, (1994).

[15]T. Kumagai, H. Soekawa, T. Yuhara, and H. Kajioka. "Fiber optic gyroscopes for vehicle navigation systems". Proceedings of SPIE, **20**(70) 181–191, (1994).

[16] Pinto, A., and Lopez-Amo, A., "Photonic Crystal Fibers for Sensing Applications", Journal of Sensors, **2012**, 1-21, (2012).

[17] P. Joshi, R. Share, J. Kishore and S. Kher, “Fabrication of Photonic Crystal Fiber", Current Science, **93** (10)1214-1215, (2007).

[18] J. D. Joannopoulos, S. G. Johnson, J. N. Winn and R. D. Meade, “Photonic Crystals Molding The Flow of Light”, 2nd Ed. Book, Princeton University Press UK , (2008).

[19] Mathew, J., Semenova, Y., and Farrell, G., 2012, "Photonic Crystal Fibre Interferometer for Humidity Sensing", Ch.8,"Photonic Crystals - Introduction, Applications and Theory",edited by:Massaro, A., In Tech.

[20] Frazao, O., Santos, J., Araujo, F., and Ferreira, L., "Optical sensing with photonic crystal fibers", Laser &Photon., **2**(6). 449-459,(2008).

[21] Chen, J.,2010, "Nanochemistry and Sensing in Photonic Crystal Fibers",Ph. D. thesis, University of Erlangen-Nuremberg, Germany.

[22] Kim, D., Kang, J.,"Sagnac loop interferometer based on polarization maintaining photonic crystal fiber with reduced temperature sensitivity",Optics Express, **12**(19) 4490-4495,2004.

[23] Alwis, L., Sun, T., and Grattan, K., "Optical fiber-based sensor technology for humidity and moisture measurement", Measurement **46(11)**, 4052-5074, (2013).

[24] G.keiser, "optical fiber communications", Mcgraw-Hill series in electrical engineering, 2nd addition, (1991).

[25] K., Fidanboylu, and H.s.,Efendioglu, "Optical fiber Sensors and their Applications", 5th International Advanced Technologies Symposium (IATS'09), Karabuk, Turkey, 13-15, May (2009).

[26] M. Arumugam , "Optical Fiber Communication -An Overview", PRAMANA - journal of physics, **57**(5) &(6), 849–869, (2001).

[27] DeGrandpre, M. D.; Burgess, L. W., App. Spec. **44**,273- 279(1990).

[28] B.H. Timmer, K.M.v. Delft, R.P. Otjes, W. Olthuis, A.v.d. Berg, ," A miniaturized measurement system for Ammonia in air", Anal. Chim. Acta **507** (1) 139–145,(2004).

[29] Kim, J., "Analysis and Applications of Microstructure and Holey Optical Fibers",Ph. D. thesis, Blacksburg, Virginia.(2003)

[30] Quimby, R., "Photonics and Lasers,An Introduction",Worcester Polytechnic Institute,Wiley-Interscience Publication,(2006).

[31]. Gong, Q., Hu, X.,"Photonic Crystals, Principles and Applications",Pan Stanford Publishing, (2013).

[32] Sukhoivanov, I., Guryev, I., "Introduction to Photonic Crystals" Ch. 1,"Photonic Crystals, physics and practical modeling", Springer, (2009).

[33] Joannopoulos, J., Johnson, S., Winn, J., Meade, R.,"Photonic Crystals, molding the flow of light",Second Edition,Princeton University Press, (2007).

[34] Yasin, M.,Harun, and Arof, H.,"Recent Progress in Optical Fiber Research", InTech,Croatia, (2012).

[35] Buczynski, R., "Photonic Crystal Fibers",Act Physic Polonic, **106**(2) 141-167, (2004).

[36] Poli, F., Cucinotta, A., Selleri, S., "Photonic Crystal Fibers, Properties and Applications", Springer, (2007).

[37] Zolla, G., Nicolet, A.,Kuhlmey, B.,Guenneau, S., and Felbacq, D.,"Foundations of Photonic Crystal Fibers",Chapter 1,Imperial College Press; 2 edition, (2012).

[38] Jr, A., "Recent progress and novel applications of photonic crystal fibers", IOP publishing, Repots on Progress in Physics, **73**,1-21,(2010).

[39] Mehra R, Tripathi J"Mach-zehnder Interferometer and it's Applications" International Journal of Computer Applications, 31-36 (2014).

[40] Ritari, T., "Novel Sensorand Telecommunication Applications of Photonic Crystal Fibers", Ph.D. thesis,Helsinki University of Technology, Finland,(2006).

[41] Eichenholz, J., "Photonic crystal fibers have many uses", Optoelectronics World, (2004).

[42] A. Ferrando, E. Silvestre, J. J. Miret, P. Andrés, and M. V. Andrés, "Full vector analysis of a realistic photonic crystal fiber" Optics. Letter. **24**, 276-278, (1999).

[43] J. C. Knight, T. A. Birks, P. St Russell and D. M. Alkin, "All-Silica Single Mode Optical Fiber With Photonic Crystal Cladding", Optics Letters, **21**(19) 1547-1549, (1996).

[44] G. Keiser. "Optical Fiber Communications", United States, 3rd edition, (2000).

[45] C. H. Jeong, C. H. Oh, and H. J. Kang, “Simultaneous independent long-period fiber gratings inscribed in holey fibers depending on air-hole size” Optic. Letter. **32**, 2245–2247, (2007).

[46] T. A. Birks, J. C. Knight, and P. St. Russell, “Endlessly single- mode Photonic Crystal Fiber”, Optics Letters **22**, 961-963,(1997).

[47] Hilligsoe, K.," Nonlinear Wave Propagation in Photonic Crystal Fibers and Bose-Einstein Condensates",Ph.D. thesis, University of Aarhus, Denmark, (2005).

[48] Knight, J., Birks, T.,Cregan R., and Russell, P.,"Large mode area photonic crystal fiber", *Electronics Letters*, **34**, 1347-1348, (1998).

[49] Baggett, J.,Monro, T.,Furusawa, K., and Richardson, D.,"Comparative study of large mode holey and conventional fibers", Optics letters, **26**(14) 1045-1047,(2001).

[50] Saitoh, K.,Tsuchida, Y., andKoshiba, M.,"Endlessly single-mode holey fibers: the influence of core design",Optics Express, **13**(26) 10833-10839, (2005).

[51] Ferrando, A., Silvestre, E.,Miret, J., Andrés, V., and Andrés, P.,"Full-vector analysis of a realistic photonic crystal fiber", Optics letters, **24**(5) 1-13,(1999).

[52] Keiser, G.," Optical Fiber Communications", 2nd Edition,Mc-Graw Hill, Inc, New York,(2000).

[53]. Flanagan, J.,Finazzi, V.,Monro, T., Furusawa, K., and Richardson, D., "Understanding bending losses in holey optical fibers",Optics Communications, **227** (4) 1-45, (2003).

[54] Wong, W., Chan, C., Chen, L.,Li, T., Lee, K., Leong, K.,"Polyvinyl alcohol coated photonic crystal optical fiber sensor for humidity Measurement", Sensors and Actuators B **174(3)**,563-569, (2012).

[55] Mathew, J.,Semenova, Y.,Rajan, G., and Farrell, G.," Humidity sensor based on photonic crystal fiber interferometer", Electronics Letters, **46**(19), (2010).

[56] Wu, Y.,Rao, Y., Chen, Y., "Miniature fiber-optic temperature sensors basedon silica/polymer microfiber knot resonators", Optics Express, **7503** (75),1-4, (2009).

[57] Shao, M., Qiao, X., Fu, H.,Li, H., Zhao, J., Li, Y., "A Mach–Zehnder interferometric humidity sensor based on waist-enlarged tapers",Optics and Lasers in Engineering, **52**(12) 86-90, (2014).

[58] Mathew, J., "Development of Novel Fiber Optic Humidity, Sensors and Their Derived Applications",Ph. D. thesis,Dublin Institute of Technology, Dublin, Ireland,(2013).

[59] Jha, R.,Villatoro, J., and Badenes, G., "Ultra stable in reflection photonic crystal fiber modal interferometer for accurate refractive index sensing", Applied Physics Letters, **93**(7), (2008).

[60] Villatoro, J.,Finazzi, V.,"Temperature-insensitive photonic crystal fiber interferometer for absolute strain sensing", Applied Physics Letters **91**, 1-3, (2007).

[61] Tatara, T., T. suzaki, K. "An apnea monitor using a rapid-response hygrometer". J. Clin. Monit. Comput., **13**(1) 5–9, (1997)

[62] Lin, Y.C. "Breath sensor based on reflective optical lensed fiber". Microw. Opt. Technol. Lett., **55**, 450–454, (2013)

[63] Kastner, W.; Neugschwandtner, G.; Soucek, S.; Newmann, H.M. "Communication systems for building automation and control". Proc. IEEE, **93**, 1178–1203, (2005)

[64] Laville, C.; Pellet, C. "Interdigitated humidity sensors for a portable clinical microsystem". IEEE Trans. Biomed. Eng., **49**(1) 1162–1167, (2002)

[65] Habib Ahsan, A.H.M.; Lange, C.F.; Moussa, W. "Development of a Humidity Microsensor with Thermal Reset. In Proceedings of the International Conference on MEMS, NANO and Smart Systems", Banff, AB, Canada, **20**(23), 89–93, July (2003)

[66] C. Y. Lee, and G. B. Lee," Humidity sensors: a review, Sensor Letters**1**(4), 1- 15, (2005).

[67] T.L. Yeo , T. Sun, K.T.V. Grattan, "Fiber-optic sensor technologies for humidity and moisture measurement", Sens Actuators A Phys, **144**(1) 280–295, (2008).

[68] sigma. “Agarose.” Http://Www.sigmaaldrich.com/Content/Dam/Sigma-Aldrich/Docs/Sigma/Product_Information_Sheet/a9539pis.Pdf, 2 Oct. (2017).

[69] Mathew, J.,Semenova, Y., and Farrell, G., "Effect of coating thickness on the sensitivity of a humidity sensor based on an Agarose coated photonic crystal fiber interferometer", Optics Express, **21**(5) 6314-6320, (2013).

[70] Mathew, J., Semenova, Y., and Farrell, G., "Relative Humidity Sensor Based on an Agarose-Infiltrated Photonic Crystal Fiber Interferometer", IEEE Journal of Selected Topics in Quantum Electronics, **18**(5) 1553-1559, (2012).

[71] A.P. Russell, K.S. Fletcher, "Optical sensor for the determination of moisture", Anal. Chim. Acta, **170**, 209-216, (1985).

[72] R. Aneesh, and S. K. Khijwania, "Titanium dioxide nanoparticle based optical fiber humidity sensor with linear response and enhanced sensitivity", Applied Optics, **51**(12) 2164-2171, (2012).

[73] A. Alvarez-Herrero, H. Guerrero, D. Levy," High-sensitivity sensor of a low relative humidity based on overlay on side-polished fibers", IEEE Sens. J., **4** (1) 52–56, (2004).

[74] P. J. Rivero, A. Urrutia, J. Goicoechea, and F. J. Arregui, "Optical fiber humidity sensors based on Localized Surface Plasmon Resonance (LSPR) and Lossy mode- resonance (LMR) in overlays loaded with silver nanoparticles", Sensors and Actuators B: Chemical. **173**, 244–249, (2012).

[75]J. Lu, Z. Chen, F. Pang, and T. Wang, “Theoretical analysis of fiber-optic evanescent wave sensors,” in Proceedings of IEEE Microwave Conference, (China-Japan Joint, 2008), doi: 10.1109/CJMW.4772500, 583–587, (2008)

[76] Mathew, J., Thomas, K., Nampoori, V., and Radhakrishnan, P.,"A Comparative Study of Fiber Optic Humidity Sensors Based on Chitosan and Agarose", Sensors & Transducers Journal, **84**(10) 1633-1640,(2007).

[77] Viegas, D.,Goicoechea, J., Santos, J.,Araújo, F., Ferreira, L.,Arregui, F., and Matias, I., "Sensitivity Improvement of a Humidity Sensor Based on Silica Nanospheres on a Long-Period Fiber Grating ", Sensors, **9**(1) 519-527,(2009).

[78] Hernaez, M.,Zamaareno, C.R., Del Villar, I.,Arregui, F.,Matias, I.,"Optical fiber humidity sensor based on lossy mode resonances", International Journal on Smart Sensing and Intelligent Systems, **2**(4), 653-660,(2009).

[79] Zamarreno, C.,Hernaez, M., Del Villar, I.,Matias, I.,Arregui, F., "Tunable humidity sensor based on ITO-coated optical fiber", Sensors and Actuators B, **146**, 414-417, (2010).

[80] Wu, Q., Semenova, Y., Mathew, J., Wang, P., and Farrell, G.,"Humidity sensor based on a single-mode hetero-core fiber structure", Optics Letters, **36** (10), 1752-1754, (2011).

[81] Mathew, J.,Semenova, Y., Rajan, G., Wang, P., Farrell, G.,"Improving the sensitivity of a humidity sensor based on fiber bend coated with a hygroscopic coating", Optics & Laser Technology, **43**, 1301-1305,(2011).

[82] Noor, M.,Khalili, N., Skinner, I., and Peng, G.,"Optical Humidity Sensor Based on Air Guided Photonic Crystal Fiber", Photonic Sensors, **2**(3), 277–282, (2012).

[83] Correia, S.,P.Antunes, P., Pecoraro,E.,Lima, P., Ferreira, R., and André, P."Optical Fiber Relative Humidity Sensor Based on a FBG with a Di-Ureasil Coating",Sensors, **12**, 8847-8860,(2012).

[84] Mathew, J.,Semenova, Y., and Farrell, G.,"Fiber Optic Hybrid Device for Simultaneous Measurement of Humidity and Temperature", IEEE Sensors Journal, **13**(5), 1632-1636,(2013).

[85] Wales, D., Parker, R., Gates, J., Grossel, M., Smith, P.,"An investigation into relative humidity measurement using analumino silicate sol–gel thin film as the active layer in an integrated optical Bragg grating refractometer", Sensors and Actuators B, **188**, 857-866, (2013).

[86] Zheng, S., Zhu, Y., Krishnaswamy, S., "Fiber humidity sensors with high sensitivity and selectivity based on interior nanofilm-coated photonic crystal fiber long-period gratings",Sensors and Actuators B, **167**, 264-274, (2013).

[87] You, Y., Dai, J., and Lee, C.,"Highly Hygroscopic Polymer Microcavity Fiber Fizeau Interferometer for Humidity Sensing",PIERS Proceedings, 25-28, (2014).

[^8] Lokman A., BatumalayM., Harun S. W. and Arof H., "Humidity sensor based on tapered single mode fiber coated with a hydroxyethyl cellulose/poly-vinylidene fluoride composite",Ukr. J. Phys. Opt. **15**(2), 96-101, (2014).

[89] Xie, W.,Yang, M., Cheng, Y., Li, D., Zhang, Y.,Zhuang, Z,"Optical fiber relative-humidity sensor with evaporated dielectric coatings on fiber end-face", Optical Fiber Technology, **20**, 314-319, (2014).

[90] Shao, M., Qiao, X., Fu, H.,Li, H., Zhao, J., Li, Y., "A Mach–Zehnder interferometric humidity sensor based on waist-enlarged tapers", Optics and Lasers in Engineering, **52**, 86-90, (2014).

[91] Yang, J., Dong, X., Ni, K., Chan, C., and Shun, P., "Intensity-modulated relative humidity sensing with polyvinyl alcohol coating and optical fiber gratings",Applied Optics, **54**, (10), 2620-2624,(2015).

[92] Liu, H., Miao, Y., Liu, B., Lin, W., Zhang, H., Song, B., Huang, M., and Lin, L., "Relative Humidity Sensor Based on S-Taper Fiber Coated With SiO2 Nanoparticles", IEEE Sensors Journal, **15**, (6), 3424-3428, (2015).

[93] Suaad Sahib Hindal, Hanan J. Taher, "Performance of humidity sensor based on photonic crystal fiber interferometer", Iraqi Journal of Physics, **14** (30), 83-89,(2016).

[94] Xing long Pan . et al, "Effective Enhancement of Humidity Sensing Characteristics of Novel Thermally Treated MWCNTs/Polyvinyl pyrrolidone Film Caused by Interfacial Effect "Qingdao 266580, P. R. China 1-7, (2016)

[95] Diego Lopez-Torres ,et al., Photonic crystal fiber interferometer coated with a PAH/PAA nanolayer as humidity sensor , **242**, 1065-1072, April (2017)

[96] Habibah Mohamed et al." Optical Humidity Sensor Based on Tapered Fiber with Multi-walled Carbon Nanotubes Slurry " **6**(1),. 97 ~ 103, April (2017)

[97] Saeed Azad , et al. , "Sensitivity optimization of ZnO clad-modified optical fiber humidity sensor by means of tuning the optical fiber waist diameter" , Optics & Laser Technology **90(**33**)**, 96–101 , (2017)

[98] Joaquin Ascorbe , et al. , "Humidity Sensor Based on Bragg Gratings Developed on the End Facet of an Optical Fiber by Sputtering of One Single Material" , Sensors, 17, 991; doi:10.3390/s17050991 , 1-13,(2017)

[99] Qifei Ma, Kai Ni ⇑ , Ran Huang , A carboxy-methyl cellulose coated humidity sensor based on Mach-Zehnder interferometer with waist-enlarged bi-tapers "Optical Fiber Technology **33**, 60–63, (2017)

[100] Kai Ni , et al. "A chitosan-coated humidity sensor based on Mach-Zehnder interferometer with waist-enlarged fusion bitapers" Optical Fiber Technology **33**, 56–59 , (2017)

[101] : Diego Lopez-Torres ,et al." Enhancing sensitivity of photonic crystal fiber interferometric humidity sensor by the thickness of SnO2 thin films", Sensors and Actuators B , SNB 22409,1-30, (2017)

LIST OF PUBLICATIONS (Journal Papers)

1- Hassan F. Hassan, Hanan J. Taher, Saif Akeel," Enhancement the sensitivity of humidity sensor based on an agarose infiltration reflection-type photonic crystal fiber", Iraqi Journal Physics.
(**Accepted**)

2- Hassan F. Hassan, Hanan J. Taher, "Enhancement the sensitivity of humidity sensor based on an agarose coating transmission-type photonic crystal fiber" Iraqi Journal of laser .
(**Accepted**)

Appendices

Appendix……..(A)

Specifications of arc fusion splicer (FSM-60S)

Item	Specifications
Applicable fibers	SMF ,MMF ,DSF ,NZDSF etc.
Cladding dia./sheathe dia.	80 to150 µm / 100 to 1000 µm
Splice mode	Total 100 modes
Automatic fiber identification	SMF ,MMF ,NZDSF
Splice loss estimate	Equipped
Attenuation splice	0.1 dB to 15dB by 0.1 dB step
Splice result storage	Last 2000 splices
Viewing methods	2 axis 2CMOS camera with 4.1 LCD
Tension test	1.96 to 2.25 N
Protection sleeve	60mm ,40mm and Fujikura micro sleeves
Diagnostic function	Equipped

Appendix……..(B)

NKT Photonics
the power of light

Crystal Fibre • aeroLASE • Koheras • SuperK

LMA-10

Single-mode 10 µm core fiber

- Low fiber loss from 500 to 1700 nm
- Single-mode at all wavelengths
- Radiation hard pure silica fiber
- Wavelength independent MFD

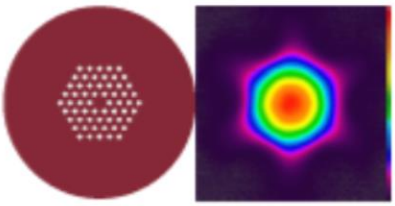

This single-mode photonic crystal fiber is optimized to exhibit low loss across the widest possible wavelength region from 500 nm to above 1700 nm while keeping an almost constant mode field diameter.

The fiber is endlessly single-mode with no higher order mode cut-off and delivers pristine mode quality at all wavelengths.

The fiber has a standard 125 µm outer diameter and is compatible with all common fiber tools.

This product is also available in a polarization-maintaining version as the LMA-PM-10.

Applications

- Single-mode high power delivery
- Mode filtering
- Single-mode pigtailing

Optical properties	
Single mode cut-off wavelength*	None
Attenuation @ 532 nm	< 25 dB/km
Attenuation @ 632 nm	< 10 dB/km
Attenuation @ 1064 nm	< 5 dB/km
Mode field diameter @ 532 nm (1/e²)	8.4 ± 0.5 µm
Mode field diameter @ 1064 nm (1/e²)	8.8 ± 0.5 µm
NA @ 1064 nm (5%)	0.11± 0.02
Physical properties	
Core diameter	10.1 ± 0.5 µm
Outer cladding diameter, OD	125 ± 5 µm
Coating diameter	245 ± 10 µm
Core and cladding material	Pure silica
Coating material, single layer	Acrylate
Coating concentricity	< 10 µm
Proof test level	0.5 %

Standard interfacing options	
FC/PC connector	0.0 ± 0.5 deg angle
FC/APC connector	8.0 ± 0.5 deg angle
Collapse and cleave	0.0 ± 0.5 deg angle

All interfaces are provided with a 150 ± 25 µm sealing length of the PCF structure.

Please contact us for other custom interfacing options.

* TA-455-80-C standard

Typical spectral attenuation and dispersion

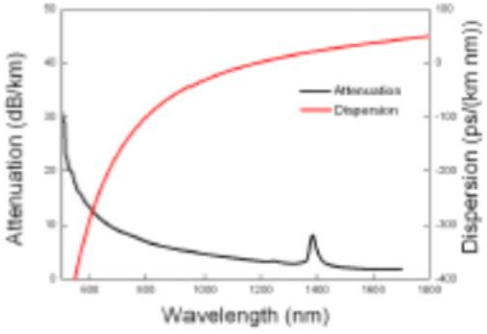

Typical MFD and NA

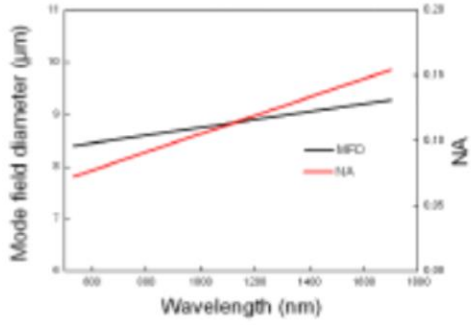

LMA

NKT Photonics A/S (Headquarters)
Blokken 84 • 3460 Birkerød • Denmark
Phone: +45 4348 3900

NKT Photonics GmbH
Schanzenstrasse 39 • Bldg D9-D13
51063 Cologne • Germany

NKT Photonics Inc.
1400 Campus Drive West • Morganville
NJ 07751 • USA

Appendix……..(C)

CIRCULATOR TEST DATA SHEET

Description: Polarization Insensitive Fiber Optics Circulator,C+L band, 3-port , SMF-28e, 900um loose tube, 1.0m, LC/UPC, 5.5×50mm

Part Number:CIR-3-C+L-1-LU

S/N: 840115230

Parameters	Unit	Specification	Test Data
Operating Wavelength	(nm)	C+L	C+L
Operating Wavelength Range	(nm)	/	/
Insertion Loss(Port 1 to Port 2)@1550nm(23℃)	(dB)	≤ 1.5	0.68
Insertion Loss(Port 2 to Port 3)@1550nm(23℃)	(dB)	≤ 1.5	0.65
PDL(Port 1 to Port 2)@1550nm	(dB)	≤ 0.15	0.02
PDL(Port 2 to Port 3)@1550nm	(dB)	≤ 0.15	0.09
Minimum Isolation at 23℃	(dB)	≥ 40	43
DIR	(dB)	≥ 50	53
Return Loss	(dB)	≥ 50	53
PMD	(ps)	0.1	Pass
Connector		LC/UPC	
Fiber Type		SMF-28e with 900um loose tube	
Fiber Length	(m)	1.0	
Power Handling	(mW)	≤300	
Operating Temperature	(℃)	0 to +70	
Storage Temperature	(℃)	-40 to +85	
Dimension	mm	¢5.5×50	

Remark: Port 1 is red marked, Port 2 is blue, Port 3 is white

Package Dimensions:

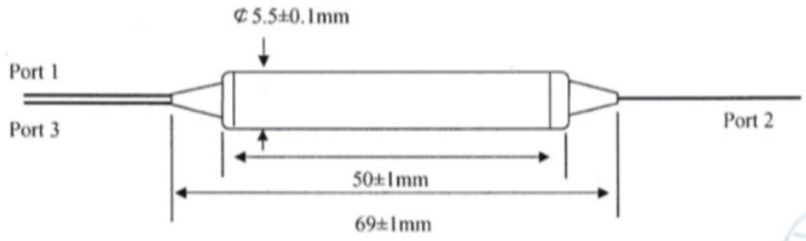

Check by: Lilai

Review by:Zhangfan

Date: 2015-3-31

QA PASS 04

Appendix……..(D)

Product Specification Sheet

Benchtop Laser Source

S1FC1550

Description

Thorlabs Benchtop Fiber Pigtailed Laser Sources are ideal for fiber based applications. Our S1FC Series comes with a pigtailed Fabry-Perot Laser diode with single mode fiber behind an FC/PC bulkhead connector. Our fiber pigtailed lasers utilize an angled fiber ferrule at the internal laser/fiber launch point to minimize reflections back into the laser diode, thereby increasing the overall stability.

Specifications

Specification	Value
Wavelength	1550 nm
Min Full Output Power	1.5 mW
Stability	15 min: ±0.05 dB, 24 hr:±0.1 dB (After 1 hr Warm-up at 25 ± 10 °C Ambient)
Display Accuracy	±10%
Setpoint Resolution	0.01 mW
Adjustment Range	~0 mW to Full Power

Specification	Value
Operating Temperature	15 to 35 °C
Storage Temperature	0 to 50 °C
AC Input	115 VAC / 230 VAC (Switch Selectable) 50 - 60 Hz
Modulation Input	0 - 5 V = 0 - Full Power, DC or Sine Wave Input Only
Modulation Bandwidth	5 kHz Full Depth of Modulation 30 kHz Small Signal Modulation
Fiber	SMF-28e

Drawings

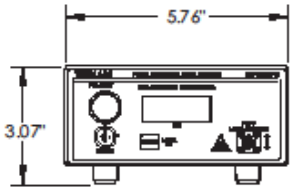

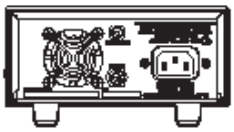

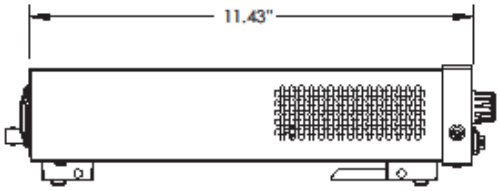

USA, Canada, & S. America
Thorlabs, Inc.
435 Route 206
Newton, NJ 07860, USA
Tel: 973-579-7227
Fax: 973-300-3600
www.thorlabs.com
email: feedback@thorlabs.com

Europe
Thorlabs GmbH
Hans-Böckler-Str. 6
85221 Dachau, Germany
Tel: +49-(0)8131-5956-0
Fax: +49-(0)8131-5956-99
www.thorlabs.com
email: Europe@thorlabs.com

UK and Ireland
Thorlabs LTD.
1 Saint Thomas Place, Ely
Cambridgeshire CB7 4EX, GB
Tel: +44 (0)1353-654440
Fax: +44 (0)1353-654444
www.thorlabs.com
email: sales.uk@thorlabs.com

Scandinavia
Thorlabs Sweden AB
Box 141 94
400 20 Göteborg, Sweden
Tel: +46-31-733-30-00
Fax: +46-31-703-40-45
www.thorlabs.com
email: scandinavia@thorlabs.com

Japan and Asia
Thorlabs Japan Inc.
5-17-1, Ohtsuka
Bunkyo-ku, Tokyo 112-0012, Japan
Tel: +81-3-5977-8401
Fax: +81-3-5977-8402
www.thorlabs.jp
email: sales@thorlabs.jp

2554-S01 – October 3, 2008

Appendix……..(E)

Specifications of Power Meter

Model	FPM-300/FLS-300/FOT-300
Power meter port	Ge
Power range (dBm)	10 to -60
Range displayed	Down to -65
Number of calibrated wavelength	10
Power uncertainty	±5% ±1 nW
Resolution (dB)	0.01
Automatic offset nulling	Yes
Display units	dB/dBm/W
Automatic wavelength recognition	Yes
Screen refresh rate (Hz)	3
Tone detection (Hz)	270 , 1 K ,2K
Battery life (hours) (typical)	>300

الخلاصة

مقياس التداخل للألياف البلورية الفوتونية تستعمل بشكل واسع في تطبيقات التحسس . وفي هذا العمل تم توصيف وتصنيع متحسسان للرطوبة النسبية بالاعتماد على مقياس التداخل لماخ زيندر . تم حقن قطعة من الليف البلوري الفوتوني بمادة الاكاروس لتحسين الحساسية والذي يعمل في نمط الانعكاس ومتحسس اخر تم طلاءه بنفس المادة والذي يعمل في نمط النفاذية . تم تصنيع هذين المتحسسين ببساطة بواسطة لحام ليف مقياس التداخل لليف الفوتوني البلوري (LMA-10) مع ليف ذو نمط مفرد (SMF-28) . يتم عمل المتحسس المحقون بمادة الاكاروس بالاعتماد على امتزاز بخار الماء عند حاجز سيليكا -هواء مع الليف البصري البلوري الفوتوني . المتحسس ابدى حساسية عالية لمقدار التغير بالرطوبة (٢٧%- ٩٥%) و زحزحة لموقع قمم التداخل نحو الأطوال الموجية الطويلة مع زيادة في قيم الرطوبة النسبية وقد حصل على اعلى مقدار للحساسية (٨,٤٩) بيكو متر / النسبة المئوية للرطوبة النسبية عند طول (٤) مليمتر مع زمن الاستجابة سريع (١,٤) ثانية والذي يمكنه من الاستعمال في جهاز التنفس للمريض في العيادات الطبية. اما المتحسس الأخر الذي تم طلاءه بمادة الاكاروس المعتمد على مقياس التداخل لماخ زندر ذو نمط النفاذية فمن خلال النتائج التجريبية أبدى المتحسس حساسية عالية لمقدار التغير بالرطوبة (٢٧%- ٩٥%) وقد حصل على أعلى مقدار للحساسية (٢٩،٣٧-) بيكو متر / النسبة المئوية للرطوبة النسبية عند سمك طبقة الطلاء بمقدار (٥،٩٩٦) مايكرو متر.

وقد اثبت ان متحسس الرطوبة المصمم يعتمد على سمك طبقة الطلاء . فعند اعلى مقدار حساسية بين المتحسس هناك استجابة خطية وزحزحة لموقع قمم التداخل نحو الاطوال الموجية القصيرة مع زمن الاستجابة سريع (٠,٨) ثانية للتغير من (٥٠%- ٩٠%) . كذلك فان متحسسي الرطوبة المصممين لهما عدة مزايا حجم صغير ، مستقرين ، ذوي قياسات دقيقية ، تحسس لمدى واسع من الرطوبة.

تم استخدام برنامج COMSOL multiphysics٥،١ لتصميم الليف البلوري الفوتوني وعند حقن وطلاء الليف البلوري بمادة الاكاروس وايجاد توجيه دايود الليزر ١٥٥٠نانومترداخل الليف البصري البلوري .

وزارة التعليم العالي والبحث العلمي
جامـــعة بغـــداد
معهد اللـــيزر للدراســـــات العليا

دراسة تحسين متحسس الرطوبة المستند على مقياس التداخل لليف البلوري الفوتوني

رسالة مقدمة إلى

معهد الليزر للدراسات العليا /جامعة بغداد /لاستكمال متطلبات نيل شهادة ماجستير علوم في الليزر/ الفيزياء

من قبل

حسن فالح حسن

بكالوريوس علوم فيزياء -٢٠٠٠

بإشراف

الأستاذ المساعد الدكتورة حنان جعفر طاهر

١٤٣٩ هـ **٢٠١٧ م**